Universitat Autònoma de Barcelona

THE ROLE OF ATR KINASE DURING MAMMALIAN GAMETOGENESIS

Memòria presentada per

Sarai Pacheco Piñol

Per obtar al títol de

Doctor en Biologia Cel·lular

Tesi doctoral dirigida per

Ignasi Roig Navarro

Departament de Biologia Cel·lular, Fisiologia i Immunologia

Universitat Autònoma de Barcelona

Director — Ignasi Roig Navarro

Doctoranda — Sarai Pacheco Piñol

Bellaterra, abril de 2015

This work received financial support from:

- Ministerio de Ciencia e Innovación grant (BFU2010-18965)
- APOSTA award for young investigators from Universitat Autònoma de Barcelona (APOSTA2011-03)

Als meus pares,

"El calidoscopio ha dado una pequeña vuelta,

y otras leyes rigen este mundo en el que sólo persiste

un elemento común: mi ojo que mira, que mira"

Julio Cortázar

INDEX

ABSTRACT

ATR kinase is one of the main players of the DNA damage response (DDR) machinery involved in maintaining genome integrity. ATR is mainly activated in response to ssDNA structures present at resected double strand breaks (DSBs) and in aberrant replicative structures. During meiosis, the specialized cell division that generates haploid gametes, hundreds of programmed DSBs are introduced in the genome. DSB repair promotes pairing, synapsis and recombination of homologous chromosomes creating connections between them to promote proper chromosome segregation, thus avoiding the formation of defective gametes. The correct execution of these processes is essential for meiocytes viability and is carefully controlled by different signaling mechanisms involving ATM and ATR proteins. Some studies have reported that ATR associates with meiotic chromosome axes. ATR colocalizes with other DDR proteins on meiotic recombination nodules and accumulates on unsynapsed chromosomes participating in meiotic transcriptional silencing of those regions. These evidences underline ATR involvement in DSB repair and mediating checkpoint responses. Here we used mouse model of human ATR-Seckel syndrome and a novel testis organ culture in order to investigate the role of ATR during mammalian meiosis and gametogenesis. Our findings showed that down-regulation of ATR function during meiotic prophase results in defective meiotic homologous recombination and reduced local DSB accumulation on unsynapsed axes as prophase progresses. Both alterations particularly concern XY pair leading to inaccurate sex chromosomes synapsis. Moreover, deficient ATR levels impair folliculogenesis progression compromising proper follicular development.

ACRONYMS AND ABREVIATIONS

γH2AX – *Phosphorylated H2AX*
β-ACTIN – *ACTIN isoform β*
°C – *Celsius degrees*
9-1-1 – *Rad9-Hus1-Rad1 clam complex*
µl – *microliter*
µm – *micrometer*
µM – *micromolar*
A – *Adenine*
AE – *Axial Element*
APS – *Ammonium Persulfate*
ATM – *Ataxia Telangiectasia Mutated*
ATR – *Ataxia Telangiectasia and Rad-3 related*
ATRIP – *ATR Interacting Protein*
ATRi – *ATR inhibitor*
avg – *Average*
bp – *Base pair*
BAC – *Bacterial Artificial Chromosome*
BRCA1 – *Breast Cancer Protein 1*
BSA – *Bovine Serum Albumin*
C – *Cytosine*
CDC25 – *Cell Division Cycle protein 25*
CDK – *Cyclin-Dependent Kinase*
cDNA – *complementary DNA*
CE – *Central Element*
CEEAH – *Ethics Committee for Animal and Human Experimentation*
CHK1 – *Checkpoint Kinase 1*
CO – *Crossover*
CO_2 – *Carbon dioxide*
Cy3 – *Cyanine 3*
Cy5 – *Cyanine 5*
DAPI – *4',6-diamidino-2-phenylindole*
dHJ – *Double Holliday junctions*
DAAM – Ministry of farming, ranching, Fishery, alimentary and environment
DDX4 – *DEAD box polypeptide 4*
DMC1 – *DNA Meiotic Recombinase 1*
DMSO – *Dimethyl sulfoxide*
DNA – *Deoxyribonucleic acid*
dNTP – *Desoxinucleotid Phosphate*
dpc – *days post-coitum*
dpp – *days post-partum*
DSB – *Double Strand Break*
DTT – *Dithiothreitol*
dUTP – *2'-deoxyuridine 5'-triphosphate*
EDTA – *Ethylenediaminetetraacetic acid*
EdU– *5-ethynyl-2'-deoxyuridine*
EtOH – *Ethanol*
FISH – *Fluorescence In Situ Hybridization*
Fig – *Figure*
FITC – *Fluorescein Isothiocyanate*
FSH – *Follicle-Stimulating Hormone*
G – *Guanine*
GD – *Gamma distribution*
gDNA – *genomic DNA*
H1T – *Testicular H1 histone*
H2AX – *X variant of 2A histone family*
HCl – *Hydrogen Chloride*
HORMAD – *HORMA Domain containing proteins*
Hop1 – *Homolog pairing protein 1*
HR – *Homologous Recombination*
HRP – *Horseradish Peroxidase*
IH – *Inter-Homologous*
kDa – *Kilodalton*
KU70 – *Lupus Ku autoantigen protein 70*
LH – *Luteinizing Hormone*
M – *Molar*
MCM2 – *Minichromosome Maintenance complex component 2*
MDC1 – *Mediator of DNA-damage Checkpoint 1*
MI – *Metaphase I*
ml – *milliliter*
MLH1 – *MutL Homolog protein 1*
mM – *millimolar*
Mec1 – *Mitosis Entry Checkpoint protein 1*
Mei-41 – *Meiosis 41 protein*
$MgCl_2$ – *Magnesium chloride*
mg – *milligram*
MRN – *Mre11-Rad50-Nbs1 complex*
mRNA – *messenger RNA*
MSCI – *Meiotic Sex Chromosomes Inactivation*
MSUC – *Meiotic Silencing of Unsynapsed Chromosomes*
mTOR – *mammalian Target Of Rapamycin protein*
MUS81 – *MMS and UV Sensitive protein 81*
NaCl – *Sodium chloride*
NCO – *Non-Crossover*
NHEJ – *Non-Homologous End Joining*
nm – *nanometer*
OCT – *Optimum Cutting Temperature compound*

OMIM – *Online Mendelian Inheritance in Man*
PAR – *Pseudo-Autosomal Region*
PAS – *Periodic Acid Schiff*
PBS – P*hosphate-Buffered Saline*
PBST – *PBS-Tween*
PCR – *Polymerase Chain Reaction*
PFA – *Paraformaldehyde*
PGC – *Primordial Germ Cell*
PIC – *Protein Inhibitor Cocktail*
PI3K – *Phosphoinositide 3-kinase*
PTBG – *PBS-Tween-BSA-Gelatin*
PTEN – *Phosphatase and Tensin homolog protein*
RAD17 – *Radiation Sensitive protein 17*
RAD51 – *Radiation Sensitive protein 51*
RAD52 – *Radiation Sensitive protein 52*
RAD54 – *Radiation Sensitive protein 54*
RNA – *Ribonucleic Acid*
RPA – *Replication Protein A*
rpm – *revolutions per minute*
RT-PCR – *Reverse Transcription - PCR*
S317 – *Serine 317*
S345 – *Serine 345*
SAC – *Spindle Assembly Checkpoint*
SEM – *Standard Error*
SC – *Synaptonemal Complex*
SCD – *S/T-Q Cluster Domain*
Scml2 – Scm-like 2 X-linked gen
SDS – *Sodium dodecyl sulfate*
SDSA – *Synthesis-Dependent Strand-Annealing*
SDS-PAGE – *SDS Polyacrylamide Gel Electrophoresis*
ssDNA – *Single stranded DNA*
SPO11 – *Sporulation Protein 11*
Sry – Sex-determining region Y
SUMO-1– *Small Ubiquitin-related Modifier 1*
SYCP1 – *Synaptonemal complex protein 1*
SYCP2 – *Synaptonemal complex protein 2*
SYCP3 – *Synaptonemal complex protein 3*
T – *Thymine*
TdT – *Terminal deoxynucleotidyl Transferase*
Tel1 – *Telomere maintenance protein 1*
TEMED – *Tetramethylethylenediamine*
TOPBP1 – *DNA Topoisomerase 2-Binding Protein 1*
TRIP13 – *Thyroid Receptor-Interacting Protein 13*
Tris-HCl – *Tris(hydroxymethyl) aminomethane hydrochloride*
TSC – *Tuberous Sclerosis Complex*
TUNEL– *Terminaldeoxynucleotidyl Transferase dUTP Nick End Labeling*
uH2A – *H2A histone ubiquitination*
– N*umber of*
Zfx – Zinc finger X-linked gene
ZMM – *Synapsis initiation complex proteins*

INTRODUCTION

Chapter 1

1.1 Gametogenesis

During the sexual reproduction process, two gametes merge to produce new progeny. Thus, the genome copy number in the gametes must be reduced by half in order to prevent the doubling of genetic material every new generation. This reduction in ploidy takes place during the process that generates gametes, known as gametogenesis, in which meiosis occurs. Meiosis is an unusual type of cell division, presenting one round of genome replication, followed by two rounds of chromosome segregation generating haploid daughter cells. In view of gametes are the precursor cells of new generations, it is not surprising that gametogenesis is cautiously controlled by an extended network of signaling pathways that elicits the appropriated responses, in which ATR kinase is involved. As male and female gametes present several differences in morphology, as well as, in the functions during early stages of embryo development, numerous events taking place during gametogenesis exhibit a high sexual dimorphism, whilst others appear to be largely conserved.

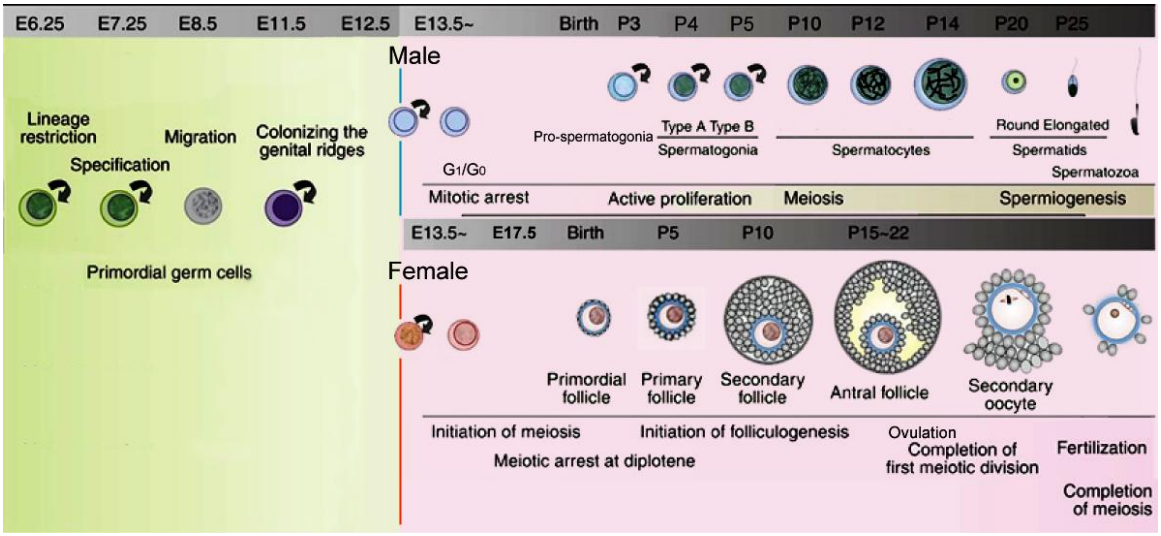

Figure 1.1. Mammalian gametogenesis is sexually dimorphic. Schematic representation showing germ cell development in mice from embryonic PGC specification until gamete formation. In both sexes PGC undergo mitotic proliferation and migration to colonize genital ridges prenatally. Male germ cells development (upper right) in the fetal testis suffers an extended period of mitotic arrest, which will resume after birth. First wave of spermatogenesis initiate around 5 dpp (P5) with first spermatogonia differentiating into spermatocytes that undergo meiosis entry. Spermatocytes are subject to two meiotic divisions, followed by spermiogenesis, to form four haploid spermatozoa. As a result of a continuous spermatogonia proliferation and differentiation, meiosis and spermatozoa formation is maintained throughout the male lifespan. By contrast, all female germ cells (lower right) entry into meiosis at the fetal ovary to become oocytes. Oocytes suffer a meiotic arrest at diplotene stage and remain arrested until ovulation. Then, oocyte resumes meiosis I to become a secondary oocyte arrested at metaphase II. Once the oocyte is fertilized, it resumes meiosis II. Because all female oogonia initiate meiosis prenatally, gametogenesis continues until the pool of oocytes is depleted. E in grey bars indicates the embryonic day of development and P the post-natal day of development. Arrows in the figure signify self-renewal of the indicate cells. Image modified from Saitou & Yamaji 2012.

1.1.1 Early events occurring during gametogenesis

Primordial germ cells (PGCs) are the embryonic progenitors of the gametes, thus, they are fundamental for sex reproduction and are the responsible to pass genetic information to new generations.

In the mouse embryo, around 6.25 days post-coitum (dpc) a small group of cells acquire the competence to become PGCs as a consequence of paracrine signaling molecules secreted from the extra-embryonic ectoderm (Chiquoine 1954; Lawson & Hage 1994)(**Fig. 1.1**). Then, around 7.25 dpc, only a subset of the PGC-competent precursor cells complete the specification process and acquire a PGC fate (Ohinata et al. 2005). At this time, these PGCs migrate from the extra-embryonic site of specification, the base of the allantois, to the primitive gonads or genital ridges, which are colonized around 10-12.5 dpc (Molyneaux et al. 2001). Additionally, during the migratory period, PGCs proliferate and initiated a genome-wide epigenetic reprogramming (Tam & Snow 1981; Surani 2001; Seki et al. 2007). To expand their numbers, PGCs proliferate mitotically increasing from approximately 50-100 cells at 8.5 dpc to 25000 cells in the 13.5 dpc (Tam & Snow 1981; De Felici et al. 2005). Upon colonization of the gonads, bipotential PGC initiate to change their gene expression profile and must differentiate in order to establish the gametes of each sex required at fertilization. This sexual differentiation is determined by the sexual phenotype of their somatic environment (Adams & McLaren 2002; Bowles & Koopman 2010). From this point, around 12.5-13.5 dpc, PGCs cease mitotic cell divisions and development of the male and female embryo undertakes divergent trajectories marked by the formation of testes or ovaries, respectively (Ewen & Koopman 2010; Feng et al. 2014).

1.1.2 Spermatogenesis

The genital ridges are sexually ambiguous, although in the XY embryo around 10.5 dpc, somatic cells begin to express the male fate determination gen Sry to lead the gonad to testis development. Sry expression leads to differentiation of some somatic cells to Sertoli cells (Sekido et al. 2004; Kanai et al. 2005). Sertoli cells are the organizing center of testis differentiation, and act as a regulatory center in testis organogenesis, including differentiation of PGCs (Palmer & Burgoyne 1991). In the absence of Sry expression, concurrently with expression of other genes of the XX embryo, gonads are lead to develop into ovaries (Wagner et al. 1994; Barrionuevo et al. 2006; Svingen & Koopman 2013). At approximately 12.5 dpc, PGCs in the testis exhibit a morphology corresponding to post-mitotic G_1 phase of the last pre-meiotic cell cycle, and several genes specific of meiosis are up-regulated (Di Carlo et al. 2000; Nakatsuji & Chuma 2001). However, around 12.5-14.5 dpc, PGCs undergo mitotic arrest remain in this quiescent state, called pro-spermatogonia state, until shortly after birth, when they resume proliferation and develop the capacity to migrate to the peripheral basement membrane of the seminiferous tubules of the testis (Hilscher et al. 1974; McLean et al. 2003). After migration to the basement membrane, pro-spermatogonia differentiate into

spermatogonial stem-cells. These spermatogonia have the capacity to self-renew, proliferating to increase population of germ cells, but also to produce cells that initiate sperm differentiation (de Rooij 1998; McLean et al. 2003). In the mouse testis, different types of spermatogonia have been described, undifferentiated type A spermatogonia, which undergo mitosis to form differentiated type A spermatogonia, intermediate and type B spermatogonia. This last type of spermatogonia differentiate to spermatocytes, which enter meiosis to form haploid spermatids and eventually spermatozoa (de Kretser et al. 1998; de Rooij 2001).

The development of the first pro-spermatogonia into mature sexual cells is known as the first wave of spermatogenesis, which begins at approximately 5 days post-partum (dpp) in mouse. This is accompanied by extensive germ cell apoptosis to adjust the number of germ cells to that which can be maintained by the available Sertoli cells (Rodriguez et al. 1997; Print & Loveland 2000). From this point, spermatogonium proliferation and spermatozoa generation is maintained throughout the life time of the male. Thus, in the testis spermatogonia are continuously stimulated to differentiate in spermatocytes, which undergo meiotic division and produce four spermatids. During the post-meiotic events, known as spermiogenesis, spermatids develop into spermatozoa. This process involves tight packing of the chromatin, growth of the sperm flagellum and the removal of the remaining cytoplasm into the residual bodies (de Kretser et al. 1998; Sakai & Yamashina 1989; Peschon et al. 1987).

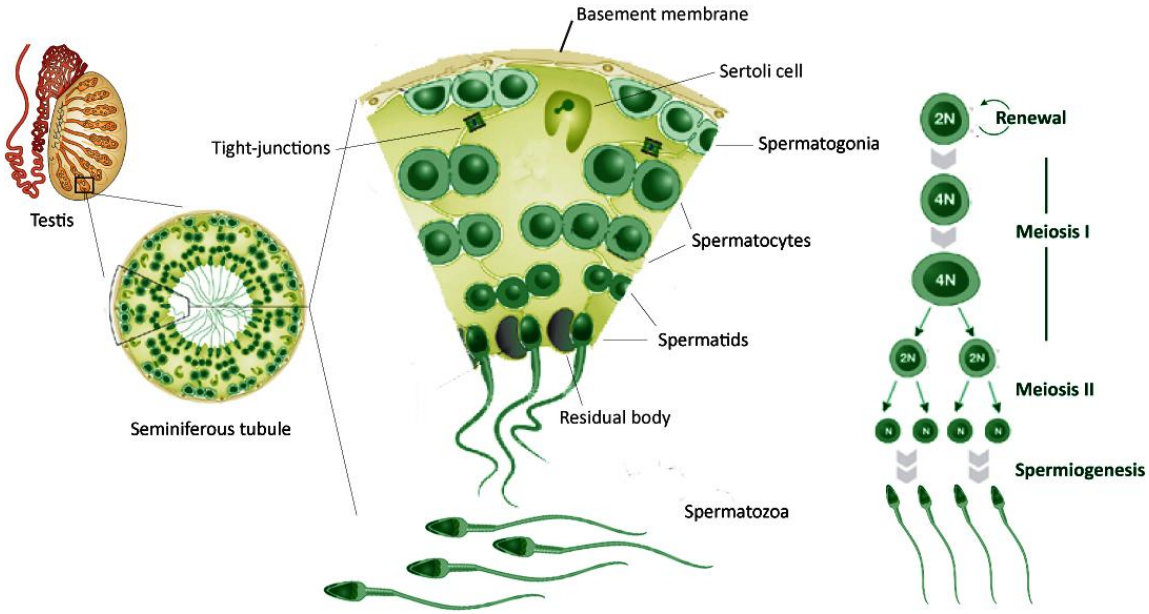

Figure1.2. Organization of the testis. Representative figure of the architecture of mammalian testis. Seminiferous tubules within the testis comprise all spermatogenic germ cells, from spermatogonial cells to spermatozoa, and supporting Sertoli cells. Note the progression of germ cell differentiation from the basement membrane region, where spermatogonia are located, followed by spermatocytes at different stages of meioisis and haploid spermatids (round and elongated). Once spermiogenesis is completed mature spermatoza are released into the lumen of the tubule. In the seminiferous tubules, tight junctions between Sertoli cells define two compartments. Spermatogonia and pre-meiotic cells reside in one side of the junctions, and meiotic and post-meiotic cells reside on the other organized in strict order of maturation. Image adapted from Krawetz et al. 2009 and Cooke & Saunders 2002.

Spermatogenesis is a highly ordered process that takes place in the seminiferous tubules. In mouse, the entire process takes approximately 35 days, in which mitotic phase takes about 10 days, meiotic phase about 11 days, and post-meiotic or spermiogenesis phase about 14 days. In the adult testis, every 8-9 days there is a group of cells that initiate spermatogenesis, consequently different spermatogenetic waves overlap (Oakberg 1956; Clermont & Trott 1969; Eddy 2002). Within the seminiferous tubules, the different waves organize in layers of cohorts of germ cells developing in synchrony (**Fig. 1.2**). Spermatogonia are located directly on the basement membrane where Sertoli cells rest. Sertoli cells act as the epithelial supporting cells of the seminiferous tubules. Moreover, Sertoli cells are connected to each other by tight-junctions forming a blood-testis barrier that separates the intra-tubular epithelium in two different compartments. A basal compartment, where cells are exposed to the extra-tubular environment, and a luminal compartment that provides a microenvironment for spermatogenesis produced by Sertoli cells and germ cells as well (Griswold 1998). In the luminal compartment are located the meiotic, primary and secondary spermatocytes, and post-meiotic cells that move from the periphery to the lumen of the tubule as spermatogenesis progresses. An interesting feature of spermatogenesis is that when a differentiated spermatogonia divides mitotically, the progeny remain connected by cytoplasmatic bridges (Greenbaum et al. 2011). These incomplete cytoplasmatic divisions allow cytoplasmatic molecules pass through the intercellular bridges leading to a synchronous maturation. Furthermore, due to the presence of these intercellular bridges, germ cells can be supplied with all gene products of a complete diploid genome after meiosis (Fawcett 1959; Braun et al. 1989). Thus, germ cells remain connected by cytoplasmatic bridges until individual spermatozoa are released into the lumen of the seminiferous tubules. Because the initiation of a new wave of spermatogenesis occurs meanwhile previous waves are still in progress, the epithelium of each tubule contains germ cells at various steps of development.

1.1.3 Oogenesis

As mentioned above, early stages of germ cell development in both sexes are undistinguishable until PGCs arrive at the gonads. Once PGCs colonized the genital ridge, they divide by mitosis until approximately 13.5 dpc (McLaren 1984; Pepling 2006). This phase of mitotic proliferation is characterized by an incomplete cytokinesis, leading to the formation of germ cell cysts, which divide synchronously and are connected by intercellular bridges. While germ cells are dividing, they interact with somatic cells in the ovary that appear surrounding the cyst (**Fig. 1.3**) Within the cyst, around 12.5 dpc, germ cells nuclei enter a premeiotic state marked by up-regulation of meiotic genes (Di Carlo et al. 2000; Nakatsuji & Chuma 2001). Nevertheless, it is not before 13.5 dpc when PGCs in the ovary become oocyte by entering meiosis. This point is the hallmark of differentiation to the female gonads (Hilscher et al. 1974; McLaren 1984; Ewen & Koopman 2010). Meiosis entry in the female embryo is not synchronous and apparently, proceeds in a wave from the anterior to the posterior end of the ovary (Menke et al. 2003; Bullejos & Koopman 2004). By 15.5 dpc the majority of the oocytes

have entered into meiotic prophase I and arrest at diplotene stage beginning at 17.5 dpc with most cells reaching diplonema by 5 dpp (Borum 1961). Oocytes remain arrested in this stage until after ovulation when meiosis is resumed. Around the time of meiotic arrest, germ cell cysts breakdown and oocytes separate and become surrounded by flattened pre-granulosa cells to form primordial follicles. During cyst breakdown, two-thirds of oocytes undergo programmed cell death (Pepling & Spradling 2001; Tingen et al. 2009). The cyst breakdown and the oocyte loss occurs simultaneously, suggesting these two processes are linked and involve communication between oocytes and granulosa cells (Robles et al. 2000; Pepling & Spradling 2001).

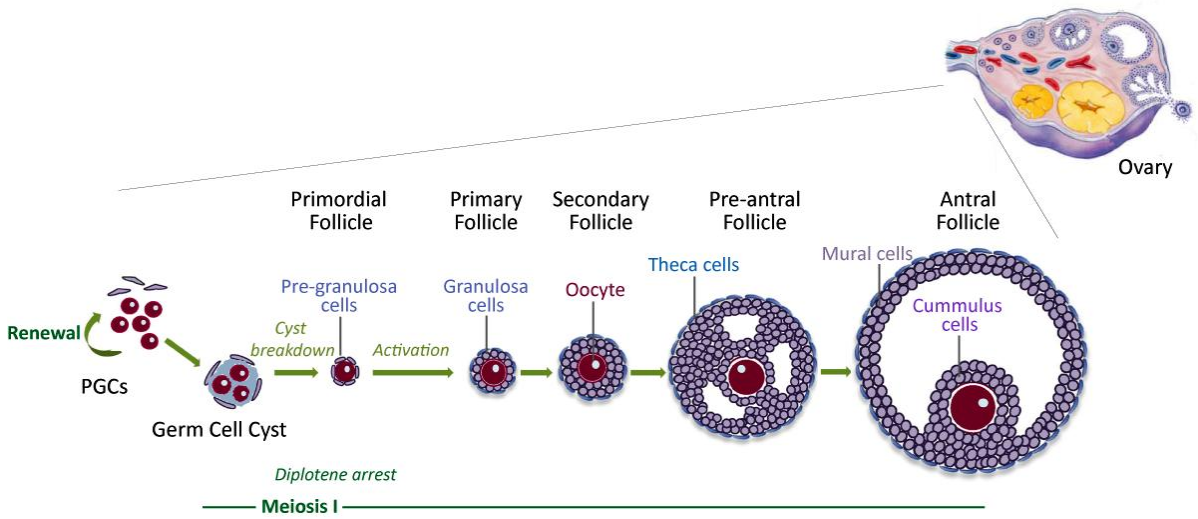

Figure 1.3. Mammalian folliculogenesis and oocyte growth. Schematic representation of oocyte development and follicle formation within the ovary. Following the arrival of PGCs at the fetal ovary germ cell cyst begin to form. Within the cyst, oocytes enter into meiosis and progress through prophase I, arresting at diplonema. Soon after birth, cysts breakdown and oocytes become enclosed individually by somatic pre-granulosa cells to form primordial follicles. Primordial follicles remain quiescent waiting to be activated and recruited into the growing follicle pool. As oocyte grow, and folliculogenesis progress, granulosa cells proliferate mitotically until a fluid-filled cavity, known as the antrum, appears at the latest stages of follicle development. Once the antrum is completely formed the pre-ovulatory oocyte remains surrounded by cumulus cells, which are essential for oocyte maturation, and mural cells rest surrounding the atrum. Once ovulation is accomplished mural cells differentiate to form the corpus luteum (yellow body in the ovary representation). Image modified from Sánchez & Smitz 2012.

It is widely accepted that primordial follicles constitute the total reservoir available during the entire period of female reproductive lifespan. Folliculogenesis initiates, once these dormant primordial follicles are activated and recruited into the growing follicle pool in a continuous manner. The total process of folliculogenesis involves a remarkable increase in the size of the oocyte, which in mice imply from 10-20 µm in the primordial follicles to greater than 70 µm in the antral follicle. Furthermore, oocyte growth is accompanied by a substantial proliferation of granulosa cells that surround the oocyte, increasing its total volume more than 100-fold (Picton et al. 1998; van den Hurk & Zhao 2005). Thus, folliculogenesis is a very dynamic and tightly controlled program that comprise multiple mechanisms of cell-cell

communication, in particular between oocytes and granulosa cells (Gilchrist et al. 2004; Sánchez & Smitz 2012; Li & Albertini 2013).

In the mouse, an initial wave of primordial follicle activation occurs within a few days after birth. At this point, primordial follicles become primary follicles, in which flattened granulosa cells, surrounding the diplotene arrested oocyte, develop into a single layer of cuboidal granulosa cells. This step involves many molecular mechanisms that are still not fully understood. Recent studies have revealed that control of initiation grow, proliferation of granulosa cells and oocyte activation requires synergistic actions of PI3K/PTEN pathway, involved in cell survival pathways, and TSC/mTOR pathway, a tumor suppressor complex, via interaction of KIT ligand and its receptor KIT expressed by somatic cells and oocytes, respectively (Liu et al. 2006; Zhang et al. 2014).

By 10-12 dpp, primary follicles progress to the secondary follicular stage, in which oocytes at midgrowth become surrounded by two or more layers of granulosa cells. This step is driven by intraovarian paracrine factors produced by oocytes and follicular cells (Pangas 2012). Next, secondary follicles continue to grow and progress through pre-antral stages. Granulosa cells at this stage proliferate at very high rate to generate a multilayer pre-antral follicle. The path to reach pre-antral stages and develop to more advanced follicular stages relies on intraovarian factors, as well as, to gonadotropins (Cortvrindt et al. 1997; Baker & Spears 1999). From pre-antral stage, follicles express functional FSH and LH and become gonadotropin-dependent for survival. During this period granulosa cells undergo profound changes progressively acquiring differentiated characteristics to support the growing oocytes (Li & Albertini 2013). One example of the importance of granulosa-oocyte communication during folliculogenesis is the expression of gap-junctions proteins (e.g., connexins 43 and 37) by the time follicles have developed to the secondary stage. In mice, ovaries lacking connexins 43 or 37 do not progress normally due to the impaired oocyte-granulosa communication. These mutant follicles are able to progress normally until pre-antral stage but mutant ovaries generate a limited number of antral follicles. These follicles do not reach full size and the oocyte is compromised (Simon et al. 1997; Carabatsos et al. 2000). Moreover, when follicle attains multilayer stage, more somatic cells, called theca cells, enclose the follicle, providing structural and vascular support for the growing follicles until ovulation (McGee & Hsueh 2000; Tajima et al. 2007).

Under the influences of gonadotropins, FSH and LH, follicles synthesize androgens and estrogens, which induce granulosa cells proliferation and differentiation (Drummond & Findlay 1999; Hu et al. 2004). Between 15-25 dpp the antrum formation starts when fluid-filled cavities appear between the layers of granulosa cells. The formation of the antrum divides granulosa cells into two different populations: mural granulosa cells, more proximal to the basal lamina, and cumulus granulosa cells, which remain closest to the oocyte (Sánchez & Smitz 2012; Li & Albertini 2013). Coinciding with the antrum formation, oocytes that have increased their size to around 80% of their final growth acquire the meiotic competence, which is the capacity to resume meiosis (Szybek 1972; Park et al. 2004). Meiotic competence is

associated with the accumulation of cell cycle regulatory factors and reorganization of chromatin and microtubule configuration (Wickramasinghe et al. 1991; Chesnel & Eppig 1995). Nuclear maturation is coordinated with cytoplasmic maturity of the oocyte, which defines the capacity of the oocyte to be fertilizable, to prevent polyspermy and to develop into an embryo. Cytoplasmatic maturation occurs right after acquisition of meiotic competence and involves synthesis and accumulation of transcripts, as well as, transcriptional silencing required to support early stages of embryo development (Eppig 2001; Gosden 2002).

Both critical events that lead to the completion of meiosis are, indeed, influenced by oocyte-granulosa cells communication. Once the antrum is formed and pre-antral granulosa cells become separated in mural and cumulus granulosa cells, the oocyte promotes the expression of cumulus cell-specific transcripts and regulates metabolic activity of cumulus cells. Thus, oocytes play a crucial role in driving cumulus cell differentiation (Diaz et al. 2007; Su et al. 2009). Furthermore, after LH induction to stimulate meiotic resumption, the oocyte also participates in the expansion of cumulus cells, which is a prerequisite for a successful ovulation (Chen et al. 1993; Dragovic et al. 2007).

Finally, antral follicles containing full grown oocytes are ready to ovulate, a process triggered by gonadotropins. At this time, ovulation occurs when a rupture is created in the apical follicle wall and the cumulus-oocyte complex is released. Then, the oocyte resumes meiosis and progresses to metaphase of the second meiotic division, where it awaits fertilization to complete meiosis (Russell & Robker 2007; Li & Albertini 2013). Once ovulation is accomplished, granulosa and theca cells differentiate to form the corpus luteum that supports gestation (Stocco et al. 2007).

Therefore, bidirectional communication between oocyte and its surrounding follicular cells, and intra- and extra-ovarian produced factors, are essential for both oocyte development and granulosa cells differentiation.

1.2 Meiosis

Meiosis is the specialized cell division that generates haploid gametes. This is a unique process in which the number of chromosomes per cell is reduced by half allowing a diploid number of chromosomes to be restored at fertilization. Genome reduction is achieved by a single round of DNA replication followed by two rounds of division and chromosome segregation (Kleckner 1996; Page & Hawley 2003).

Following a DNA replication during meiotic S-phase, germ cells initiate meiotic prophase I, which is divided into four substages –leptonema, zygonema, pachynema and diplonema- distinguishable based on the configuration and structure of chromosomes and the formation of a proteinaceous meiotic scaffold along them, the synaptonemal complex (SC). During prophase I chromosome morphology changes as a result of pairing, synapsis and desynapsis of

the homologous chromosomes. This chromosomal choreography is concomitant to meiotic recombination. At the onset of prophase multiple double strand breaks (DBSs) are introduced in the DNA. At this point, homologous recombination (HR) is initiated when DSBs are repaired using the homologous chromosome as a template and consequently, homologous chromosomes start to pair and synapse. Most DSBs are repaired by non-crossover (NCO) pathways, while some of them, ~10% in mice (Cole et al. 2012), are repaired forming crossovers (CO). CO events provide the physical connections required for proper homologous chromosome segregation during meiosis I, also known as chiasma. The first meiotic division is reductional and segregates homologous chromosomes to produce secondary meiocytes containing one set of chromosomes, each of them with two sister chromatids. The Second meiotic division is an equal segregation that separates sister chromatids to ultimately generate haploid gametes (**Fig. 1.4**).

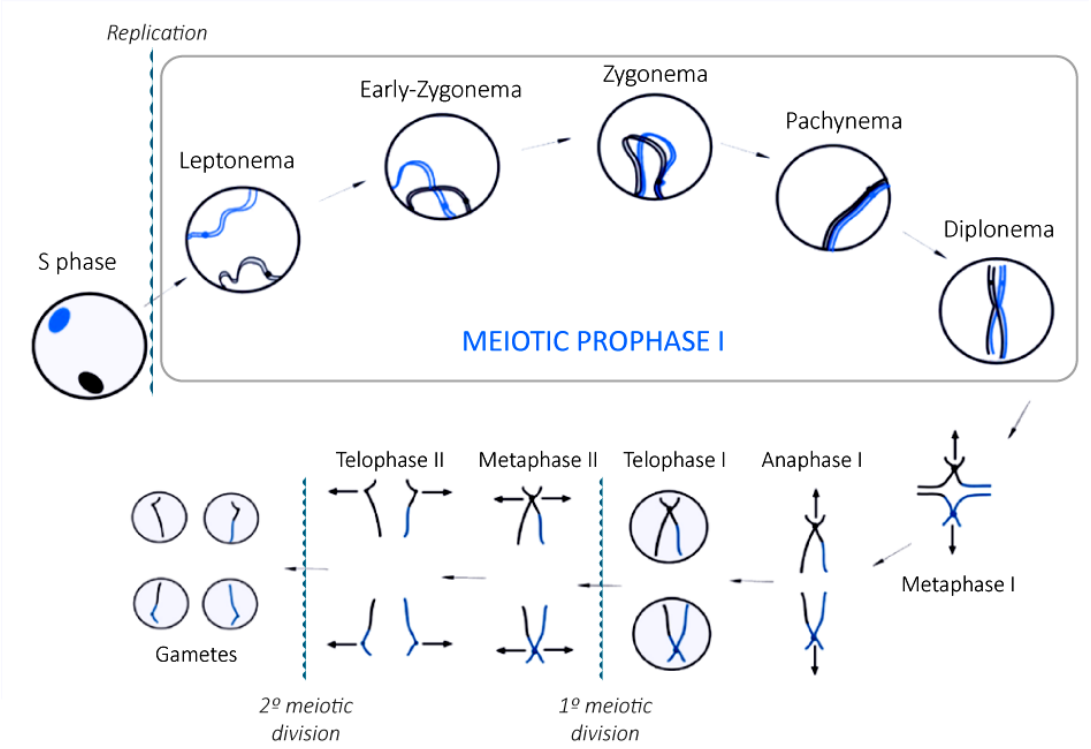

Figure 1.4. Mammalian meiotic progression. Meiosis is preceded by replication in pre-meiotic S-phase to produce cells with 4n DNA content. Following, 4n meiocytes undergo two consecutive rounds of division to eventually produce haploid gametes. Both meiotic divisions are divided in prophase, metaphase, anaphase and telophase stages, although prophase II is practically inexistent. During first meiotic division, specifically at prophase I (grey box) chromosomes pair, synapse and recombine to provide physical connections between them. Chromosome organization is depicted by two pair of homologous chromosomes formed by two sister chromatids. Meiotic recombination starts with the formation of DSBs at leptonema, when chromosomes ends become tethered to the nuclear envelope. By the time of zygonema homologous chromosomes initiate synapsis at the sites of homologous DSB repair. At pachynema synapsis is completed and DSBs are repaired originating CO and NCO events. Homologous chromosomes disassemble at diplonema and remain attached only at CO sites. Image modified from Roig 2005.

Thus, meiosis events are carefully monitored in order to promote homologous chromosomes find each other, synapse and create stable connections between them to avoid the formation of defective gametes (Handel & Schimenti 2010). Most of these intricate processes that take place during meiosis I, and particularly in the context of prophase I, are coordinated on a network of signaling mechanisms highlighted in the following sections.

1.2.1 The role of the synaptonemal complex

The synaptonemal complex is a zipper-like tripartite proteinaceous structure that holds together homologous chromosomes during prophase of the first meiotic division. The SC is formed by two lateral elements, one per each homologous chromosome, that are linked together by a central element (CE). This functional architecture is highly conserved among different organisms, although the proteins that constitute the SC are divergent (Bogdanov et al. 2007). The assembly of the SC mediates homologous chromosome synapsis. Furthermore, the SC, and thus, synapsis, are used to define the progression of meiotic prophase I (Page & Hawley 2004; Yang & Wang 2009).

SC assembly initiates after pre-meiotic replication and early at leptonema, when the proteins SYCP2 and SCYP3 are recruited to the chromosome axes in an inter-dependent manner, after of the assembly of a cohesion core (Pelttari et al. 2001; Yang et al. 2006; Llano et al. 2012; Syrjänen et al. 2014). These two proteins are the major components of the axial elements (AE), which maintain each pair of sister chromatids anchored at their bases into a series of loops (**Fig 1.5a**). At zygonema, following homologous recognition, alignment and pairing, the AE of homologous chromosomes are progressively connected by interdigitating SYCP1 transverse filaments, which are the principal constituents of the central elements (CE) of the SC, and lead to homologous synapsis (de Vries et al. 2005) (**Fig. 1.5b**). At pachynema, the SC is fully formed and consequently, autosomal homologous chromosomes are completely synapsed forming bivalents. In the case of males, X and Y chromosomes are synapsed only by a small homologous region they share, called the pseudoautosomal region (PAR). Finally, the SC dissembles at diplonema promoting desynapsis of the homologs. However, at this stage homologous chromosomes remain linked to each other by chiasma, which are the cytological manifestation of COs that facilitate the stable biorientation of the bivalents on the metaphase I spindle (Page & Hawley 2004; Yang & Wang 2009; Fraune et al. 2012).

Therefore, the formation of this dynamic protein complex provides chromosome compaction and juxtaposition of homologous chromosomes, to allow an efficient execution of meiotic recombination events. Thus, there is a clear evidence for a mutual dependency between meiotic homologous recombination and homologous synapsis mediated by SC assembly during prophase I. These processes show temporal correlation, so that failure in one process disturbs the correct execution of the other.

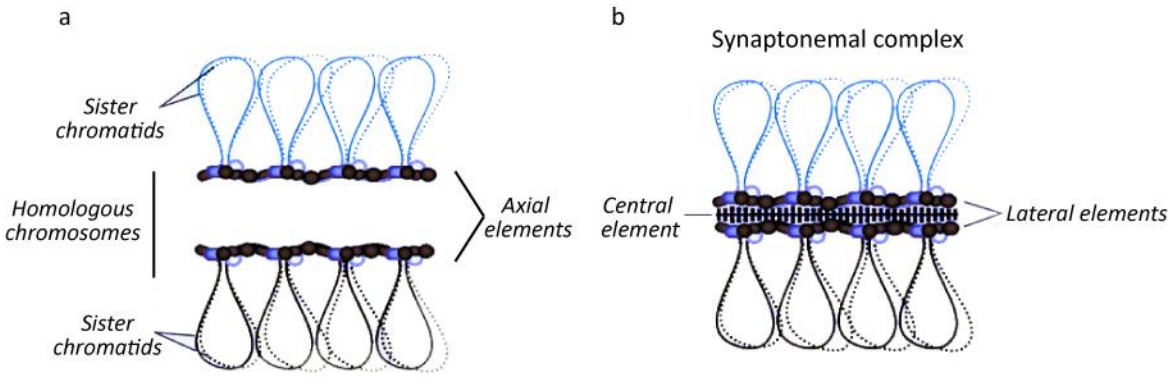

Figure 1.5. Synaptonemal complex structure and chromosome organization. a) At the onset of prophase SYCP2, SYCP3 proteins and cohesins (blue and black ovals) lodge along the chromosomal axes forming filaments denominated axial elements. This structure facilitates chromosome organization into chromatin loops anchored at their bases. **b)** At zygonema, homologous chromosomes initiate synapsis when a central element holds axial filaments together forming a tripartite structure composed of two lateral elements and a central element. Central element is constituted by SYCP1 and other proteins forming the transverse filaments. Image modified from Lam & Keeney 2014.

1.2.2 Meiotic recombination initiation

Meiotic recombination requires the induction of programmed DNA double strand breaks (DSBs) across the genome for initiation. DSBs are generated by the evolutionary conserved topoisomerase-like protein SPO11 (Keeney et al. 1997; Baudat et al. 2000; Romanienko & Camerini-Otero 2000). At the onset of prophase, SPO11 and several other DSB proteins assemble on chromosome axes and then capture DNA loops segments and inflict breaks in the DNA (Blat et al. 2002; Keeney et al. 2014) (**Fig. 1.6a**). SPO11 remains attached to the 5' end of each broken strand and is eventually released by endonucleolytic cleavage resulting in the formation of SPO11-oligonucleotide covalent complexes. DNA ends are then resected generating 3' single stranded tails in both sites of the DSB, which are detected by recombination intermediate proteins to signal the damage and initiate DSB repair originating recombinant products.

Although the risks that it imply to the meiocytes, the production of self-inflicted DNA damage is an inherent process of meiotic prophase I and is required for a successful meiosis. Thus, DSBs formation is a highly regulated process to avoid any possible deleterious effects of an overactivation. Recent findings have elucidated some information about the regulation of SPO11 activity. In the first place, a pathway involving ATM kinase as a negative regulator of DSBs formation has been demonstrated. DSBs levels increase in ATM-lacking testes suggesting that ATM controls a negative feedback loop that regulates the number of DSBs created (Lange et al. 2011). More recently, it has been demonstrated that the MRE11 complex –which activates ATM– is required to perform this negative feedback loop in mouse spermatocytes (Pacheco et al. 2015). Interestingly, different studies in S. cerevisiae also show the elevated DSB formation in yeasts lacking the ATM ortholog Tel1 (Zhang et al. 2011; Carballo et al. 2013) proposing the existence of an evolutionary conserved pathway to control DSB numbers. Additionally, further studies in S. cerevisiae indicate the existence of a more complex network

regulating DSB formation in which defects in the amount of DSBs formed or in their repair modulate the levels of DSBs by promoting or suppressing DSB formation (Carballo et al. 2013; Gray et al. 2013; Thacker et al. 2014). In this way, Gray and colleagues have revealed that when the catalytic activity of Spo11 is compromised the yeast ATR orthologue, Mec1, is activated to promote DSB formation to obtain optimal levels of recombination. Additionally, studies in yeast and mice, suggest the existence of a feedback between DSB formation and the completion of homologous interactions in which unsynapsed axes continue to accumulate DSBs until synapsis is completed (Kauppi et al. 2013; Thacker et al. 2014).

1.2.3 DSB repair by homologous recombination

Spo11-generated DSBs originate an extensive activation of DNA damage repair machinery, which involves the detection of breaks and the recruitment of several recombination intermediate proteins to catalyze homology search, DNA strand exchange and finally, resolution of the interhomolog joint molecules. Following breakage, DNA ends are rapidly processed to promote homologous recombination. One of the first signals that appear in response to DSB formation at leptonema is the phosphorylated form of the histone variant H2AX, which is phosphorylated by ATM kinase to trigger a network of DSB repair responses (Fernandez-Capetillo et al. 2003; Barchi et al. 2005; Bellani et al. 2005). Nucleolitically DSB resection generates 3' single stranded tails in both sides of the DSB, which attract replication protein A (RPA) (**Fig. 1.6b**), a single-stranded DNA (ssDNA) binding protein. RPA acts like a primary effector of the homology search, promoting the load of two RecA homologs, RAD51 and DMC1, into DSB sites forming the early recombination nodules (Bannister & Schimenti 2004a; Moens et al. 2007). RAD51 and the meiosis specific recombinase DMC1 are strand exchange proteins which form nucleoprotein filaments with the ssDNA that unwounds the homologous DNA to promote homology search and catalyze strand invasion (Brown & Bishop 2014) (**Fig. 1.6c**). These recombination intermediates are cytologically detected early at leptonema by formation of approximately 200-300 discrete foci marking sites of DSBs and ongoing recombination (Moens et al. 2007; Baudat et al. 2013).

Strand invasion occurs by insertion of the resected end into the template duplex leading to the formation of a displacement loop (D-loop) and the synthesis-dependent extension of the invading end. At this point, the D-loop can be stabilized forming an intermediate called single-end invasion (SEI), in which the other resected end is incorporated or "captured" forming a stable double Hollliday junction (dHJ). Most dHJ are resolved to generate crossovers (CO), reciprocal exchanges of DNA sequences, leading to the formation of chiasma. When the D-loop is not stabilized, the invading strand is displaced and the DSB is repaired by a synthesis-dependent strand annealing (SDSA) mechanism **(Fig. 1.6d**). In this case, there is not reciprocal exchange of DNA and the extension and ligation with his opposite end produces a non-

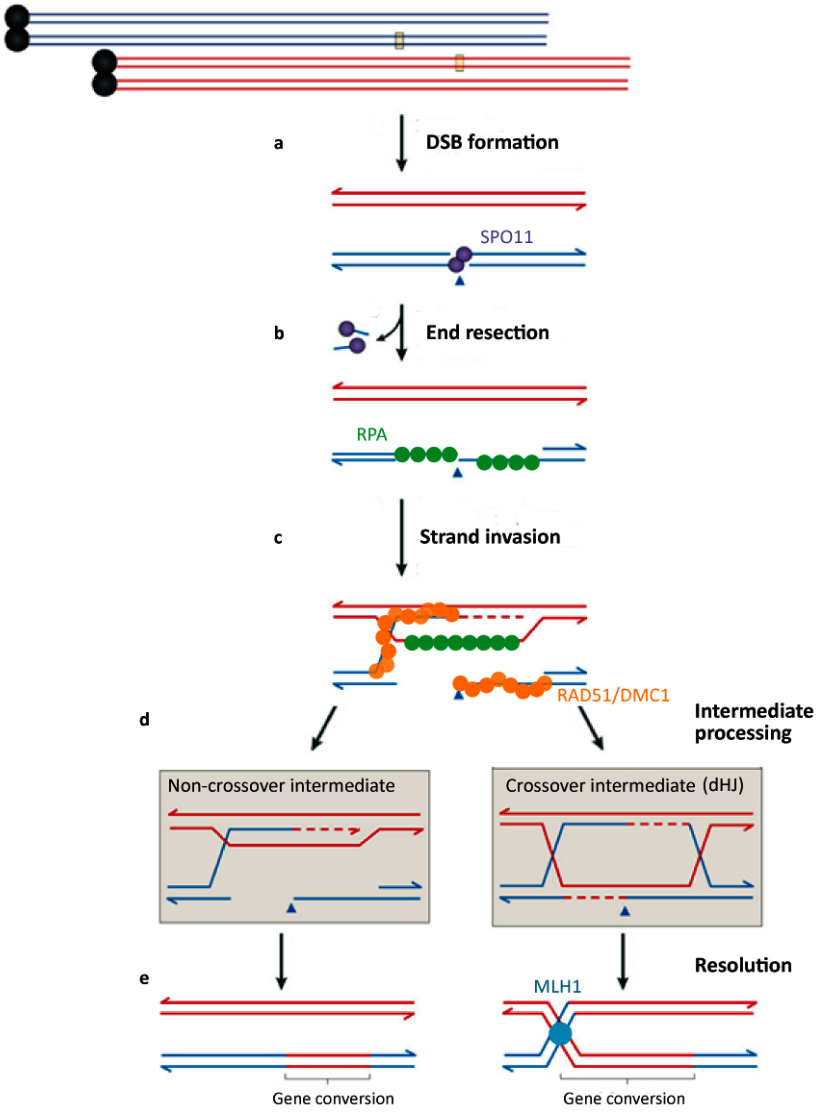

Figure 1.6. Model of major meiotic recombination pathways. Schematic representation of different recombination pathways of meiotic DSB repair and the proteins involved in each step. At the top, two acrocentric homologous chromosomes formed by four sister chromatids are represented. DNA strands are depicted with blue and red lines. Homologous recombination of two homologous chromosomes (yellow boxes) is represented. **a)** Recombination initiates by the programmed induction of DSBs in the genome by SPO11 protein (purple circle) and associated proteins. **b)** Endonucleolytic cleavage on either side of the DSB, evolving MRN (MRE11-RAD50-NBS1) complex, releases SPO11 covalently attached to a short oligonuceotide. DNA ends undergo 5' to 3' resection generating 3'ssDNA tails. RPA protein (green circle) recognizes and coat ssDNA tails. **c)** Displacement of RPA by RAD51/DMC1 proteins (orange circle) occurs on recombination sites. These proteins catalyze strand invasion generating a D-loop intermediate. **d)** Recombination intermediates can be processed by non-crossover pathways when the invading strand associates with the opposite end of the original DSB by a synthesis-dependent strand-annealing (SDSA). Contrarily, when the second end of the original DSB also engages with the homologous chromosome, double Holliday junctions (dHJ) are created and recombination intermediates are processed by CO pathways. **e)** Whereas, SDSA resolution results in no reciprocal exchange in the recombination product, dHJ resolution involve MLH1 protein (blue circle) and generates a CO in which the flanking DNA sequences are reciprocally exchanged. Image adapted from Baudat et al. 2013**.**

crossover (NCO) event resulting in gene conversion (Baudat & de Massy 2007; Youds & Boulton 2011). Resolution of most dHJ into CO events require MutL protein homolog 1 (MLH1) (**Fig. 1.6e**), as MLH1-deficient spermatocytes do not achieve sufficient number of chiasma and do not progress beyond pachynema (Edelmann et al. 1996; Guillon et al. 2005). Although in mammals the vast majority of COs originate from the MLH1-mediated resolution of dHJs, there are alternative pathways that result in the formation of COs (Edelmann et al. 1996; Holloway et al. 2008). The final product of meiotic recombination, CO and NCO, are generated at mid-pachynema (Anderson et al. 1999; Guillon & de Massy 2002).

Although DSB repair by homologous recombination could be mediated by the invasion of a homolog chromatid or a sister chromatid, consistent with the importance of recombination to promote homologous chromosome pairing, SPO11-generated DSBs are preferentially repaired by interhomologous (IH) recombination. To achieve this goal, several studies suggest the presence of a mechanism that prevents DSB repair using the nearby sister chromatid as a template and that promotes HR between non-sisters (Carballo et al. 2008; Callender & Hollingsworth 2010; Wu et al. 2010). As mentioned before, DSB repair takes place in the context of the chromosome axes, which organize chromatids forming DNA loops. This architecture is also involved in the establishment of IH recombination (Humphryes & Hochwagen 2014). Studies in S. cerevisiae suggest that regulation of the repair partner choice involves phosphorylation of the chromosomal axis protein Hop1 in response to DSB formation via the ATM and ATR orthologues, Tel1 and Mec1 respectively. Activation of Tel1 and Mec1 in meiotic prophase leads to the activation of Mek1 kinase that promotes IH recombination by phosphorylating several proteins, like the abovementioned Hop1 or the Rad51 partner Rad54 required to perform intersister repair (Carballo et al. 2008; Callender & Hollingsworth 2010; Wu et al. 2010).

The crucial role of COs in maintaining homologous chromosomes together until the anaphase I stage of meiosis supports the fact that CO formation is subject to an strict regulation to ensure that each bivalent receive at least one CO. The mechanisms that regulate CO formation are generally grouped under the CO control term. Furthermore, CO control also sets CO homeostasis, allowing the maintenance of the adequate number of CO events when DSBs levels are disrupted at the expense of NCO (Martini et al. 2006; Cole et al. 2012). This mechanism warranties that when low DSBs are created CO formation will be favored to ensure that every bivalent has at least one CO event. Finally, CO control also regulates CO distribution. It is widely accepted that CO are not-randomly distributed along chromosomes, and that the position of each CO event is influenced by a positive interference (Jones & Franklin 2006). Adjacent COs in the same bivalent tend to occur more separated than expected if they were randomly positioned (Berchowitz & Copenhaver 2010).

Nonetheless, the control mechanisms that regulate meiotic recombination are not yet fully understood. Whether crossovers and non-crossovers originate from the same pathway (Guillon et al. 2005; Cole et al. 2014), whether certain DNA sequences act like a target of

chromatin epigenetic modifications directing SPO11 to particular sites on the genome (Baudat et al. 2010; Wu et al. 2013), or whether the recruitment of the DSBs machinery into the different sites of the genome are influencing recombination patterns (Borde et al. 2009; Brick et al. 2012), are unanswered questions that still required further investigation.

1.2.4 Special features of X and Y chromosomes

The heterologous X and Y chromosomes entail an additional challenge for male meiotic recombination machinery. The X and Y chromosomes share a short homology region called the Pseudoautosomal region (PAR) and despite the differences in their size, they may act as homologous chromosomes ensuring pairing and CO formation to achieve a correct segregation (Rouyer et al. 1986). However, compared to autosomes that are homologous in their entire length, the size of the homologous region available in the sex chromosomes to achieve these processes is minute (Raudsepp et al. 2012). Consequently, PAR in mouse exhibit a crossover density higher than is required in autosomal chromosomes (Soriano et al. 1987).

Thus, to ensure a correct meiotic recombination of X and Y chromosomes the PAR presents a distinct chromosome organization in which the chromatin is packed in longer axes than the autosomes thus making the chromatin organize in smaller loops. Since SPO11 generates DSBs at the loops (see above), this configuration creates more potential sites for break formation (**Fig. 1.7a**)(Kauppi et al. 2011). Furthermore, DSB formation on the PAR is boosted by the existence of positive feedback mechanism that promotes break formation on unsynapsed regions of the genome as meiotic prophase progresses (Kauppi et al 2013). Interestingly, similar mechanisms have been identified in yeast. At present, we know two mechanisms that promote DSB formation during meiotic prophase, one dependent on Mec1 and another one dependent on the absence of interaction between homologous chromosomes (Gray et al 2013 and Thacker et al 2014). Thus, the continuous production of DSBs on unsynapsed chromosomes and the particular compaction of the chromatin on the sex chromosomes ensure that DSBs are formed on the small PAR. The higher frequency of DSBs generated in sex chromosomes facilitate homology search and stable interaction originated by homologous recombination. Consistent with this idea, PAR pairing is temporally different from that of autosomal chromosomes. The X and Y chromosomes pair late at zygonema coinciding with sex body formation (see below), which maintains the XY chromosomes in proximity and may also facilitate pairing.

At pachynema, when autosomal chromosomes are completely synapsed, the heterologous regions of the X and Y chromosomes remain unsynapsed and undergo a programmed transcriptional silencing called meiotic sex chromosome inactivation (MSCI) resulting in the formation of the sex body (McKee & Handel 1993; Turner 2007). MSCI have been thoroughly studied and is considered a specific form of a more general mechanism responsible for transcriptional silence of unsynapsed chromosome regions during meiotic prophase, also known as Meiotic Silencing of Unsynapsed Chromosomes (MSUC) (Turner et al.

2005; Baarends et al. 2005). Recent studies propose a model that integrates the stage-specific proteins required to achieve meiotic silencing based on evidences from MSCI (Royo et al. 2013) (**Fig. 1.7b**). During zygonema the unsynapsed axes accumulate HORMAD1 and HORMAD2 (Wojtasz et al. 2009) which attracts BRAC1 protein (Turner et al. 2004; Daniel et al. 2011; Wojtasz et al. 2012). BRCA1 acts as a sensor to recruit ATR and their cofactors, ATRIP and TOPBP1, at these sites. ATR then maintains asynapsis signaling at AE during late-zygonema by continuing recruiting BRCA1. At pachynema, ATR translocates into chromatin loops of the unsynapsed chromosomes in an MDC1-dependent manner (Ichijima et al. 2011) and catalyzes the phosphorylation of H2AX histone (γH2AX)(Fernandez-Capetillo et al. 2003) in a positive feedback loop with MDC1. Thence, MDC1 acts as a mediator to spread ATR and γH2AX signal into X and Y chromatin, along with other epigenetic modifications as SUMO-1 or uH2A (Baarends et al. 1999; Vigodner 2009), that induce post-translacional modifications and gene silencing.

Therefore, MSCI is an essential process in which the persistence of unsynapsed chromosomes triggers a global epigenetic modification of the sex chromatin that leads to the repression of gene transcription.

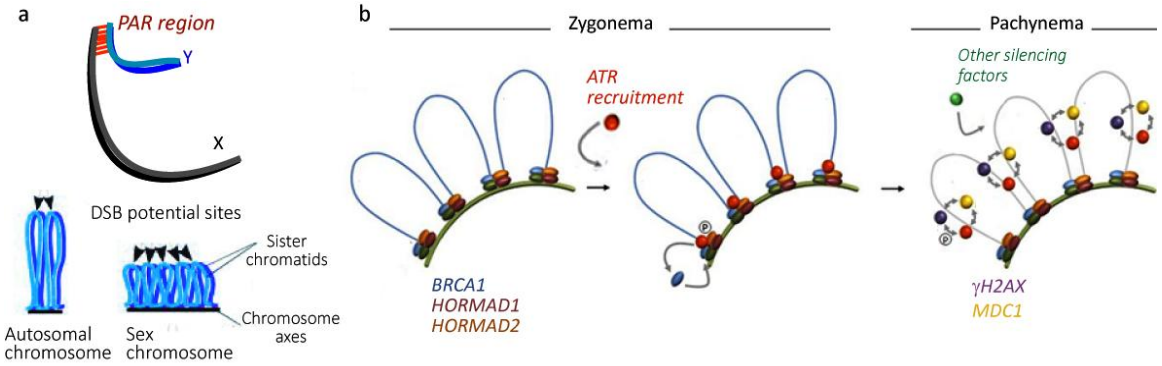

Figure 1.7. Specific sex chromosome features during meiotic prophase. **a)** Schematic representation of X and Y chromosomes (grey and blue lines, respectively, top figure) sharing only a small region of homology, the pseudo-autosomal region (PAR). Axis-loop chromatin organization on sex chromosomes differs from autosomal organization (only one homolog consisting in two sister chromatids is represented as blue lines, bottom figure). DNA on sex chromosomes is organized in longer axis and smaller loops, providing more potential DBS sites (black arrowheads) than in autosomal chromosomes, which present DNA organized in less and longer loops. **b)** Because of the heterologous nature of sex chromosomes, they become transcriptionaly silenced. During zygotene, BRCA1 protein (blue ovals) and HORMAD1/2 proteins recognize and associate with unsynapsed axes and mediate ATR kinase (red circle) recruitment at these sites. ATR maintains asynapsis signaling by promoting continuous BRCA1 loading on AEs. At pachynema ATR translocates into the chromatin loops and catalyze H2AX phosphorilation (purple circle) in a MDC1-dependent manner (yellow circle). Epigenetic modifications lead to sex chromosome silencing. Images adapted from Kauppi et al. 2012 and Royo et al. 2013.

1.2.5 Checkpoint mechanisms regulate meiotic progression

Meiotic prophase comprises many crucial processes in order to provide gametes with the correct chromosome number. Germ cells undergoing meiosis have to coordinate the progression of different events, such as DSB repair, chromosome dynamics and homologous synapsis, and respond to errors occurring in any of these processes. Thus, defects in the correct execution of these processes can activate different responses that lead to arrest, or delay, cell cycle progression to allow more time to correct them or, in some cases, activate apoptosis to remove cells that are unable to repair these errors. In mammals, there are two major stages in which spermatocytes arrest and ultimately apoptose, pachytene stage and metaphase I.

The pachytene checkpoint prevents that meiocytes progress beyond pachynema before recombination and synapsis are completed. The responses that trigger the checkpoint arrest can be separated depending on the inability to complete recombination once it has begun, as seen in Dmc1 or Trip13 mutant spermatocytes (Pittman et al. 1998; Li et al. 2007; Roig et al. 2010) or, opposite, the absence of DSBs, as seen in Spo11 mutants (Baudat et al. 2000; Romanienko & Camerini-Otero 2000). In males, recombination-dependent and DSB-independent responses lead spermatocytes to arrest at early and late-pachynema respectively (Barchi et al. 2005). However, in females, although both checkpoint responses has been proposed to be less stringent (Hunt & Hassold 2002), recombination-dependent response occurs around the time oocytes undergo meiotic arrest at diplonema and ovaries become depleted of oocytes within a few days after birth. In contrast, synaptic defective oocytes, which trigger DSB-independent response, are eliminated later, around two weeks after birth (Di Giacomo et al. 2005).

The checkpoint signaling machinery also responds to defects during metaphase to anaphase I transition. During both mitosis and meiosis, the spindle assembly checkpoint (SAC) arrests the progression of the cell cycle in response to disrupted spindle microtubules or defective connections to chromosomes (Gorbsky 2014). During meiotic metaphase I, the presence of misaligned homologous chromosomes on the spindle apparatus due to crossover defects could predispose meiocytes to aneuploidy (Morelli & Cohen 2005; Hall et al. 2006). For this reason, SAC comprises a complex set of signaling pathways that involve microtubule dynamics, biomechanical kinetochores forces, and highly regulation of protein interactions and post-translational modifications to prevent the generation of unbalanced gametes (Sun & Kim 2012). Nevertheless, several studies suggest that meiotic SAC executes different responses in spermatocytes and oocytes. One example can be found in Mlh1-deficient spermatocytes and oocytes in which homologous chromosomes fail to remain attached once the SC is dissembled at diplonema (Edelmann et al. 1996; Baker et al. 1996). Thus, homologous chromosomes appear separated at MI, as univalents and consequently, chromosome alignment and spindle formation are defective in these meiocytes. However, whereas all Mlh1-/- spermatocytes arrest at MI and undergo apoptosis, some Mlh1-/- oocytes are able to progress through

anaphase I and extrude the first polar body (Woods et al. 1999; Eaker et al. 2002). Therefore, even though SAC regulates the correct segregation of chromosomes during first meiotic division to ensure success of meiosis, SAC in females displays lower stringency than in males.

1.3 ATR: a master regulator of the DNA damage response

The DNA damage response (DDR) is a highly organized network of cellular pathways that sense, signal and repair DNA lesions. In response to DNA damage, surveillance proteins that monitor DNA integrity can activate repair pathways, arrest cell-cycle progression or induce apoptosis. The major regulators of the DDR are the phosphoinositide 3-kinase related proteins (PIKKs), including ataxia telangiectasia mutated (ATM) and ataxia telangiectasia mutated and Rad-3 related protein (ATR), which share similar domain and several modes of regulation (Harper & Elledge 2007; Maréchal & Zou 2013).

1.3.1 ATR function in the DNA damage response in somatic cells

ATR maintains genome integrity by playing different roles in response to DNA damage and replication stress. ATR is a key sensor of ssDNA that is activated every mitotic S phase to regulate firing of replication origin, to stabilize stalled replication forks and to prevent the premature mitotic entry (Cimprich & Cortez 2008; Nam & Cortez 2011)(**Fig. 1.8**).

The processing of many types of DNA damage leads to the presence of ssDNA, which activates ATR, as base adducts, crosslinks, DSBs and replication stress. Single stranded DNA structures are bound by RPA, which stimulates the binding of the ATR-interacting protein (ATRIP) to the ssDNA, and consequently, ATR is recruited to the sites of damage (Cortez et al. 2001). Nevertheless, activation of ATR requires the independent recruitment of the RAD9-RAD1-HUS1 complex (9-1-1) to the DNA end adjacent to a stretch of RPA-ssDNA, which is accompanied by another crucial activator of ATR, topoisomerase-binding protein-1 (TOPBP1) (Yan & Michael 2009). TOPBP1 contains an activation domain that interacts with ATR-ATRIP complex and allows ATR kinase to be activated. Once an activated ATR complex is assembled to the DNA damage site, it mediates phosphorylation of several substrates to coordinate the DDR pathway. One of the most understood pathways is the one dependent on CHK1 activation. ATR phosphorylates CHK1, in the presence of additional factors, on at least 2 residues, S317 and S345 (Cimprich & Cortez 2008; Stracker et al. 2009). Claspin protein accompanied by RAD17, interacts with CHK1 in a DNA damage-dependent manner and it is necessary to mediate the activation of CHK1 by ATR (Wang et al. 2006). Activated CHK1 functions to spread the DNA damage signal to the rest of the nucleus and controls principally the intra-S and G_2/M phase transitions. During replication, obstacles in the DNA template, as DNA damage, can lead to the stall or collapse of the replication machinery at the fork. Under these conditions efficient CHK1 activation mediates the phosphorylation of one of its central targets CDC25 family of phosphatases, which act removing inhibitory phosphorylations from

cyclin-dependent kinases (CDKs). CHK1 negatively regulates CDC25s by phosphorylation and prevents CDKs activation. This mechanism leads to the activation of the intra-S checkpoint that slows DNA replication under DNA-damaging conditions and prevents meiotic entry (Feijoo et al. 2001; Chen & Poon 2008; Cimprich & Cortez 2008).

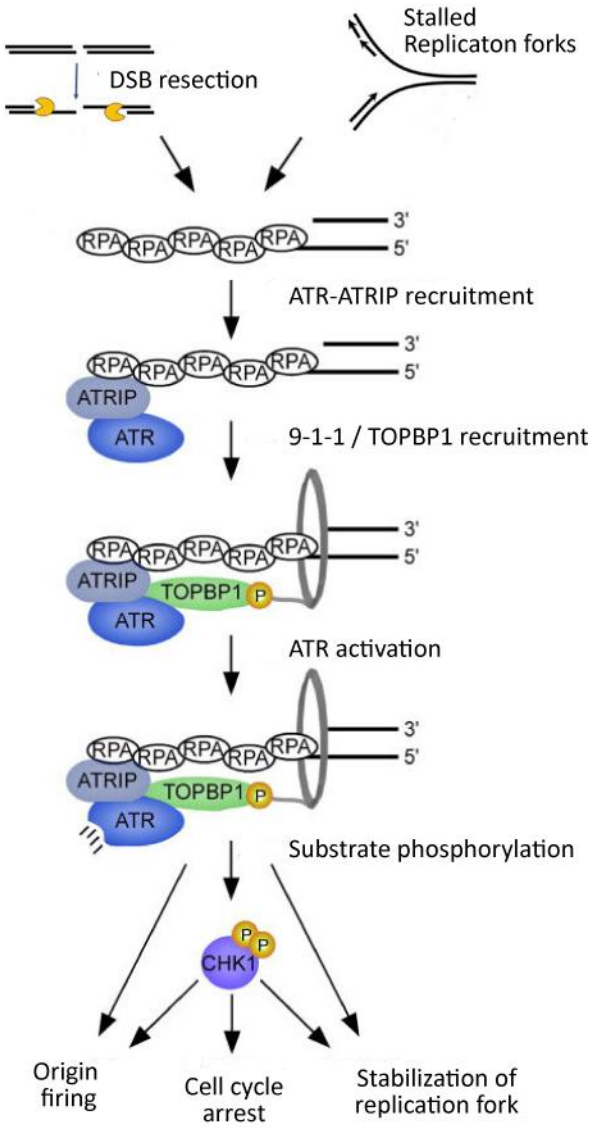

Figure 1.8. ATR activity in DNA damage response. ssDNA generated during replication or at resected DSBs, among others, activate ATR signaling response. RPA-ssDNA structures mediate ATR-ATRIP complex recruitment to the sites of the lesion. Next, loading of 9-1-1 complex to DNA brings the ATR activator TOPBP1 close to ATR kinase, facilitating TOPBP1-ATR binding. ATR becomes activated in an ATRIP dependent manner. ATR activation leads to phosphorylation of several substrates, including CHK1, to regulate DNA damage and replication stress. ATR signaling pathway, ultimately, slows origin firing and induces cell cycle arrest, as well as, mediates stabilization and restart of stalled replication forks. Image modified from Nam & Cortez 2011.

Moreover, ATR signaling via CHK1 phosphorylation also regulates replication origin activity. Replication-associated DNA damage not only can produce the collapse of replication forks, but can also promote firing of new replication origins to ensure completion of replication independently of the damaged fork. ATR-dependent phosphorylation of MCM2, the minichromosome maintenance subunit 2, promotes the recruitment of Polo-like kinase 1 (PLK1) to chromatin, which promotes neighboring origins to fire (Ge & Blow 2010; Nam & Cortez 2011). Consequently, PLK1 overlooks the ATR-CHK1 dependent inhibition of origin firing to complete replication. Thus, these apparently contradictory functions of ATR, reducing

replication rates by inhibiting global origin firing and, opposite, promoting new origins firing near a particular stalled fork may reflect a way to ensure completing genome replication once DNA damage is repaired (Thomson et al. 2010; Alver et al. 2014).

In addition, ATR is also directly involved in the regulation of the DNA repair. Whereas ATM is activated only in response to DSBs, ATR is activated by a large spectrum of DNA lesions, including DSBs. Thence, DSBs generated during S and G_2 phases activate both ATM and ATR kinases, and they are majorly processed for HR (Jazayeri et al. 2006; Heyer et al. 2010). Although, the activation of ATM in response to DSBs occurs immediately after the lesion is sensed, ATR responds more slowly as a consequence of DSB-end resection that expose an ssDNA region. Thus, ATR and ATM act like partners in DSB response. In addition, different studies in budding yeast also suggest that in the presence of DSBs, the ATR-CHK1 pathway promotes HR repair by phosphorylating RAD51, and that the inhibition of RAD51 phosphorylation confers hypersensitivity to DNA damage and defective HR repair (Sørensen et al. 2005; Flott et al. 2011).

Accordingly with the role of ATR kinase in DSB repair and replication stress-response, ATR is essential for cell survival. Consequently, in mammals, the loss of ATR causes lethality at embryonic stages (Brown & Baltimore 2000; de Klein et al. 2000). It has been postulated that defects in ATR might be critical for viability due to the formation of ssDNA structures under normal cell cycle conditions provoking endogenous DNA damage and creating structures that make replication complicated. Combination of ssDNA structures at stalled forks with defects in ATR activity might be the major cause of genome instability. In the absence of ATR a stalled fork will collapse and DNA damage will accumulate in these areas, causing high levels of fragile-sites breakage and, eventually, cell death (Durkin & Glover 2007; Cimprich & Cortez 2008).

1.3.2 The poorly understood role of ATR during mammalian meiosis

Since ATR is a central player in mediating DNA damage responses during mitosis in somatic cells, it is coherent to reason that ATR is also playing central roles in the extensive network of signaling mechanisms taking place during meiosis. Whereas most information regarding the implication of a particular protein in meiotic molecular pathways has been obtained studying mutant models lacking that protein, until few years ago, there were not available models to study the implications of ATR deficiency in germ line because loss of ATR is critical for embryo development (O'Driscoll 2009). Consequently, little is known about ATR function during mammalian meiosis.

The ATR signaling pathway during meiosis has been proposed to monitor both recombination events and chromosomal synapsis in order to coordinate the proper meiotic progression. Accordingly, it has been demonstrated that Atr transcripts and ATR protein are expressed in high levels in testes, and specifically, are expressed most highly in the cells

undergoing meiotic prophase I, suggesting an essential role for ATR in this organ and during meiotic prophase (Keegan et al. 1996). Nevertheless, in mammals most evidences of ATR function in meiosis have been inferred by cytological studies. Several immunofluorescence studies have revealed that ATR associates with meiotic chromosome axes. ATR is present at recombination nodules during early meiotic prophase forming foci that colocalize in part with RAD51 foci (Keegan et al. 1996; Plug et al. 1998; Moens et al. 1999). In addition, ATR is present on unsynapsed chromosome axes. It is now clear that ATR plays a role in the initiation of meiotic sex chromosomes inactivation (MSCI) (Royo et al. 2013), being the major kinase that phosphorylates H2AX to promote sex body formation (see section 1.2.4). In the same way, according to the fact that MSCI is a particular form of MSUC, it has been demonstrated the presence of ATR in autosomal axes that still remain unsynapsed during late meiotic prophase participating in the transcriptional silence of this regions (Turner et al. 2004; Burgoyne et al. 2009). These evidences suggest that ATR might be involved in meiotic recombination, as well as, mediating checkpoint responses.

However, because ATR is a highly evolutionary conserved kinase, the current understanding of the possible roles for ATR during meiosis encompasses a more extensive network of signaling mechanisms. Evidences from different organism have elucidated a new perception of ATR implications during meiotic prophase. In budding yeast, the ATR ortholog Mec1 is implicated in S-phase progression, in meiotic recombination and promotion of IH recombination pathways, in the completion of homologous synapsis by regulation of Spo11-generated breaks, as well as, in CO distribution (Carballo & Cha 2007; MacQueen & Hochwagen 2011; Subramanian & Hochwagen 2014). Additionally, studies carried out in Drosophila melanogaster have revealed that the ATR ortholog Mei-41 is directly involved in CO distribution and mutation of this protein leads to defects in CO regulation (Carpenter 1979). Furthermore, Mei-41 participates in the activation of the recombination dependent checkpoint occurring in Drosophila (Ghabrial & Schüpbach 1999).

1.4 The ATR Seckel mouse model

In light of the essential nature of ATR kinase, mutations that imply complete ATR loss of function are not compatible with mammalian embryo development (Brown & Baltimore 2000; de Klein et al. 2000). Nevertheless, an hypomorphic mutation in Atr gene that originates a significant reduction of ATR expression was found in some patients presenting a rare disease known as Seckel syndrome (OMIM210600) (O'Driscoll et al. 2003). Seckel syndrome is an autosomal recessive disorder characterized by intrauterine growth retardation resulting in low weight at birth, post-natal growth delay resulting in dwarfism, microcephaly associated to mental retardation, and characteristic facial features known as "bird-headed" (Shanske et al. 1997).

Using this mutation, Fernandez-Capetillo and colleagues created an humanized mouse model of ATR Seckel syndrome that has provided interesting insights on ATR functions (Murga et al. 2009). This mutation is a synonymous A > G transition in the exon 9 of *Atr* gene that promotes an impaired splicing of exons 8-10, resulting in the skipping of exon 9, to produce a message with premature stop codon, which originates a severe ATR hypomorphism (**Fig 1.9a**). Thus, in order to recapitulate this mutation that affects splicing, Murga et al. developed and strategy to generate an humanized allele by transferring into the ATR loci from mouse, the human genomic region containing the exons 8, 9 and 10, and their respective introns. Then, the Seckel A2101G ATR mutation (O'Driscoll et al. 2003) was introduced into exon 9 creating the Seckel allele (Atr^S). The presence of this allele in homozygosis reduces the expression of ATR to almost undetectable levels in most tissues.

ATR-Seckel mouse model ($Atr^{S/S}$) reproduces the clinical features of the human disease (**Fig 1.9b**). Seckel mouse exhibits severe dwarfism presumably associated to reduced ATR function during embryonic development. In addition, mutant mice present microcephaly accompanied by ocular dysmorphism, dental malocclusion and micrognatia characteristic of Seckel syndrome. Related to the decrease in the dimensions of their heads, Seckel mice show severe loss of astrocytes of the corpus callosum associated with reduced brain size.

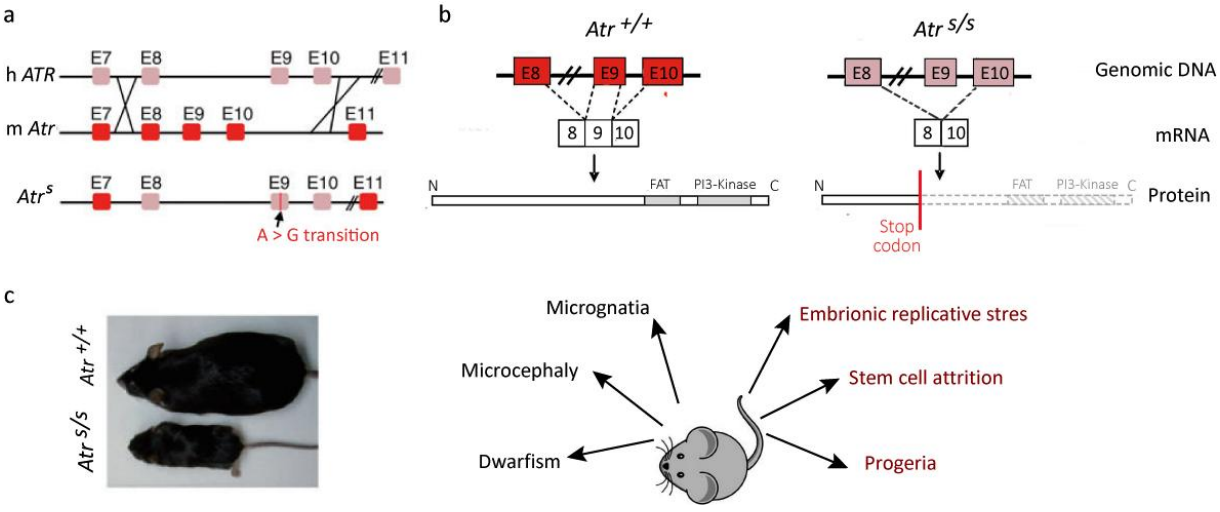

Figure 1.9. Model of the generation of a humanized allele associated with Seckel syndrome and the related mice phenotype. **a)** Schematic representation of the approach used to generate the humanized ATR-Seckel syndrome mouse model. ATR genomic region from mouse (red squares) incorporating the exons 8-10 and their associated introns from human sequence (pink squares). The Seckel mutation is introduced in exon 9 in the rearranged Atr^S allele. **b)** Atr^S allele affects the normal splicing of the exons 8-10. The mRNA lacking exon 9 introduces a stop codon in the transcript that results in a truncated dysfunctional protein. **c)** Seckel mouse model recapitulates the human Seckel syndrome. Because of the increased embryonic replicative stress, Seckel mice suffer an intrauterine programming of ageing resulting in post-natal reduced body size, stem cell attrition and progeria among others. Image modified from Murga et al. 2009 and O'Driscoll 2009.

Besides to this phenotype, Seckel mouse also displays very elevated levels of replication stress during embryo development. Replication stress responses are activated in order to preserve genome integrity when aberrant replication forks containing ssDNA structures are generated during DNA replication. Then, replication stress responses are primarily mediated by activation of ATR signaling pathways (Zeman & Cimprich 2014). Since, during embryogenesis cells replicate and proliferate faster than in any other stage, ATR function is particularly critical at this period. Sectioned Seckel mutant embryos exhibited increased levels of γH2AX positive cells, indicating high levels of DNA damage, which were also positive for apoptotic markers, suggesting a high loss of cells during embryogenesis due to accumulation of replication-induced DNA damage. On the basis of this observation the authors proposed a model defined as "intrauterine programming of ageing" in which the high replication stress in the embryo affects the future lifespan of the mice (Murga et al. 2009; Fernandez-Capetillo 2010). They suggest that the massive apoptotic rate found in the Seckel mouse embryo might compromise future stem cell functioning, not only by the reduction of stem cells pools, but also by alteration of stem cells niches, thence, initiating a premature program of progeria that leads young animals to early senescence.

Altogether, Seckel mouse model is the first designed viable mammalian model that introduces ATR mutation into the germ line, providing a great advantage for genetic studies of ATR functions in mammals (O'Driscoll 2009).

OBJECTIVES

Chapter 2

During meiosis hundreds of programmed DSBs are introduced in the genome. The repair of these breaks by homologous recombination promotes pairing, synapsis and CO formation among homologous chromosomes. These processes are critical to ensure an accurate segregation during the first meiotic division. Inaccurate recombination or synapsis may generate genomic instability or create unbalanced gametes. Therefore, the mechanisms that control these processes are robustly regulated by different pathways involving a large number of proteins.

The Ataxia Telangiectasia and Rad-3 related (ATR) protein is a component of the DDR network that is activated in response to ssDNA to prevent genomic instability. Since, ATR has been previously localized accumulating on unsynapsed chromosomes, where silencing of these regions occurs, and on meiotic chromosome cores co-localizing with other recombination proteins, the main aim of the present study is to characterize the functions of ATR during meiosis and consequently in gametogenesis using genetic and pharmacologic strategies.

For this purpose we established the following specific objectives:

2.1.1 *To characterize the function of ATR during male meiosis*

To achieve this objective the effects of Seckel mutation in male meiosis and the effect of ATR inhibition during in vitro meiotic prophase will be analyzed in order to characterize the functions of ATR during spermatogenesis focusing on the following specific points:

-To analyze the function of ATR in meiotic silencing of unsynapsed chromosomes. Sex body formation will be studied in Seckel mouse spermatocytes in order to investigate whether the reduced ATR expression described in Seckel mice is affecting the established function of ATR during meiotic prophase.

-To evaluate the implication of ATR in meiotic recombination and regulating DSB formation during meiotic prophase. The role of ATR during meiotic recombination will be assessed by exhaustively analyzing different proteins involved in meiotic recombination events at different stages of meiotic prophase in spermatocytes from Seckel mice and from cultured seminiferous tubules treated with ATR inhibitors.

2.1.2 *To characterize the gametogenic phenotype of Seckel females*

To accomplish this purpose the complete process of oogenesis, from meiotic prophase to folliculogenesis will be analyzed focusing on the following specific points:

- To evaluate meiotic prophase progression in Seckel mouse oocytes. Meiotic prophase processes will be analyzed in order to elucidate the involvement of ATR in oocytes mammalian prophase.

-To examine folliculogenesis progression in Atr Seckel females. Complete process of folliculogenesis, from meiotic prophase to folliculogenesis, will be analyzed in order to reveal the ATR function in this process.

MATERIAL AND METHODS

Chapter 3

3.1 Mice and biological material

3.1.1 Experimental animals

Atr Seckel and *Spo11* mutated alleles were generated previously (Murga et al. 2009; Baudat et al. 2000). The mouse lines were maintained in a C57BV6 - 129/SV mixed genetic background. All the experiments were performed using at least two mutant animals and compared to littermate control mice. In those cases in which appropriate littermates controls were unavailable, control animals were obtained from other litters of the same matings and the same age.

In order to obtain Seckel mutant mice heterozygous mice were mated owing to it was described that male Seckel mice was fertile, although it was demonstrated by in-vitro fertilization, and no viable oocytes were obtained after hormone-induced superovulation of female *Seckel* mice (Murga et al. 2009). Moreover, SPO11 mice were also obtained from heterozygous matings, due to both *Spo11*-deficient males and females are sterile (Baudat et al. 2000).

3.1.2 Biological samples

Testes were obtained from adult mice of 2 month of age for most of the experimental procedures, except otherwise mentioned (e.g. to perform seminiferous tubules cultures, where testes were obtained from 5 dpp males).

Ovarian samples were obtained from females at different ages depending on the experimental procedures. For nuclei spreading procedures, ovarian samples were obtained from embryos at 18 - 20 dpc. For histological procedures, ovarian samples were obtained from prepubertal mice at 21 dpp, or from adult females of about 3 months of age. To analyze gene expression ovaries from adult females from 2 month of age were used.

When necessary, testis or ovaries obtained were immediately cryopreserved by immersion in liquid nitrogen and storage at -80°C until use.

All the animals used for experimental procedures were sacrificed using CO_2 euthanize methods. Experimental procedures performed in the present work conform to the protocol CEEAH 1091 (DAAM6395) approved by the Ethics Committee for Animal Experimentation of the Universitat Autònoma de Barcelona and the Catalan Government.

3.2 Molecular biology techniques

3.2.1 Genomic DNA extraction from mouse tail

In order to define the genetic constitution of the mice used in this work, genomic DNA was isolated from mouse tails and subsequently amplified to screen the animals.

Protocol:

-Obtain the last 0.5 mm of the mouse tail and place it into a 1.5 ml tube containing 490 µl of lysis buffer (0.1 M Tris-HCl pH= 8.5, 0.2 M NaCl, 0.2% SDS, 5 mM EDTA in Milli-Q water) and 10 µl of 20 mg/ml proteinase K (Roche Diagnostics).
-Place the tubes in the thermomixer at 56°C and 350 rpm overnight.
-Centrifuge the tubes for 15 minutes at 13200 rpm.
-Transfer the supernatant into a new clean 1.5 ml tube containing 0.5 ml of isopropanol and shake the tube vigorously to precipitate the DNA.
-Centrifuge the tubes for 15 minutes at 13200 rpm.
-Remove the supernatant without disturbing the pellet.
-Add 0.5 ml of ice-cold 70% EtOH to the pellet and mix gently to wash it.
-Remove the supernatant and let the tubes open at room temperature until the pellet is dry.
-Dissolve the pellet in 0.1 ml of Milli-Q water and place the tubes in the thermomixer for 10 minutes at 60°C.
-Store the DNA extract at -20°C until use.

3.2.2 Genotyping PCR amplification

The Polymerase Chain Reaction method was used to genotype the mice. Genomic DNA was amplified using previously designed primers (Murga et al. 2009) to distinguish the wild type and mutant alleles based on the unique amplification products.

ATR Primers:

-3'E8 Reverse: 5'-GGAATAAATCCATGGAAGTGAGAGCAT-3'
-5'N Forward: 5'-CACTGGCCTCACAGACTTCAGCATG-3'
-5'I7 Forward: 5'-TCCTCGTGCTTTACGGTATCGCC- 3'

3'E8 and 5'N primers give a 330 bp product of the wild-type allele, whereas 3'E8 and 5'I7 give a 500 bp product from the mutant allele (**Fig. 3.1**).

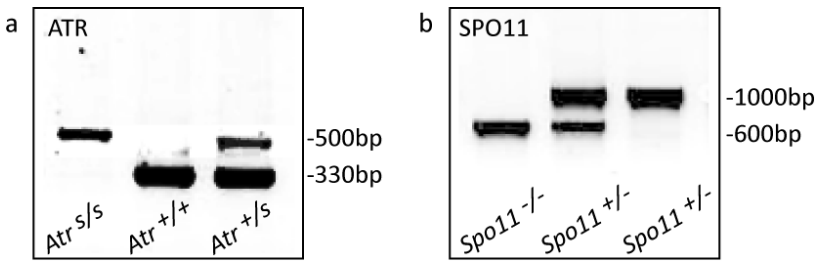

Figure 3.1. Genotyping PCR amplification. PCR products from *Atr* PCR amplification representing the wild type allele (330 bp) and the mutant allele (500 bp) from a *Seckel* homozygote, wild type and heterozygote individuals, respectively

Protocol:

-Add the following components to a 0.2 ml PCR tube according to the Horse-Power Taq DNA Polymerase recombinant Kit (Canvax) protocol:

Table 3.1. List of components for the mix used to PCR reactions

Component	Volume	Final concentration
10x PCR buffer	2 µl	1x
$MgCl_2$ 25 mM	2 µl	2.5 mM
dNTPs mix 8 mM	2 µl	0.8 mM
Forward primer 10 µM	1 µl	0.5 mM
Reverse primer 10 µM	1 µl	0.5 mM
Mutant primer 10 µM	1 µl	0.5 mM
Template DNA	1 µl	-
Horse-Power Taq DNA polymerase	0.2 µl	0.05 u/µl
Milli-Q water	up to 20 µl	-

-Perform the PCR amplification using the following cycling conditions:

ATR PCR CONDITIONS			
Predenaturation	94°C	4 minutes	
Denaturation	94°C	45 seconds	x 34 cycles
Annealling	60°C	45 seconds	
Extension	72°C	45 seconds	
Final extension	72°C	7 minutes	

SPO11 PCR CONDITIONS			
Predenaturation	94°C	4 minutes	
Denaturation	94°C	20 seconds	x 35 cycles
Annealing	59°C -0.1°C/cycle	45 seconds	
Extension	72°C	35 seconds +1 second/cycle	
Final extension	72°C	7 minutes	

-Analyze the amplification products by electrophoresis in a 1% Ethidium bromide, 1% agarose gel using appropriate molecular weight standard to determine the size of the products.

-Scan the gel using GelDoc XR+ system (Bio-Rad) to determine the presence and size of PCR products.

3.2.3 Total RNA purification from frozen tissues

The isolation of RNA from a tissue allows performing gene expression analysis. To extract total RNA from mouse testes or ovarian samples an optimized version of the protocol from RNeasy Plus Mini kit (Qiagen) was followed.

Protocol:

-Add 30 mg of frozen mouse testis or two adult mouse ovaries into a clean 1.5 ml tube.
-Disrupt it mechanically with a pestle.
-Transfer the lysate into a 2 ml microcentrifuge tube.
-Add 600 µl of Buffer RLT Plus and homogenize by passing lysate 5 times through a 20G needle fitted to an RNase-free syringe.
-Centrifuge the tube for 3 minutes at 13200 rpm.
-Remove the supernatant carefully by pipetting and transfer to a gDNA Eliminator spin column placed in a 2 ml collection tube.
-Centrifuge the tube for 30 seconds at 10000 rpm.
-Discard the column and save the flow-through. If necessary, repeat the centrifugation until all liquid has passed the membrane.
-Add 600 µl of 70% EtOH and mix by pipetting.
-Transfer 700 µl of the sample to an RNeasy spin column placed in a 2 ml collection tube.
-Centrifuge for 15 seconds at 10000 rpm and discard the flow-through.
-Add 700 µl of Buffer RW1 to the RNeasy spin column and centrifuge for 15 seconds at 10000 rpm. Discard the flow-through.
-Add 500 µl of Buffer RPE to the RNeasy spin column and centrifuge for 2 minutes at 10000 rpm.
-Place the RNeasy spin column in a new 1.5 ml tube and add 30 µl of RNase-free water to the column membrane.
-Centrifuge for 1 minute at 13200 rpm to elude the RNA.
-Quantify the final concentration of purified RNA using the NanoDrop 1000.
-Store the isolated RNA at -80°C until use.

3.2.4 Retrotranscription

The Reverse Transcription-Polymerase Chain Reaction is a PCR variant technique used to detect and semiquantitatively measure RNA expression levels. To analyze ATR expression in mutant and control samples, a SuperScript III One-Step RT-PCR system (Qiagen) was used, which performs cDNA synthesis by a reverse transcriptase followed by a standard PCR amplification in a single tube using a previously described gene-specific primers (O'Driscoll et al. 2003).

ATR Primers:

-5'Exon 8 Forward: 5'-TGTGGTATGCTCTCACTTCC-3'
-3'Exon 10 Reverse: 5'-CATTCATGTTGAGAAGTGGC-3'

In wild type samples, these primers originate a 477 bp product corresponding to the amplification of ATR exons 8, 9 and 10. In Seckel samples, a 284 bp product is amplified corresponding to the ATR exons 8 and 10, skipping exon 9 (**Fig. 3.2**)

β-actin Primers:

-5'ACTIN 1 Forward: 5'-ATCTACGAGGGCTATGCTCTC-3'
-3'ACTIN 2 Reverse: 5'-AGGTCTTTACGGATGTCAACG-3'

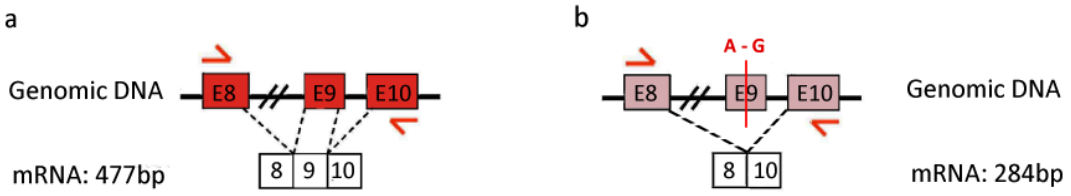

Figure 3.2. Illustration of how *Seckel* mutation in exon 9 (shaded) of ATR gene affects the normal splicing of exons 8–10. Red arrows represent where RT-PCR primers are located in de genome in wt (a) and *Seckel* alleles (b). Image modified from O'Driscoll 2009

Protocol:

-Add the following components to a 0.2 ml PCR tube for a final volume of 50 µl:

Table 3.2. List of components for the mix used in One-Step RT-PCR reactions

Component	Volume	Final concentration
2x Reaction Mix	25 µl	1x
Forward primer 10 µM	1 µl	0.2 mM
Reverse primer 10 µM	1 µl	0.2 mM
Super Script III RT/ Taq Enzyme	1 µl	-
Template RNA	0.5 µg	-
Distilled water	up to 50 µl	-

-Perform the cDNA synthesis followed immediately with PCR amplification using the following cycling conditions:

cDNA synthesis	55°C	30 minutes	
Predenaturation	94°C	2 minutes	
Denaturation	94°C	15 seconds	x 40 cycles
Annealing	59°C	30 seconds	
Extension	68°C	30 seconds	
Final extension	68°C	5 minutes	

-Analyze the amplification products by electrophoresis in a 1% Ethidium bromide, 1.5% agarose in gel using an appropriate molecular weight standard to determine the size of the products.

-Scan the gel using GelDoc XR+ system (Bio-Rad) to determine the presence and size of PCR products.

3.2.5 Protein extraction from frozen testes

Efficient extraction of the total proteins from tissues must be performed in order to analyze specific protein levels by Western Blot.

Protocol:

-Place a frozen testis into a 1.5 ml tube containing 200-500 µl of RIPA Buffer (50 mM Tris-HCl pH=8, 0.1% SDS, 1% Triton X-100, 150 mM NaCl, 1 mM EDTA, 0.5% Sodium Deoxycholate, 1x PIC (Roche Diagnostics) in MIlli-Q water).

-Grind the tissue with a pestle until disruption.

-Place the tube in a thermomixer for 10 minutes at 95°C.

-Grind the tissue again with the pestle and centrifuge the tube for 10 minutes at 13200 rpm at 4°C.

-Transfer the supernatant containing soluble proteins to a new tube.

-Take an aliquot for quantification and store the rest of the protein extract at -20°C until use.

3.2.6 Quantification of the protein extract

A colorimetric-based assay was used to determine an accurate total protein concentration in the extracts. For these purpose the BSA Protein assay kit (Thermo Scientific), which relies on a protein-copper chelation reaction was employed.

Protocol:

-Prepare the set of protein standards diluting the content of one Albumine Standard ampoule (2 mg/ml). Make nine working range dilution of 0 – 2000 µg/ml.

-Prepare Working Reagent by mixing 50 parts of Reagent A with 1 part of Reagent B.

-Pipette 50 µl of each standard and protein extract sample into a 1.5 ml tube.

-Add 1 ml of the Working Reagent to each tube and mix well.

-Measure the absorbance of all the samples at 562 nm with a spectrophotometer (Cary 400 Bio).

-Prepare a standard curve by plotting the average 562 nm measurement for each BSA standard and use the curve to determine the protein concentration of each protein extract sample.

3.2.7 *Western Blot*

Western blotting was used to separate and determine specific proteins from protein extracts. This technique allows the identification of proteins with three steps. The proteins are separated by size, based on molecular weight, through gel electrophoresis. Then, proteins are transferred to a membrane, and finally, the membrane is incubated with specific antibodies to detect the protein of interest. The intensity of the signal of the band corresponds to the amount of protein present.

Protocol:

Sample preparation

-Determine the volume of protein extract to load 50 µg of each sample and add one fifth of the volume of laemmli loading buffer.

-Equal the volume of all samples by adding laemmli buffer if necessary.

-Heat the samples for 5 minutes at 95°C with the thermomixer to denature the proteins.

-Keep samples at 4°C until use.

Gel preparation

-Prepare gel electrophoresis solutions.

Table 3.3. List of components used to prepare Western Blot gel electrophoresis

7% Running gel	Milli-Q water	**5.1 ml**
	1.5 M Tris-HCl (pH=8.8)	**2.5 ml**
	Bis-acrylamide	**2.4 ml**
	20% SDS	**50 µl**
	10% APS	**100 µl**
	TEMED	**13 µl**
4% Stacking gel	Milli-Q water	**3.7 ml**
	1 M Tris-HCl (pH=6.8)	**625 µl**
	Bis-acrylamide	**670 µl**
	20% SDS	**25 µl**
	10% APS	**50 µl**
	TEMED	**10 µl**

*Note that 10% APS and TEMED solidify the solution; therefore, both gels can be prepared at the same time, if the abovementioned reagents are not added until the end).

-Assemble the Mini-Protean cell casting module (Bio-Rad) (**Fig. 3.3**).

-Add running gel solution carefully into the glass plates up to the top of the casting frame (Bio-Rad). Immediately add Milli-Q water or isopropanol to the top. Wait for 15-30 minutes until the gel solidifies.

-Overlay the running gel with the stacking gel, after removing the Milli-Q water or isopropanol and wait until the gel solidifies. Note that solidification can be easily checked by leaving some gel solution in a tube.

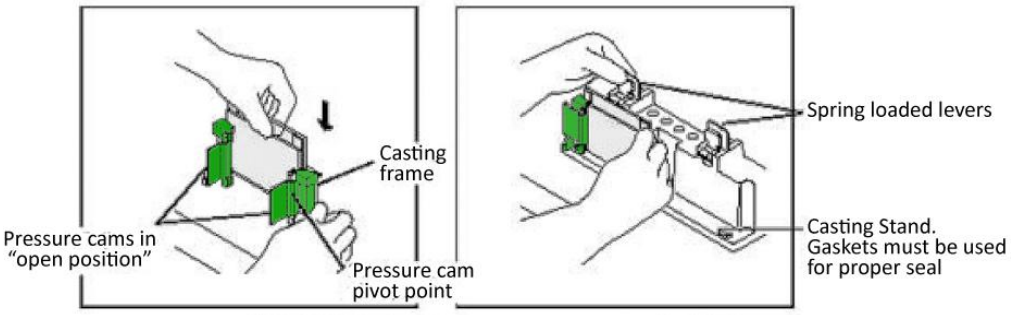

Figure 3.3. Assembling the Mini-Protean cell casting module and glasses into the casting frame. Image modified from Bio-Rad.

Electrophoresis

-Place the gel inside the electrophoretic chamber and add the running buffer (250 mM Tris, 14.4% Glycine, 1% SDS in Milli-Q water).

-Load marker and samples into the wells.

-Run the gel first at low voltage (80 V) while in the stacking gel. Once samples have penetrated running gel increase voltage (to 100-120 V) for approximately an hour.

Semi-dry Electrotransfer using Trans-Blot Turbo system (Bio-Rad)

-Position the PVDF membrane and bottom stack on the cassette.

-Place gel on the membrane and cover with the top stack using the blot roller to remove trapped air bubbles.

-Close and lock the cassette. Insert into the Trans-Blot Turbo and transfer for 7 minutes at a constant electric current of 2.5 A.

Antibody incubation

-Block the membrane with 5% skim milk in PBST (20mM Tris-HCl pH=7.4, 137 mM NaCl, 0.1% Tween 20) for 1 hour.

-Add primary antibody in 5% skim milk in PBST and incubate overnight in 4°C under constant agitation. Use β-ACTIN as a loading control in order to normalize the signals from the proteins of interest (**Table 3.4**).

Table 3.4. List of primary antibodies used in western blotting

Antigen	Host	Supplier	Final dilution
ATR (Ab-2)	Rabbit	Calbiochem	1:1500
β-ACTIN (AC-15)	Mouse	Abcam	1:10000

-Wash the membrane with PBST three times for 5 minutes at room temperature under constant agitation.

-Add secondary antibody conjugated with horseradish peroxidase (HRP) in 5% skim milk in PBST (1:3000) and incubate for 1 hour (**Table 3.5**).

Table 3.5. List of secondary antibodies used for western blotting

Target	Conjugated	Host	Supplier	Final dilution
Rabbit	HRP	Goat	Bio-Rad	1:3000
Mouse	HRP	Goat	Bio-Rad	1:3000

-Wash the membrane with PBST three times for 5 minutes at room temperature under constant agitation.
-Incubate with Luminata Forte Western HRP substrate (Millipore) for 1 minute.

Stripping
-If necessary, wash the membrane twice for 15 minutes in fresh stripping buffer (15% glycine, 1% SDS, 0.1% Tween 20) in order to strip off the antibodies before applying another primary antibody incubation.

3.3 Cytological techniques

3.3.1 Spermatocyte nuclei spreading from fresh testes

In order to obtain high-quality preparations of meiotic prophase nucleus displaying the chromatin-associated proteins, spermatocyte surface spreading was performed from fresh testes. This technique allows the study of the proteinaceus nuclear components by protein immunolabelling. Spreading protocol was adapted from Peters et al. (1997).

Protocol:

-Remove the testes from a male mouse and immediately place it in a petri dish containing PBS to rinse testes.
-Hold testes with forceps to pull out the tunica albuginea and release the seminiferous tubules into a cold PBS drop.
-Mince the sample with a scalpel.
-Pipette the cell suspension and transfer into a 15 ml tube containing 7 ml of cold PBS.
-Pipette up and down few times to homogenize the cell suspension. Let large pieces settle to the bottom for approximately 10 minutes.
-Transfer 1 ml of cell suspension into six previously marked 1.5 ml tubes.
-Centrifuge the tubes for 5 minutes at 1500 rpm
-Discard the supernatant and loose the pellet by flicking with your fingers.
-Add 40 µl of 0.5 M sucrose at 37°C into each tube and resuspend the pellet.
-Distribute 20 µl of cell suspension on a previously labeled slide containing 65 µl of cold fixative (1% Paraformaldehyde, 0.15% Triton X-100, 1x PIC (Roche Diagnostics) in Milli-Q water, pH=9.2-9.4).
-Let slides fixing for 2 hours at room temperature into a closed humidity chamber.
-Open the chamber and let the slides air dry for 30 minutes.

-Wash the slides four times in 4% Photoflo (Kodak) solution for 2 minutes. Note that different genotypes must be washed separately.
- Let slides air dry and store at -80°C until use.

3.3.2 Spermatocyte nuclei spreading from frozen testes

Obtaining meiotic spreads from frozen tissues represents an advantage considering mouse testes may be stored at -80°C, preserved, and used when necessary using only a small portion of frozen tissue. This alternative procedure adapted from Liebe et al. (2004) allows the analysis of the nuclear components from spermatocytes in high-quality surface spreads.

Protocol:

-Place a small portion of mouse frozen testis on a petri dish placed on ice.
-Mince the sample a scalpel.
-Add up to 40 µl of cold PBS and keep disaggregating until obtaining a cell suspension.
-Distribute 8 µl of the cell suspension on previously marked slides placed in a humidity chamber.
-Add 90 µl of ionic detergent solution (1% Lipsol in Milli-Q water) on the cell suspension and leave for 10-15 minutes.
-Add 95 µl of fixative solution (1% Paraformaldehyde, 0.15% Triton X-100, 1x PIC (Roche Diagnostics) in Milli-Q water, pH=9.2-9.4).
-Let slides fixing for 2 hours at room temperature into a closed humidity chamber.
-Open the chamber and let the slides air dry for 30 minutes.
-Wash the slides four times in 4% Photoflo (Kodak) solution for 2 minutes. Note that different genotypes must be washed separately.
-Let slides air dry and store at -80°C until use.

3.3.3 Oocytes nuclei spreading from fetal ovaries

Since female first meiotic prophase takes place during fetal development, obtaining and analyzing oocytes from fetal ovaries is required. To study the events that occur in the nucleus of oocytes, chromosome spreads from fetal mouse ovaries were performed.

Protocol:

-Preheat hypotonic buffer (30 mM Tris-HCl pH=8.2, 50 mM Sucrose, 17 mM Sodium Citrate, 5 mM EDTA, 0.5 mM DTT (Roche Diagnostics), 1x PIC (Roche Diagnostics) in Milli-Q water) at 37°C.
-In a 24-well plate, dispense 500 µl of M2 medium (Sigma) in row 1.
-Remove the uterus from a pregnant mouse and place in a petri dish containing PBS.
-Dissect fetuses out of the uterus and transfer them into a new petri dish containing PBS.

-Remove the ovaries from female fetuses with the help of a stereo microscope (Nikon SMZ-1) and place the two ovaries from each female into a well from row 1 containing M2 medium. Use one well for each female. Repeat this action for every female fetus found.
-Add a 25 µl of 50 mg/ml Collagenase (Sigma) in M2 medium in row 2 and transfer the ovaries from the row 1 wells to row 2 wells.
-Incubate the ovaries for 30 minutes at 37°C.
-Transfer the ovaries from row 2 wells to row 3 wells containing 500 µl of prewarmed hypotonic buffer and incubate them for 30 minutes at room temperature.
-Add a 60 µl of 100 mM sucrose pH=8.2 in row 4 and transfer the ovaries into these wells.
-Pipette the ovaries up and down using a P100. On the stereo microscope check that the tissue is disaggregated and the oocytes are thoroughly suspended.
-Distribute 10 µl of cell suspension on previously marked slides (6 slides for 1 fetus) containing 40 µl of fixative solution (1% PFA, 5 mM Sodium Borate, 0.15% Triton X-100, 3 mM DTT (Roche Diagnostics), 1x PCI (Roche Diagnostics) in Milli-Q water, pH=9.2).
-Let the slides fixing for 2 hours into a closed humidity chamber.
-Open the chamber and let the slides completely air dry.
-Wash the slides four times in 4% Photoflo (Kodak) solution for 2 minutes. Note that different genotypes must be washed separately.
-Let slides air dry and store at -80°C until use.

3.3.4 Immunofluorescence on surface spreads

To identify the presence and determine the location and the appearance of particular proteins indirect immunofluorescence was performed in surface spreads. Indirect immunofluorescence consists on the detection of the molecule of interest with a specific primary antibody and a secondary antibody chemically conjugated to a fluorescent dye that is directed towards the primary antibody.

Protocol:

-Block slides with a blocking solution (0.2% BSA, 0.2% gelatin, 0,05% Tween-20 in PBS) for 10 minutes at room temperature under constant agitation.
-Prepare the primary antibodies solution adding the appropriate volume of each primary antibody in blocking solution (**Table 3.6**).
-Add 100 µl of primary antibody solution for each slide and cover with parafilm.
-Incubate the slides in a humidity chamber overnight at 4°C.
-Wash the slides four times in blocking solution for 3 minutes.

Table 3.6. List of primary antibodies used in immunofluorescence procedures

Antigen	Host	Supplier	Final dilution
SYCP3	Rabbit	Abcam	1:200
SYCP3 (Cor 10G11/7)	Mouse	Abcam	1:200
SYCP1	Mouse	Abcam	1:400
ATR (Ab-2)	Rabbit	Calbiochem	1:100
SUMO - 1 (GMP-1)	Mouse	Life Technologies	1:100
MDC1 (aa1883-2089)	Sheep	AbdSerotec	1:100
γH2AX (Ser139)	Mouse	EMD Millipore	1:200
H1T	Guinea pig	Dr M.A. Handel, Jackson Lab	1:500
RPA	Rabbit	Dr Edita Marcon	1:100
RAD51 (ab-1)	Rabbit	Calbiochem	1:100
DMC1 (H-100)	Rabbit	Santa Cruz Biotechnology	1:100
MLH1 (G168-15)	Mouse	BD Bioscience	1:50
DDX4 - MVH	Rabbit	Abcam	1:100

-Prepare the secondary antibody solution adding the appropriate volume of each secondary antibody in blocking solution (**Table 3.7**).

-Add 100 µl secondary antibody solution for each slide and cover with parafilm.

-Incubate the slides in a humidity chamber for 1 hour at 37°C.

Table 3.7 List of secondary antibodies used in immunofluorescence procedures

Target	Conjugated	Host	Supplier	Final dilution
Rabbit	FITC	Goat	Jackson Immunoresearch	1:200
Rabbit	Cy3	Goat	Jackson Immunoresearch	1:200
Mouse	FITC	Goat	Jackson Immunoresearch	1:200
Mouse	Cy3	Goat	Jackson Immunoresearch	1:200
Mouse	Cy5	Goat	Jackson Immunoresearch	1:200
Guinea pig	Cy3	Goat	Jackson Immunoresearch	1:200
Sheep	Cy3	Donkey	Jackson Immunoresearch	1:200

-Wash the slides four times in blocking solution for 3 minutes.

-Drain slide and add 15 µl of 0.1 µg/ml DAPI in Vectashield mounting medium and cover with a coverslip.

-Analyze with an epifluorescence microscope. Store it at 4°C for short periods or at -20°C for longer periods.

3.3.5 Fluorescence in situ hybridization on spermatocyte spreads using Bacterial Artificial Chromosomes

Fluorescence *in situ* hybridization (FISH) technique using Bacterial Artificial Chromosomes (BAC) probes allows the identification of certain chromosomes. In this particular

case, FISH was performed on spermatocyte spreads previously immunostained in order to study different recombination events in the X chromosome.

Protocol:

Pre-hybridization treatments

-Carefully remove the coverslip from the slides that have been previously analyzed by immunofluorescence.

-Wash the slides for 1 minute in Milli-Q water and let them air dry.

-Immerse the slides in a prewarmed denaturation solution (70% formamide in 2% SSC, pH= 7.2-7.4) for 20 minutes at 74° in a water bath.

-Wash the slides for 1 minute in Milli-Q water.

-Add 100 µl of 1 M Sodium thiocyanate and cover with parafilm.

-Let the slide incubating into a humidity chamber for 2.5 hour at 65°C.

-Remove the parafilm and let the slides air dry.

-Immerse the slide in a denaturation solution for 20 minutes at 74° in a water bath.

-Dehydrate the slide by successive immersion in 70%, 90% and 100% EtOH solutions at -20°C for 2 minutes each one and let the slide completely air dry at room temperature before adding the probe.

Hybridization

-Add 5 µl of Smcl2 probe previously labeled with digoxigenin in a clean 1.5 ml tube and add one volume of hybridization buffer (4xSSC, 50% Dextran sulphate, 2 mg/ml BSA, 2 mM Vanadyl ribonucleoside)

-Place the tube containing the hybridization mix in the thermomixer for 10 minutes at 75°C to denature the probe and incubate for 10 minutes at 37°C to reanneal highly repetitive sequences..

-Add 10 µl of hybridization mix on the desired region of the denatured slide and cover with a 20x20 mm coverslip. Ensure no air bubbles are trapped below the coverslip.

-Let slides hybridize in a humidity chamber for 72 hours at 37°C.

Post-hybridization treatments

-Remove the coverslip carefully and wash the slide three times for 5 minutes in washing solution (50% formamide, 2×SSC pH= 7.2-7.4) at 45°C in a water bath.

-Wash the slide three times for 5 minutes in 2× SSC at 45°C in a water bath.

-Rinse the slide once in a 4xSSC 0.1% Tween 20 at room temperature.

-Add 200 µl of blocking buffer (40% BSA mg/ml, 20% 20xSCC, 0.1% Tween 20 in Milli-Q water), cover with parafilm and incubate into a humidity chamber for 30 minutes at 37°C.

-Prepare the detection solution (10% Anti-Digoxigenin-Fluorescein (ApopTag Plus Fluorescein In Situ Apoptosis Detection kit - Millipore) in a 4xSSC 0.1% Tween 20).

-Add 30 µl of detection solution on the hybridized region from each slide, cover with parafilm and incubate into a humidity chamber for 1 hour at 37°C.

-Wash the slide three times for 5 minutes in 4xSSC, 0.1% Tween 20 at room temperature.

-Drain the slides and add 15 µl of 0.1 µg/ml DAPI in Vectashield mounting medium and cover with a coverslip.

-Analyze with an epifluorescence microscope or store at -20°C until use.

3.4 Histological techniques

3.4.1 Sample preparation for microtome sectioning

In order to section, stain and study the histological structure of ovarian and testicular samples, a protocol for fixation and paraffin embedding of the specimens was performed. The histological standard preparation is composed of three major steps. The first one is fixation which preserves the integrity of the tissue. The second, processing, substitutes the water of the tissue by paraffin, to do so samples are dehydrated, cleared and infiltrated with paraffin. Finally, the embedding step includes the tissue in a block that can be sectioned for analysis and easily stored.

Protocol:

Fixation

-Remove the testes or the ovaries from a mouse and immediately place in a petri dish containing cold PBS to rinse the organs.

-Immerse the tissue in a precooled fresh fixative solution and fix overnight at 4°C. Note that different fixative solutions were used according to the purpose of the study. PFA (4% paraformaldehyde in PBS, pH=7.4) was used to perform TUNEL assays, instead, Bouin's solution (70% Saturated picric acid, 25% Formaldehyde, 5% Glacial acetic acid) was used to study histological structure by PAS-Hematoxilin staining.

-Wash tissue in PBS twice for 30 minutes at 4°C.

Processing

-Wash the tissue with 50% EtOH for 20 minutes at 4°C

-Transfer the specimen to 70% EtOH for 30 minutes at 4°C. At this step the tissue can be stored for 4-5 weeks at 4°C).

-Wash the tissue for 30 minutes with 85% EtOH at room temperature.

-Transfer the specimen to a solution containing 95% EtOH, 0.1% eosin for 30 minutes at room temperature to dye the tissue.

-Continue dehydration by washing twice in 100% EtOH for 30 minutes at room temperature.

-Wash the tissue with Histo-Clear (National Diagnostics) three times for 30 minutes at room temperature.

-Place the tissue in a cassette previously marked and immerse it in a pre-embedding solution (50% Histo-Clear, 50% paraffin) for 45 minutes at 56°C.

-Submerge the tissue overnight in 100% paraffin solution at 56°C.

Embedding

-Removed the tissue from cassettes, place it in an embedding centre and position on a metallic mold.

-Orientate the sample determining the plane through which it will be cut.

-Place a new cassette appropriately marked on top of the mold and add more paraffin to cover the tissue.

-Let the paraffin completely solidify on a cold surface before removing the mold.

-Store the block containing the specimen at 4°C until sectioning.

Sectioning with microtome

-Attach the block into the microtome (Reichert-Jung) with the proper orientation.

-Cut sections at a thickness of 5-6 µm ensuring that only a single layer of cells makes up the section.

-Transfer the section to the surface of warm water bath to smooth it out.

-Pick the sections up onto poly-L-lysine-coated slides.

-Let the slides completely dry overnight at 37°C and store them at room temperature until use.

3.4.2 Sample preparation for cryostat sectioning

Cryosections provide an efficient method to detect and visualize fine details of a sample. Despite cryosections are less stable than paraffin sections, they allow a better molecular characterization of the sample. Hence, in order to study cell proliferation by measuring EdU incorporation into the DNA on ovarian samples the following protocol for fixation, processing and cryosectioning frozen tissues was performed.

Protocol:

Fixation

-Remove the ovaries from a mouse and immediately place them in a petri dish containing cold PBS to rinse them.

-Immerse the tissue in a precooled fresh fixative solution (4% paraformaldehyde, see Table 3.6) and fix overnight at 4°C.

-Wash tissue twice in PBS for 30 minutes at 4°C.

Processing

-Immerse the fixed specimen in a sucrose solution (30% sucrose in PBS) overnight at room temperature to cryoprotect the tissue.

-Place the sample over a filter paper in order to remove the excess of sucrose from the tissue

Embedding

-Place a plastic mold on dry ice for embedding the tissue.
-Add a drop of embedding medium OCT compound (Sakura) at the bottom of the mold and bind the tissue in the appropriate orientation to determine the plane through which the section will be cut.
-Add OCT compound to cover the tissue.
-Let the block completely solidify on dry ice before removing it from the mold.
-Store the block at -80°C until sectioning.

Sectioning with cryostat
- Adjust the temperature of the cryostat (SME Thermo electron corporation) using the following conditions for ovarian samples: Temperature of the cutting chamber= -17°C; Specimen temperature= -15°C.
-Attach the block to the cryostat block holder with the proper orientation.
-Cut sections at a thickness of a 10 µm.
-Transfer cryosections to poly-L-lysine-coated slides.
-Dry the slide on a slide warmer for 30 minutes at 37°C and store at -80°C until use.

3.4.3 PAS-Hematoxylin staining

The Periodic Acid Schiff staining is a method used to detect structures rich in carbohydrate macromolecules, such as glycogen, typically found in connective tissues and basal laminae. This staining was used to analyze the structure and morphology of testicular and ovarian histological sections.

Protocol:

Deparaffinization and rehydration of the sections
-Wash the slide in xylene three times for 5 minutes.
-Rehydrate the tissue washing the slide using a gradient of ethanol solutions:

100% EtOH twice for 3 minutes
96% EtOH twice for 2 minutes
70% EtOH twice for 2 minutes
Distilled water for 2 minutes

Staining
-Oxidize the slide in a 1% Periodic Acid in distilled water solution for 15 minutes at room temperature.
-Wash the slide twice in distilled water for 3 minutes.
-Immerse the slide in Schiff reagent for 30 minutes at room temperature. Note that Schiff reagent must be stored a 4°C in darkness. Red colored solution indicates a deteriorated Schiff reagent.

-Wash twice in Sulphurous water (10% Potassium metabisulfite, 0.1 M HCl in Milli-Q water) for 3 minutes at room temperature.
-Wash twice for 3 minutes in distilled water.
-Counterstain in Mayer's Hematoxylin (Sigma) for 1 minute at room temperature**.**
-Rinse with tap water for 1 minute.

Dehydration and mounting
-Dehydrate the tissue washing the slide using a gradient of ethanol solutions:
70% EtOH twice for 2 minutes
96% EtOH twice for 2 minutes
100% EtOH twice for 3 minutes
-Wash the slide in xylene twice for 5 minutes.
-Add a drop of DPX mounting medium (Sigma) on each section and cover with a coverslip ensuring no air bubbles are trapped.
-Let the slide completely air dry. Analyze with a brightfield microscope or store at room temperature.

3.4.4 In situ cell death detection on testicular paraffin sections

The Terminal deoxynucleotidyl transferase dUTP nick end labeling or TUNEL reaction technique was used to detect and quantify programmed cell death. The TUNEL reaction labels DNA double strand breaks generated during apoptosis. To analyze spermatocytes apoptosis a TUNEL staining protocol optimized for the *In situ* cell death detection kit (Roche Diagnostics) was performed on testis sections.

Protocol:

Deparaffinization and hydration
-Wash the slide in xylene three times for 5 minutes.
-Rehydrate the tissue washing the slide using a gradient of ethanol:
100% EtOH twice for 3 minutes
96% EtOH twice for 2 minutes
70% EtOH twice for 2 minutes
Distilled water for 2 minutes

TUNEL staining
-Rinse the slide once in PBS for 2 minutes at room temperature.
-Wash the slide in a cell permeabilization solution (0.5% Triton X-100 in PBS) for 15 minutes.
-Wash the slide in PBS twice for 2 minutes at room temperature.
-Add 100 µl of Background reducing solution (Dako) on each slide, cover with parafilm and incubate in a humidity chamber for 15 minutes at room temperature.

-Rinse the slide once in PBS and remove the excess of liquid remaining around the section.

-Add 25 µl of TUNEL reaction mixture (10% TdT enzyme solution, 90% label solution) on each section and incubate the slides into a humidity chamber for 1 hour at 37°C.

-Wash the slide in PBS three times for 5 minutes.

-Drain the slide and add 15 µl of 0.1 µg/ml DAPI in Vectashield mounting medium and cover with a coverslip.

-Analyze with an epifluorescence microscope or store at-20°C until use.

3.4.5 Indirect In situ cell death detection on ovarian paraffin sections

In order to detect and quantify apoptosis in ovarian sections an optimized TUNEL staining protocol from ApopTag Plus Fluorescein *In Situ* Apoptosis Detection kit (Millipore) was performed.

Protocol:

Deparaffinization and rehydration

-Wash the slide in xylene three times for 5 minutes.

-Rehydrate the tissue washing the slide using a gradient of ethanol solutions:

100% EtOH twice for 3 minutes

96% EtOH twice for 2 minutes

70% EtOH twice for 2 minutes

Distilled water for 2 minutes

TUNEL staining

-Wash the slide twice in PBS for 2 minutes at room temperature.

-Add 75 µl of equilibration buffer on each slide and incubate for at least 10 seconds.

-Add 55 µl of working strength TdT enzyme (30% TdT enzyme solution, 70% reaction buffer) on each slide and incubate the slides in a humidity chamber for 1 hour at 37°C.

-Wash the slides in working strength stop buffer for 10 minutes at room temperature.

-Wash the slide in PBS three times for 1 minute at room temperature.

-Add 65 µl of detection solution (30% Anti-Digoxigenin conjugate antibody, 70% blocking solution) on each slide and incubate in a humidity chamber for 30 minutes at 37°C.

-Wash the slide in PBS four times for 2 minute at room temperature.

-Drain the slide and add 15 µl of 0.1 µg/ml DAPI in Vectashield mounting medium and cover with a coverslip.

-Analyze with an epifluorescence microscope or store at-20°C until use.

3.4.6 *Click-iT EdU Cell proliferation assay*

To measure follicular cells proliferation rate, a cell proliferation assay was used on ovarian cryosections. This method is based on the incorporation of EdU (5-ethynyl-2'-deoxyuridine), a nucleoside analog of thymidine into DNA during active DNA synthesis. This nucleoside is then detected through the covalently ligation of a fluorescent dye via a Click-it kit. Thus, following the described protocol for Click-It EdU Imagine Kits (Invitrogen), follicular replicating cells were detected and quantified by *in vivo* EdU incorporation in ovaries.

Protocol:

In vivo incorporation of EdU

-Administer 300 µl of EdU solution (EdU 1 mg/ml in PBS) by single intraperitoneal injection to 21 dpp female mouse. Note that the solution must be prewarmed at 37°C to be injected at body temperature.

-Euthanize mouse 24 hours after injection and process ovaries for cryostat sectioning (see 1.4.2 section).

EdU detection

-Thaw slides containing cryosections incubating them for 30 minutes at 37°C.

-Wash the slides in permeabilization buffer (0.5% Triton X-100 in PBS) for 20 minutes at room temperature.

-Block the slides with blocking solution (3% BSA in PBS) for 10 minutes at room temperature.

-Prepare the reaction cocktail adding the following compounds in the order listed (**Table 3.8**). Use the solution within 15 minutes of preparation.

Table 3.8. List of components for EdU detection reaction

Click-iT reaction cocktail	Reaction buffer – Component D	**86 µl**
	CuSO4 – component E	**4 µl**
	Alexa Flour azide – component B	**0.25 µl**
	Reaction buffer additive – component F	**10 µl**

-Add 100 µl of Click-iT reaction cocktail on each slide and incubate into a humidity chamber for 30 minutes at room temperature.

-Wash the slides in blocking solution for 5 minutes at room temperature.

-Wash the slides in PBS for 5 minutes at room temperature.

-Drain the slides.

-Add 15 µl of 0.1 µg/ml DAPI in Vectashield mounting medium and cover with a coverslip or, alternatively, proceed to perform immunofluorescence (see section 3.4.7 section).

3.4.7 Immunofluorescence staining on ovarian sections

To identify more easily follicles within the ovarian sections, on both paraffin-embedded or cryosections, the oocytes enclosed in follicles were immunodetected using an antibody against DDX4 protein, which is a germ cell marker

Protocol:

Deparaffinization and rehydration

-Wash the slide in xylene three times for 5 minutes.

-Rehydrate the tissue washing the slide using a gradient of ethanol solutions:

100% EtOH twice for 3 minutes

96% EtOH twice for 2 minutes

70% EtOH twice for 2 minutes

Distilled water for 2 minutes

Antigen retrieval

-Pre-heat a water bath with a coplin jar containing Sodium Citrate buffer (10mM Sodium Citrate, 0.05% Tween 20 in Milli-Q water, pH 6.0) to 95-100°C.

-Immerse slides in the Citrate buffer and incubate for 20 minutes.

-Remove the coplin jar from the water bath and allow the slides to cool for 20 minutes at room temperature.

Immunofluorescence

-Block the slides with blocking solution (0.2% BSA, 0.2% gelatin, 0.05% Tween-20 in PBS) for 10 minutes at room temperature under constant agitation.

-Add 100 µl of primary DDX4 antibody in blocking solution (1:100; see Table 3.6) for each slide and cover with parafilm.

-Incubate the slides in a humidity chamber at 4°C overnight.

-Wash the slides four times in blocking solution for 3 minutes.

-Add 100 µl of secondary antibody solution (0.5% anti-mouse Cy3 conjugated antibody in blocking solution) for each slide and cover with parafilm.

-Incubate the slides in a humidity chamber for 1 hour at 37°C.

-Wash the slides four times in blocking solution for 3 minutes.

-Drain slide and add 15 µl of 0.1 µg/ml DAPI in Vectashield mounting medium and cover with a coverslip.

-Analyze with an epifluorescence microscope or store at -20°C (or 4°C for short periods of time).

3.5 Organ culture protocols

3.5.1 In vitro neonatal mouse testis organ culture

New developed organ culture systems have allowed progression of spermatogenesis *in vitro* by cultivating neonatal mouse testis (Sato et al. 2011). This method enables the *in vitro* study of meiotic prophase.

Using this method it was possible, cultivating testis tissue fragments from neonatal mouse, to reproduce the events that take place during *in vivo* meiotic prophase. Therefore, this system could be useful for evaluating the effect of different drugs on meiosis. In this particular case, a recently discovered drug that selective inhibits ATR (AZ-20) (Foote et al. 2013) was tested on testis organ culture modifying the protocol described in Sato et al. (2011) to evaluate the effects of suppressing ATR function during meiosis.

Protocol:

Culture dish preparation

-Prepare agarose solution (1.5% agarose in Milli-Q water) and sterilize it by autoclaving (2 atmospheres at 121°C for 20 minutes).

-Pour agarose solution into petri dishes and leave at room temperature until polymerizes.

-Cut the agarose gel into cubes of about $10 \times 10 \times 5$ mm in size with the help of a scalpel.

-Place two cubes into each well of a 6-well plate and add culture medium (10% Knockout Serum Replacement (Invitrogen), 1% Antibiotic-Antimycotic 100x (Gibco), 0.37% Sodium Bicarbonate in α-Minimum Essential Medium (Invitrogen)) to completely submerge the cubes.

-Equilibrate in a culture incubator supplied with 5% CO_2 in air and maintained at 34°C overnight or longer in order to replace water from agarose cubes with medium culture.

-On the day 0 of the culture, remove old medium and add fresh culture medium until it reaches half of the height of the agarose cubes.

-Leave again the 6-well plate in the incubator at 34°C with 5% CO_2 in air.

Testis organ culture

-Remove testes from 5 dpp mouse and immediately place them in a petri dish containing washing solution (1% Antifungic-Antymicotic 100x in α-Minimum Essential Medium).

-Hold testes with forceps to cut the testis in half and pull out the tunica albuginea.

-Transfer one or two half testis onto an agarose cube.

-Incubate in an incubator supplied with 5% CO_2 in air and maintained at 34°C for one or two weeks. Note that medium culture must be replaced once a week.

Control spreads day 0 (D0)

-Collect the washing solution used for handling testes from each individual in different 1.5 ml tube.

-Centrifuge for 3 minutes at 3000 rpm.

-Discard the supernatant and break up the pellet.

-Add 20 µl of 100 mM sucrose at 37°C into each tube and resuspend the pellets.

-Transfer the 20 µl of cellular suspension on a previously marked slide containing 40 µl of cold fixative solution (1% Paraformaldehyde, 0.15% Triton X-100, 1x PCI (Roche Diagnostics) in Milli-Q water, pH=9.2-9.4).

-Let the slides fixing for 2 hours at room temperature in a closed humidity chamber.

-Open the chamber and let the slides completely air dry.

-Wash the slides four times in 4% Photoflo (Kodak) solution for 2 minutes. Note that different individuals must be washed separately.

Drug administration

-After 7 days of culture (D7), replace old culture medium with fresh culture medium supplemented with 0.2 µM, 1 µM or 5 µM AZ-20 (Selleckchem) dissolved in DMSO (Sigma), and with the equivalent volumes of DMSO for each ATR inhibitor concentration used in corresponding control wells.

-Incubate at 34°C with 5% CO_2 in air for one more week.

Processing of cultured testis fragments

-After 7 (D7) or 14 days of culture (D14), freeze each fragment in liquid nitrogen.

-Store frozen testis fragments at -80°C until use.

Meiotic spreads from cultured fragments of testis

-Place a fragment of testis on a slide and mince it with a scalpel.

-Add 20 µl of cold PBS and keep mincing the sample until obtaining a cellular suspension.

-Distribute 10 µl of the cellular suspension on another slide and place both slides in a humidity chamber.

-Add 90 µl of ionic detergent solution 1% on the suspension and leave for 12 minutes.

-Add 95 µl of fixative solution (1% Paraformaldehyde, 0.15% Triton X-100, 1X PCI (Roche Diagnostics) in Milli-Q water, pH=9.2-9.4).

-Let slides fixing for 2 hours at room temperature in a closed humidity chamber.

-Open the chamber and let the slides completely air dry.

-Wash the slides four times in 4% Photoflo (Kodak) solution for 2 minutes. Note that slides from fragments treated with different doses of AZ-20 must be washed separately.

-Let slides air dry and store at -80°C until use.

3.6 Microscopy, image processing and data analysis

3.6.1 Microscopy and image acquisition

PAS-Hematoxilin stained tissue sections were analyzed on a brightfield microscope Olympus CH2 and images were captured using Zeiss Axiophot Microscope and Olympus C5060 camera.

For fluorescent sample analysis and image capturing a Zeiss Axioskop fluorescence microscope connected with a ProgRes Jenoptik camera was used. The image capture software ProgRes CapturePro was employed for image acquisition and image processing.

3.6.2 Image analysis and processing

All microscopy images were processed and different fluorescent channels overlaid using Adobe Photoshop CS2.

The Java-based image processing program ImageJ (imagej.nih.gov/ij/) was used to quantify fluorescence intensity levels and to measure length and areas.

The analysis of position and distribution of MLH1 foci was performed using MicroMeasure version 3.3 (www.colostate.edu/Depts/Biology/MicroMeasure/).

3.6.3 Statistical analysis

Data analysis and statistical inference were performed using the GraphPad InStat, GraphPad QuickCalcs (http://www.graphpad.com/quickcalcs/) and GraphPad Prism 5 softwares. For MLH1 foci distribution and inter-focus analyses the following pages were used: http://www.physics.csbsju.edu/stats/ and http://www.wessa.net/rwasp_fitdistrgamma.wasp, respectively.

RESULTS

Chapter 4

4.1 Characterization of ATR functions during male meiosis

Investigating the role of ATR during spermatogenesis is fundamental to understand how recombination and chromosome silencing take place during meiotic progression. For this purpose in the present study we use a recently generated murine model that recapitulate the human Seckel syndrome, as well as, new organ culture methods that allow the use of pharmacologic strategies in order to evaluate the effects of ATR deficiency during prophase.

4.1.1 Analysis of the expression of ATR in Seckel mice testis

Seckel mouse model ($Atr^{s/s}$) carries a hypomorphic mutation that impairs proper *Atr* splicing producing a defective transcript and originating a message with a premature stop codon. Thus, when the Seckel allele is in homozygosis this leads to a severe down-regulation of ATR protein levels in most tissues (Murga et al. 2009). In order to determine whether ATR levels were reduced in Seckel testis we performed RT-PCR from whole testis in Seckel and control mice using two oligonucleotides that bind *Atr* exon 8 and 10 (**Fig. 3.2**, see section 3.2.4). The retrotranscription analysis detected a reduced expression of the ATR transcript in Seckel testis compared with control mice (**Fig. 4.1a**). As previously described, we noticed that Seckel mice showed two RT-PCR products, one corresponding to the product lacking exon 9 (284 bp) and a second one, which is present also in control samples, corresponding to the product including exon 9 (477 bp)(O'Driscoll et al. 2003). These results indicate that some of the *Atr* transcripts are properly spliced in Seckel mice, although most of them suffer an aberrant splicing, creating an isoform lacking exon 9, which introduces a stop codon generating a truncated ATR protein.

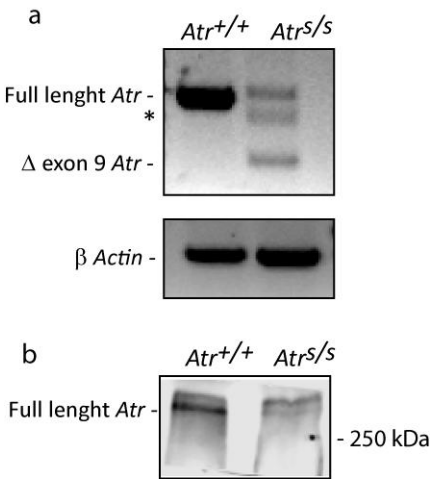

Figure 4.1. Seckel mouse testis present reduced expression of ATR. a) RT-PCR of ATR products using primers at exon 8 and exon 9 for the indicated genotypes. RT-PCR product corresponding to full length Atr (477 bp) is several reduced in $Atr^{s/s}$ testis. Note another RT-PCR product corresponding to Atr lacking exon 9 (284 bp) is present in $Atr^{s/s}$ testis. Asterisk denote unspecific RT-PCR product. **b)** Western blot analyses of ATR for the indicated genotypes. $Atr^{s/s}$ testis show decreased signaling corresponding to ATR protein.

To evaluate the degree of ATR reduction in testis we also performed Western blot analysis from whole testes lysates from control and Seckel mutant mice. Consistent with the results observed by RT-PCR, Seckel mice showed a substantial decrease of the amount of ATR

protein compared to control mice (**Fig. 4.1b**). Thus, these data indicate that indeed, ATR expression is significantly reduced in Seckel mice testis.

4.1.2 Histological characterization of Seckel testis

To investigate the effects of an ATR expression reduction in testicular development we performed histological analysis of testes from adult males. One of the first indicators of a defective spermatogenesis observed in most mutations that compromise meiosis is a decrease in the testicular size (Yuan et al. 2000; Romanienko & Camerini-Otero 2000). Anatomical comparison of mouse testes from Seckel and control animals showed that Seckel males had normalized testis size comparable to the one found in control littermates (0.72 ± 0.02% of total body mass in $Atr^{+/+}$ (avg. ± SEM, N=20); 0.65 ± 0.05% in $Atr^{s/s}$ (N = 20); p>0.05, t test).

Next, we analyzed histological sections from testes. Spermatogenesis takes place in the seminiferous tubules. These contain pre-meiotic (spermatogonia), meiotic (spermatocyte) and post-meiotic cells (spermatids). These different cell types are stratified in the seminiferous tubule, where mitotic and early meiotic cells are located at the base of the tubule, and later meiotic and post-meiotic cells move toward the lumen (Russell et al. 1993). Histological analysis revealed that tubules cross sections from both, Seckel and control males, contained all different cell types and all spermatogenic stages, from spermatogonia to spermatozoa (**Fig. 4.2a**). These data indicate that, despite the reduction of ATR protein in Seckel mouse testes, mutant mice are capable to generate spermatozoa.

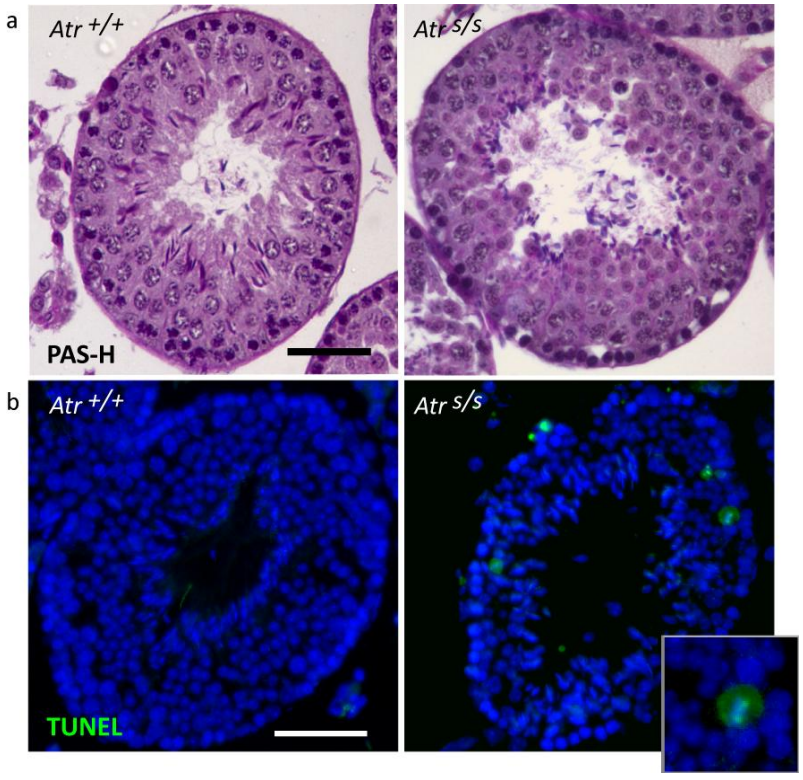

Figure 4.2. Characterization of Seckel testis. a) Seminiferous tubule cross sections from $Atr^{+/+}$ and $Atr^{s/s}$ stained with PAS-Hematoxilin containing all spermatogenic stages, from spermatogonial cells at the base of the tubule to elongated spermatids at the lumen. **b)** TUNEL staining on seminiferous tubules. Presence of apoptotic spermatocytes is marked in green. The image inserted shows an apoptotic spermatocyte at metaphase stage. Bars in the images represent 50 µm.

In addition, in order to determine whether ATR reduction could cause a minor meiotic arrest at some stage, we performed TUNEL assays on testis sections. The results obtained showed that, even thought seminiferous tubules from Seckel mice testis contained all cells going through spermatogenesis, we detected a statistically significant increase in the number of apoptotic spermatocytes. Whereas in control testis we found only 3.7% of the seminiferous tubules exhibit ≥5 TUNEL-positive cells (N=350), in Seckel mouse testis we found that 10.9% of the tubules had ≥5 TUNEL-positive cells (N=276, p=0.0013, Fisher's exact test, **Fig. 4.2b**). Interestingly, most of this apoptotic cells were at metaphase I stage (**Fig. 4.2b-inset**). Then, we decided to analyze whether the number of metaphases present in Seckel testis was higher than the observed in control testis. We reasoned that if more spermatocytes arrest and undergo apoptosis at metaphase I in Seckel testes we might observe an increase number of metaphases per tubule in these animals. Consistent with the TUNEL results, the analysis of the seminiferous tubules showed that mutant animals tended to present an increased number of spermatocytes at metaphase per tubule stage compared to control mice, although this was not statistically significant (0.23 ± 0.09 in $Atr^{+/+}$ (avg. ± SEM, N=128); 0.46 ± 0.13 in $Atr^{s/s}$ (N=170), p>0.05, t test). Together these results indicate that, even though there is a minor arrest occurring in ATR deficient mice, spermatogenesis is not essentially compromised in Seckel mice.

4.1.3 Study of ATR function in meiotic sex chromosome inactivation (MSCI)

It is now well established that the presence of unsynapsed chromosomes axes during meiotic prophase is associated with the activation of checkpoint signaling machinery (Turner et al. 2004; Turner et al. 2005; Garcia-Cruz et al. 2009; Burgoyne et al. 2009). In mammals, from late-zygonema, unsynapsed regions of the genome undergo dynamic remodeling processes related to the incorporation of several proteins to the chromatin resulting in heterochromatinization and transcriptional silencing of those regions (Burgoyne et al. 2009). Heterologous male sex chromosomes remain partially unsynapsed at pachynema and this trigger the inactivation of X and Y-linked genes (MSCI) forming a sub-nuclear domain called the sex body, which is essential for male fertility (Royo et al. 2010). Since sex body formation relies on ATR location to the sex chromatin (Royo et al. 2013), we assessed the physiological implications of *Atr* reduction expression in Seckel mice spermatocytes focusing on how this reduction affected MSCI. To perform this, we compared sex body formation in control and Seckel mouse spermatocytes by immunostaining of different proteins on surface spreads.

Firstly, we analyzed the presence of ATR on sex chromosomes at pachynema. Consistent with previously described data, we observed that ATR accumulates along the axes of the X and Y chromosomes at late-zygonema to early-pachynema transition in control mice, and immediately spreads to the surrounding chromatin forming a cloud (88.7% of the control pachytene spermatocytes analyzed (N=284), **Fig. 4.3a**). Nonetheless, in Seckel mouse spermatocytes ATR localization pattern on the sex chromosomes was disturbed. In this case,

most mutant pachytene cells presented ATR staining confined to the sex chromosome axes (76.8% (N=282), **Fig. 4.3b**). Only a small proportion of pachytene cells presented ATR staining extended to the X and Y chromatin (23.2%, p<0.0001, Fisher's exact test, **Fig. 4.3c**).

Since ATR phosphorylates the histone H2AX to promote meiotic silencing of the X and Y chromosomes (Royo et al. 2013), we investigated γH2AX presence on sex body (**Fig. 4.3d**). Despite the abnormal location of ATR, mutant pachytene spermatocytes presented γH2AX staining extended to the X and Y chromatin forming a visible sex body (**Fig. 4.3e)**. Nevertheless, comprehensive examination of the γH2AX staining showed that Seckel mouse spermatocytes presented a significant reduction of ~40% of the intensity observed on control spermatocytes (44.2 ± 0.99 in $Atr^{+/+}$ (avg. ± SEM, N=80); 27.4 ± 0.78 in $Atr^{s/s}$ (N=98), intensity is showed in arbitrary units, p<0.0001, t test **Fig. 4.3f**).

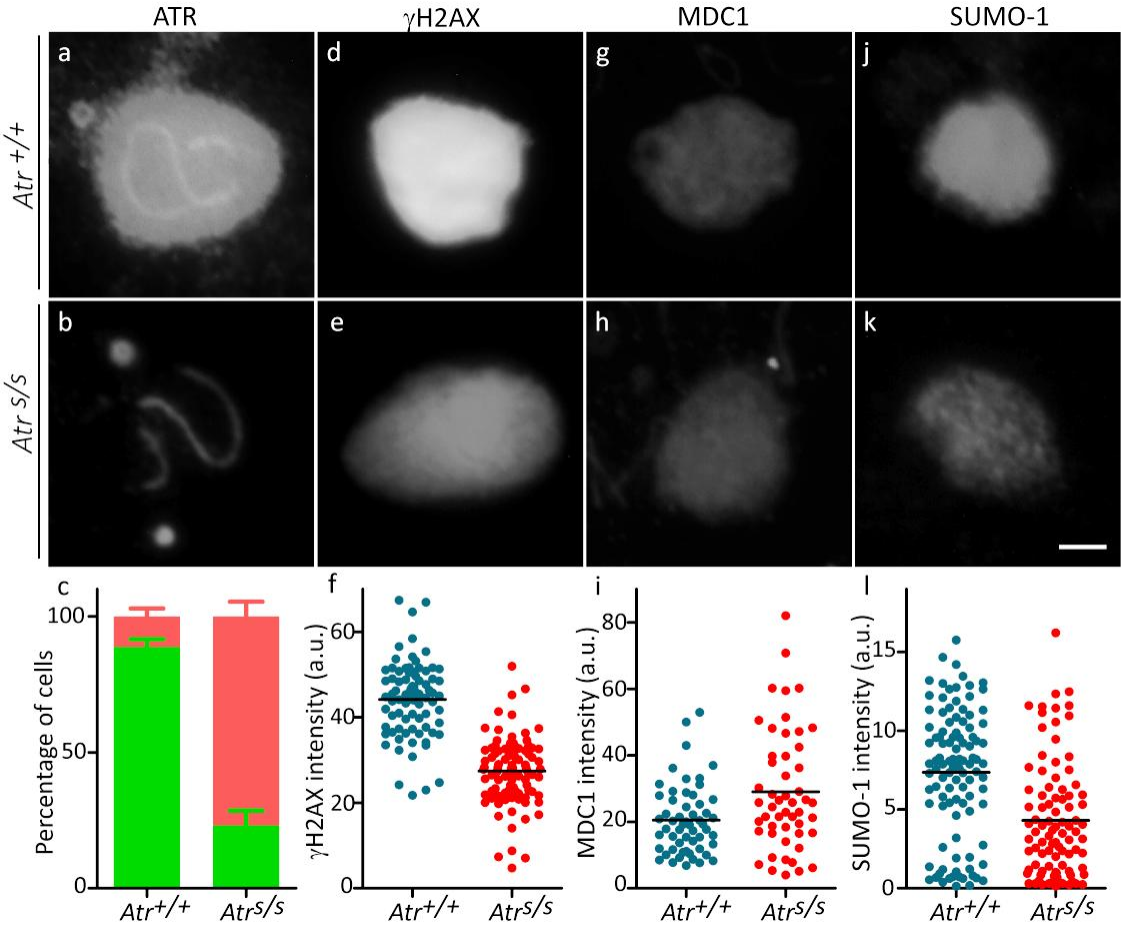

Figure 4.3. Seckel mice exhibit an abnormal sex body formation. a-k) Representative sex body images from $Atr^{+/+}$ and $Atr^{s/s}$ spermatocytes at pachynema immunostained for ATR, γH2AX, MDC1 and SUMO-1 proteins captured with the same exposure time. In $Atr^{s/s}$, sex body presents abnormal accumulation of MSCI proteins. Bar in the images represents 2µm. **c)** Percentage of cells exhibiting ATR staining extended to X and Y chromatin forming a cloud (green) or confined only to the X and Y axes (red) of the indicate genotypes. Columns and lines indicate the mean and standard error (SEM). **f, i, l)** Quantification of the intensity of γH2AX (f), MDC1 (i) and SUMO-1 (l) staining on the sex body from pachytene spermatocytes of the indicate genotypes. Horizontal black lines denote the means. Intensity is expressed in arbitrary units (a.u.).

Recent studies suggested the existence of a positive feedback loop between ATR, γH2AX and MDC1 proteins in which MDC1 was required to properly spread ATR and γH2AX to the X and Y chromatin (Ichijima et al. 2011). Since MDC1 localizes to the XY bivalent on an ATR-dependent manner (Royo et al. 2010), we analyzed the presence of this protein in the sex body of control and Seckel mice. MDC1 was present on the sex chromatin from both, control and mutant pachytene spermatocytes (**Fig. 4.3g,h**), but in contrast to what we observed for γH2AX, Seckel sex body showed a significant increase of ~40% in MDC1 staining compared to the intensity found in control spermatocytes (20.5 ± 1.4 in $Atr^{+/+}$ (N=56); 29 ± 2.5 in $Atr^{s/s}$ (N=51), p=0.0032, t test, **Fig. 4.3i**).

Finally, given that the small ubiquitin-like modifier protein 1 (SUMO-1) preceded γH2AX accumulation on the sex chromosomes during meiotic inactivation (Vigodner 2009) and its incorporation is ATR-dependent (Royo et al. 2013), we analyzed the effect of ATR reduction on this epigenetic modification in the XY pair (**Fig 4.3j,k**). As observed for γH2AX, in Seckel mice the intensity of SUMO-1 on the sex body was significantly reduced (~40%) compared to the intensity found in control cells (7.4 ± 0.4 in $Atr^{+/+}$ (N=104); 4.3 ± 0.4 in $Atr^{s/s}$ (N=94), p<0.0001, t test, **Fig. 4.3l**).

According to these findings, reduction of ATR expression in Seckel mouse testes affects the known physiological functions of ATR during meiosis. Thus, these data validate the use of Seckel mouse model to study the role of ATR during meiotic recombination.

4.1.4 Evaluating the role of ATR in homologous synapsis

One of the most relevant challenges of meiosis is the identification of homologous chromosome pairs in order to establish connections between them to achieve a proper segregation during the first meiotic division, as well as, to generate genetic diversity within a population by the transmission of new allelic combinations to the progeny. In order to achieve this goal, meiotic cells have devised different strategies. In most organisms, including mouse, the ability of homologous to find each others, pair and synapse require DNA DSBs (Baudat et al. 2000; Handel & Schimenti 2010), highlighting clear evidences for a close dependent relationship between synapsis and homologous recombination.

ATR has been previously identified in the sites where homologous recombination occurs (Keegan et al. 1996; Plug et al. 1998; Moens et al. 1999). For this reason, we decided to perform an exhaustive characterization of synapsis progression and homologous recombination during meiotic prophase to determine whether ATR deficiency was affecting these processes.

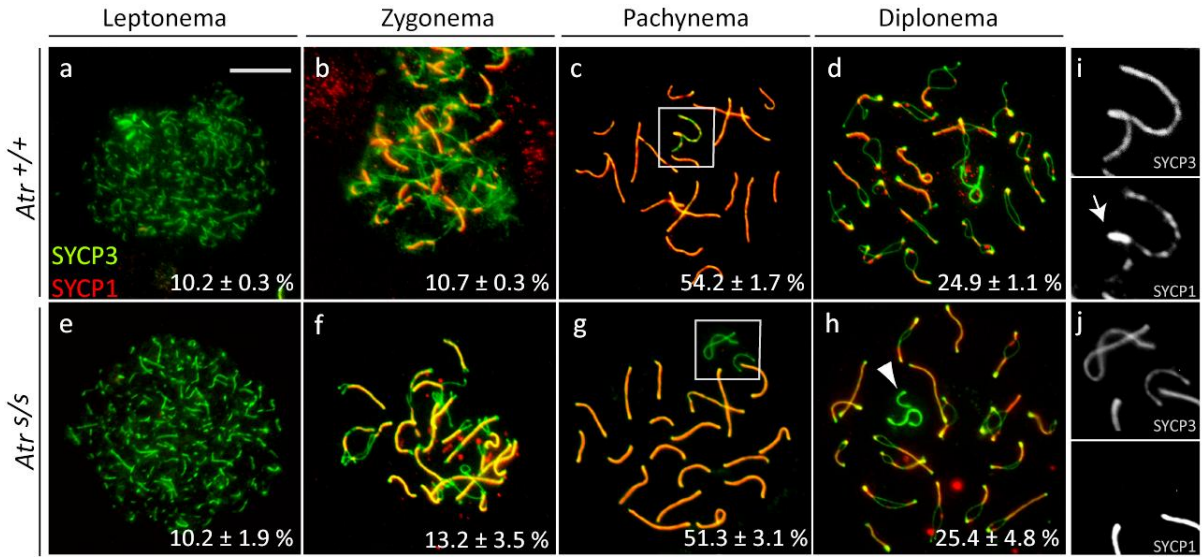

Figure 4.4. Seckel spermatocytes complete autosomal synapsis but fail to synapse the XY pair. a-h) Representative images from *Atr*$^{+/+}$ and *Atr*$^{s/s}$ showing progression of meiotic prophase followed by immunostaining of spermatocyte spreads against SYCP3 (green) and SYCP1 (red). Bar in the images represents 10 µm. Numbers indicate the percentage of spermatocytes (avg. ± SEM) found at each stage of the meiotic prophase from *Atr*$^{+/+}$ (N=402) and *Atr*$^{s/s}$ (N=370). Seckel mice spermatocytes (e-h) achieve a complete autosomal synapsis comparable to *Atr*$^{+/+}$. Note the presence of unsynapsed X and Y chromosomes in Seckel spermatocytes at pachynema (g, white box) and diplonema (h, arrowhead). **i-j)** Magnified images of sex chromosomes at pachytene stage (white boxes). In control spermatocytes sex chromosomes synapse at pachytene as demonstrated by the presence of SYCP1 in the PAR (arrow). Seckel mice spermatocytes exhibit not aligned sex chromosomes presenting only SYCP3 staining.

Firstly, we studied how synapsis was accomplished in an ATR deficient scenario. To perform this, we followed synapsis progression in control and Seckel mice by immunostaining spermatocyte spreads against SYCP3 and SYCP1 proteins, as a marker of the AE and CE of the synaptonemal complex, respectively. In control spermatocytes, we observed that at the onset of prophase SYCP3 began to appear forming the AE over the axis of each homologous chromosome (**Fig 4.4a**). At zygonema synapsis started and leading to the formation of the CE, containing SYCP1 that appears holding the AE together to form the SC (**Fig 4.4b**). At pachynema autosomal homologous chromosomes were fully synapsed and SYCP3 and SYCP1 proteins completely co-localize (**Fig. 4.4c**). At diplonema SCs dissociated, thus SYCP1 disappeared from the central region of the SC, but homologous chromosomes remained connected by chiasma (**Fig. 4.4d**). Seckel mouse synapsis progression was similar to what we observed in control cells (**Fig. 4.4e-h**). We found undistinguishable proportion of spermatocytes at different prophase stages in both genotypes (p=0.6236, G test), indicating that Seckel mice spermatocytes exhibit proper autosomal synapsis through all prophase stages. Nevertheless, we detected impaired sex chromosomes synapsis. We found that mutant pachytene spermatocytes presented two times more unsynapsed X and Y chromosomes than control cells (12.2% in *Atr*$^{+/+}$ (N=197); 25.1% in *Atr*$^{s/s}$ (N=235), p=0.0013, Fisher's exact test) (**Fig. 4.4i-j**). Moreover, the analysis of sex chromosome synapsis at late-diplonema showed that, although the number of unsynapsed sex chromosomes increased in both genotypes

compared to what we observed at pachynema, we found similar number of unsynapsed sex chromosomes in control and mutant cells (29.3% in $Atr^{s/s}$ (N=150); 32.8% in $Atr^{+/+}$ (N=259), p=0.5083, Fisher's exact test). These results suggest that, regardless autosomal synapsis is not affected in Seckel mouse spermatocytes, wild type levels of ATR are required to ensure a proper synapsis of sex chromosomes.

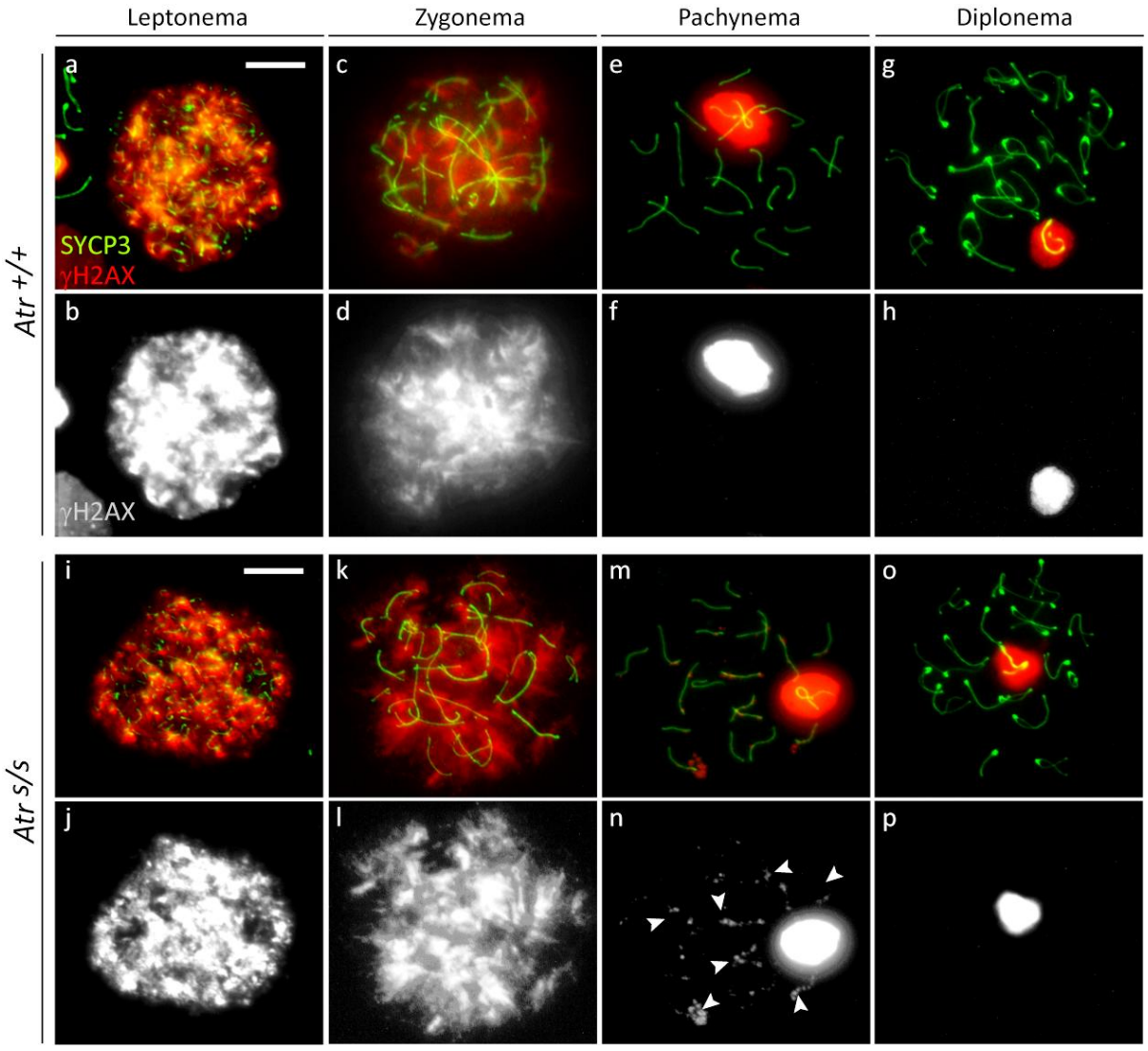

Figure 4.5. Dynamic of γH2AX staining during meiotic prophase I. a-p) Representative images of spermatocytes at different stages of meiotic prophase immunostained against SYCP3 (green) and γH2AX (red) from $Atr^{+/+}$ and $Atr^{s/s}$ mice. Bars in the images represent 10 µm. In control spermatocytes γH2AX staining appears over all chromatin in early-prophase stages in response to SPO11 generated-DSBs and begins to disappear as homologous chromosomes synapse and DSBs are repaired. From pachytene γH2AX is recruited to X and Y chromosomes (f-h). γH2AX staining in Seckel mice spermatocytes shows similar dynamic than in control cells (i-p). Nevertheless, still some patches of γH2AX are present in autosomal bivalents indicating some DSBs remain unrepaired at late-prophase stages (n, arrowheads).

4.1.5 Analysis of ATR implication in meiotic DSB repair and homologous recombination

It was long recognized that homologous recombination is required to ensure proper homology search and efficient homologue associations. Given that, defects in synapsis are strongly correlated to defects in DSBs-repair (Bannister & Schimenti 2004b), we decided to investigate whether the defects in sex chromosome synapsis found in Seckel meiocytes might as well reflect defects in meiotic recombination. Homologous recombination initiates at the beginning of leptonema by the induction of programmed DSBs catalyzed by SPO11 protein (Keeney et al. 1997). These DSBs must be repaired during meiotic prophase to achieve viable meiocytes and it occurs in the context of the SC. DSB repair can be monitored indirectly by staining different recombination intermediates. Firstly, we performed immunostaining against the histone variant γH2AX, which is phosphorylated by ATM at early prophase in response to DSBs (Mahadevaiah et al. 2001; Bellani et al. 2005; Barchi et al. 2008). In control mice, we observed that at leptonema γH2AX was accumulated on all chromatin due to the presence of SPO11-generated DSBs (**Fig 4.5a,b**). At zygotene, γH2AX progressively disappeared as DSBs were repaired in the synapsed regions (**Fig 4.5c,d**). At pachynema and diplonema γH2AX was mostly confined to the sex chromosomes (**Fig. 4.5e-h**). Similar to control spermatocytes, in Seckel mouse spermatocytes we observed a normal γH2AX dynamic during leptonema and zygonema (**Fig. 4.5i-l**). Nonetheless, at pachynema and diplonema, although γH2AX was recruited to the sex body, we observed γH2AX patches that remained on autosomal synapsed regions (**Fig. 4.5m-p**).

Previous studies of mouse recombination mutants have demonstrated that the persistence of unrepaired DSBs at pachynema causes the accumulation of γH2AX at these sites forming patches (Li et al. 2007; Barchi et al. 2008; Roig et al. 2010). Consequently to quantify the effect of an ATR activity reduction on meiotic recombination we analyzed the presence of γH2AX patches on early and late-pachytene and diplotene spermatocytes from control and Seckel mice. At the onset of pachynema, some meiotic DSBs are still present in control cells (**Fig. 4.6a**), which are almost completely repaired by the time of mid/late-pachynema (**Fig. 4.6b,c**). In order to distinguish between these two stages we performed immunostaining against the testis-specific histone H1 variant, H1t, which replace somatic H1 at mid-pachytene being incorporated to the chromatin (Drabent et al. 1996; Inselman et al. 2003). Interestingly, we observed that Seckel mouse spermatocytes tended to present more unrepaired DSBs in all stages analyzed (**Fig. 4.6d-f**). Although, at early-pachynema there were not statistically significant differences between the γH2AX patches counted in control and mutant meiocytes (16.6 ± 1.6 in $Atr^{+/+}$ (avg. ± SEM, N=49); 20.4 ± 1.4 in $Atr^{s/s}$ (N=60), p=0.0809, t test, **Fig. 4.6g**), at late-pachynema we observed a significant increase in the number of γH2AX patches on synapsed autosomes (1.8 ± 0.3 in $Atr^{+/+}$ (N=43); 5.0 ± 1.5 in $Atr^{s/s}$ (N=68), p<0.0001, t test, **Fig. 4.6h**). Moreover, whereas at diplonema in control cells the number of γH2AX patches was almost inexistent, mutant spermatocytes presented higher number of γH2AX patches (0.8 ±

0.2 in *Atr*$^{+/+}$ (N=32); 3.4 ± 0.6 in *Atr*$^{s/s}$ (N=46), p=0.0007, t test, **Fig. 4.6i**). These data suggest that Seckel mouse spermatocytes exhibit unrepaired DSBs at late-prophase stages.

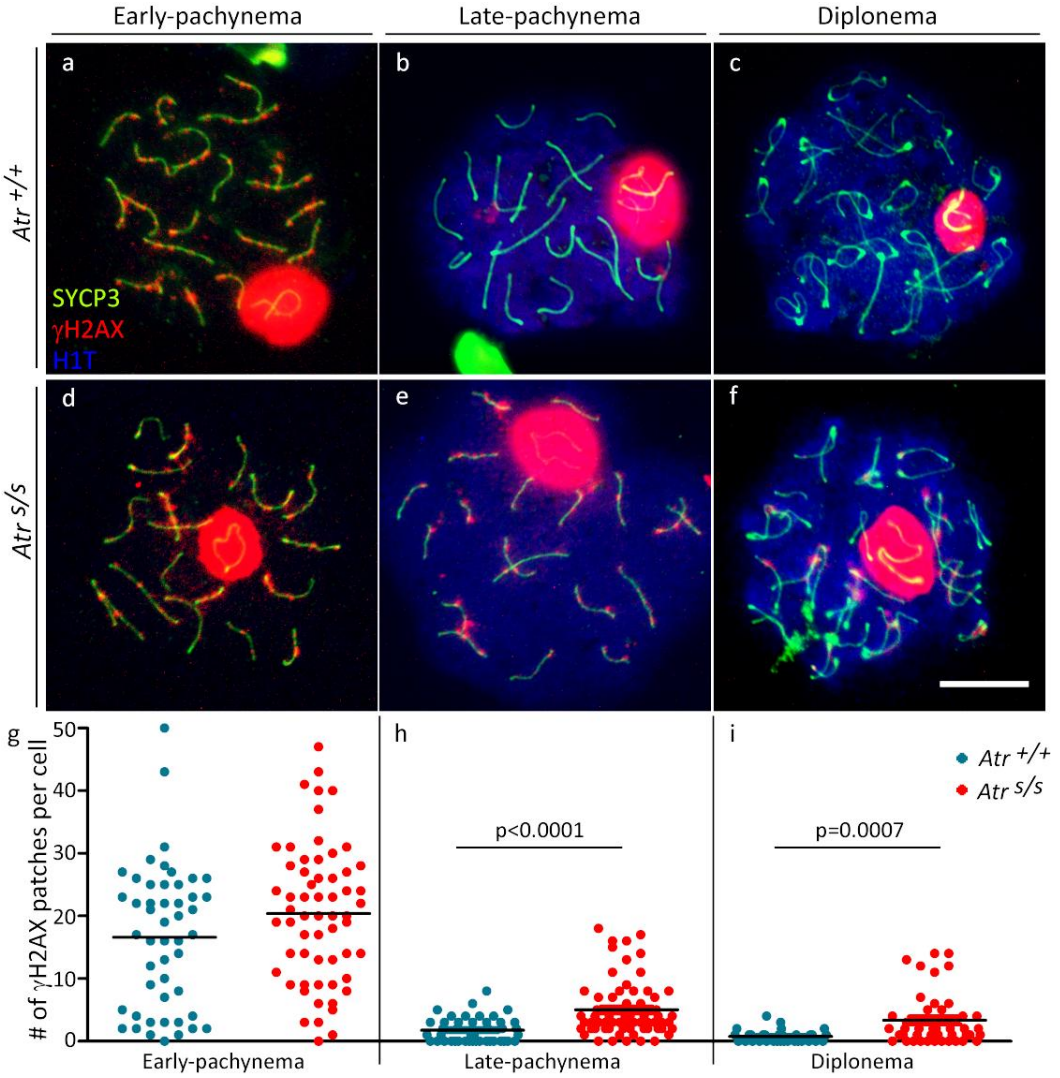

Figure 4.6. Seckel spermatocytes exhibit significant unrepaired DSBs at late-prophase stages. a-f) Immunostaining against SYCP3 (green), γH2AX (red) and H1T (blue) show the presence of meiotic DSBs in *Atr*$^{+/+}$ and *Atr*$^{s/s}$ spermatocytes. Bar in the images represent 10 µm. Note that the number of DSBs at early-pachynema (H1T-negative cells) is similar between *Atr*$^{+/+}$ and *Atr*$^{s/s}$ spermatocytes, besides, at late-pachynema (H1T-positive cells) Seckel spermatocytes accumulate more unrepaired DSBs on autosomal chromosomes than control cells. **g-i)** Quantification of total γH2AX foci present in each nucleus analyzed in *Atr*$^{+/+}$ and *Atr*$^{s/s}$ spermatocytes at the indicated stages. Horizontal black lines denote the means. A significant increase of γH2AX foci at late-prophase stages (late-pachynema and diplonema) was observed in Seckel mice spermatocytes relative to control cells.

To gain insight into the implication of ATR in homologous recombination we aimed at characterizing further recombination intermediates present at recombination nodules during different prophase stages in control and Seckel mice spermatocytes. RAD51 recombinase is a mammalian RecA-homolog protein, which associates at early stages of prophase with resected DSBs to assist homology search promoting strand invasion of the homologous chromosomes

(Kolas et al. 2005; Moens et al. 2007). Hence, RAD51 is present on DSB sites until these are repaired. Therefore, we assessed progression in DSB repair by observing changes in the RAD51 foci numbers. In control spermatocytes, we detected RAD51 foci accumulating at leptonema, where they reached a maximum peak. As meiotic prophase progressed, RAD51 foci counts dropped until diplonema, where most RAD51 foci found localized at the X and Y pair (**Fig. 4.7a**, **Table 4.1**,). In mutant spermatocytes, although RAD51 staining also decreased throughout prophase, we detected a significant increase of RAD51 foci at pachynema ($p=0.0005$, t test, **Table 4.1**). At this stage, several foci were still present on autosomal chromosomes, consistent with the persistent γH2AX patches observed at late-prophase stages. In addition, we identified that Seckel mouse spermatocytes presented a significant decrease of RAD51 foci numbers at early-leptonema compared to control spermatocytes ($p=0.0073$, t test, **Fig. 4.7a,b**). Thus, to further investigate ATR involvement in meiotic recombination, we analyzed DMC1 foci formation during meiotic prophase. The meiosis-specific RecA homolog DMC1 protein, along with RAD51, forms nucleoprotein filaments on DNA to direct homologous search and catalyze strand exchange (Bishop et al. 1992; Tarsounas et al. 1999; Cloud et al. 2012). Therefore, in control spermatocytes the appearance of DMC1 during prophase was similar to the results observed for RAD51 (**Table 4.1**). Accordingly, in Seckel mouse spermatocytes we observed a similar increase in DMC1 foci numbers at pachynema compared to control cells ($p<0.0001$, t test, **Fig. 4.7c,d**, **Table 4.1**). Moreover, during early-prophase, Seckel mice spermatocytes showed decreased number of DMC1 foci in all stages analyzed (**Fig. 4.7c**). Remarkably, while the analysis of RAD51 foci number in Seckel mice showed a significant reduction only at early-leptonema compared to control spermatocytes, the analysis of DMC1 foci number showed a more affected phenotype in mutant spermatocytes exhibiting a significant decrease at early-leptonema ($p=0.0076$, t test) and late-leptonema ($p<0.0001$, t test), as well as, at early-zygonema ($p=0.0364$, t test) and late-zygonema compared to control spermatocytes ($p=0.0355$, t test). Thereby, these observations suggest that DSB repair progression is altered in Seckel mice; first, by the reduction in the number of RAD51 and DMC1 foci at early-prophase stages, and secondly, by the presence of unrepaired breaks at late-prophase stages.

One possible explanation for the drop in the number of RAD51 and DMC1 at early-prophase is that Seckel mice exhibit defects in the formation or processing of programmed DSBs at the onset of prophase. Alternatively, Seckel mice spermatocytes might fail to load RAD51 and DMC1 to resected DSB sites. To discern between these two possibilities we examined the behavior of RPA protein. RPA is a single stranded DNA binding protein, which acts during early-recombination binding the exposed ssDNA resulting from DSBs resection, but only transiently, before RAD51 and DMC1 accumulates at these sites (Moens et al. 2007; Yang et al. 2008a). Immunostaining against RPA showed that control spermatocytes presented approximately 150 foci at early prophase reaching a peak at early-zygotene, when RPA coated ssDNA present at DSB sites as a result of homologous invasion mediated by RAD51 and DMC1 (**Fig. 4.7e, Table 4.1**). Thereafter, RPA foci number progressively disappeared as DSBs were repaired. In contrast, mutant spermatocytes showed a significant increase in the number of

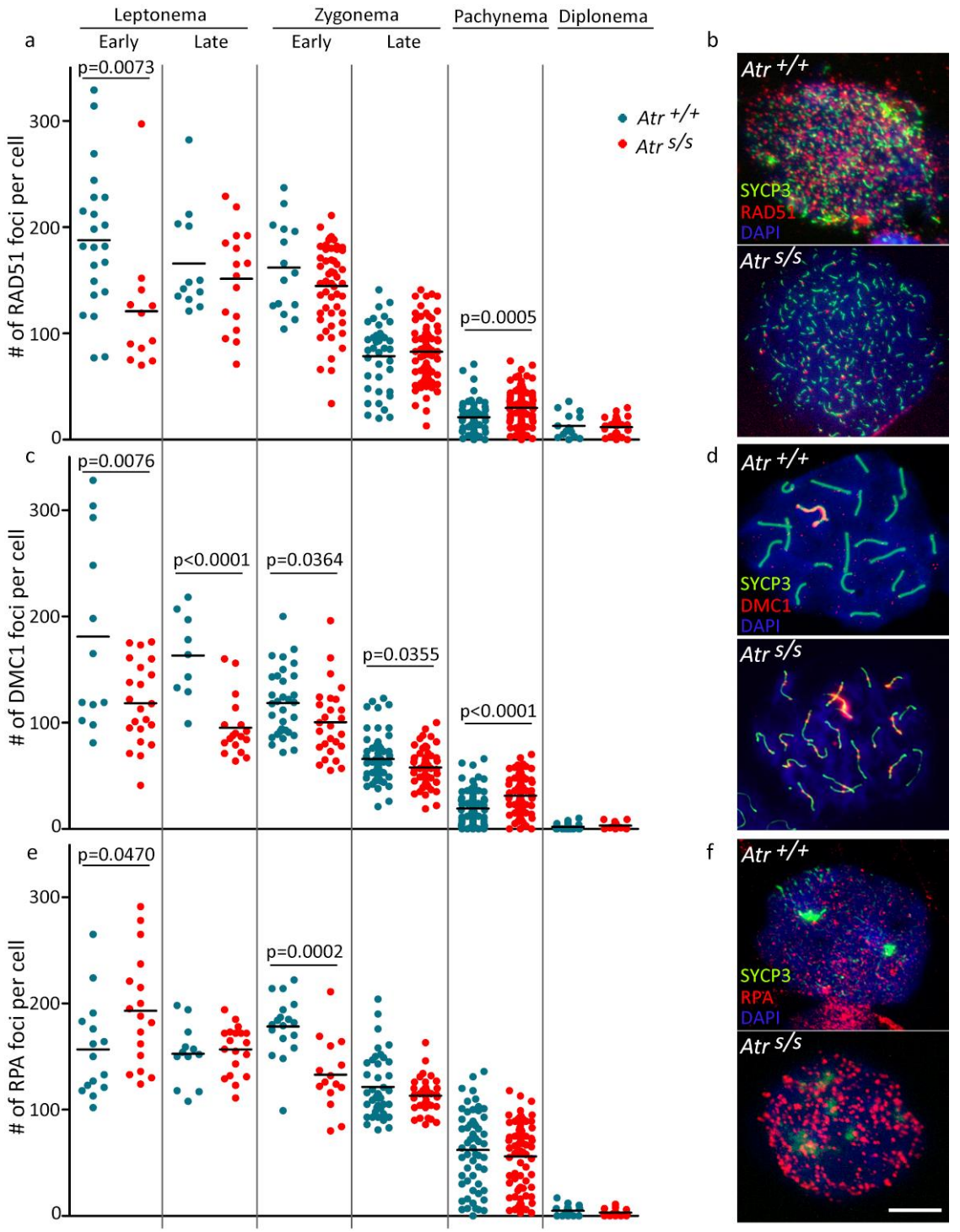

Figure 4.7. Recombination foci of DSB intermediate proteins present in control and Seckel mice spermatocytes during prophase. a) Quantification of total RAD51 foci per spermatocyte at the indicated stages. Horizontal lines denote the means. **b)** Representative images of early-leptotene spermatocytes from the indicated genotypes immunostained against SYCP3 (green), RAD51 (red) and DNA (DAPI, blue). Note the reduced number of RAD51 foci present in the *Atr*$^{s/s}$ cell. **c)** Quantification of total DMC1 foci per spermatocyte at the indicated stages. **d)** Pachytene spermatocytes from the indicated genotypes immunostained against SYCP3 (green), DMC1 (red) and DNA (DAPI, blue). Some DMC1 foci are present in autosomal bivalents in *Atr*$^{s/s}$ pachytene evidencing unrepaired DSBs. **e)** Quantification of total RPA foci per spermatocyte at the indicated stages. **f)** Representative spermatocytes at leptonema from the indicated genotypes immunostained against SYCP3 (green), RPA (red) and DNA (DAPI, blue). RPA persistence at DSB sites indicates early recombination defects in *Atr*$^{s/s}$ mice. Bar in the image represent 10µm.

RPA foci present at early-leptonema compared to control spermatocytes (p=0.0470, t test, **Figure 4.7f**, **Table 4.1**) reflecting that DSB formation was not defective in Seckel mice, otherwise the ssDNA-bound RPA persisted at DSB sites due to RAD51 and DMC1 loading was defective. Consequently, at early-zygotene, when homologous invasion occurs, Seckel mouse spermatocytes showed a significant decrease in the number of RPA foci compared to control cells (p=0.0002, t test). These data suggest that DSB repair is delayed when the amount of ATR is deficient. Together, these findings reveal that ATR is required to achieve a proper meiotic homologous recombination at early and late-stages of prophase, playing a role in the loading of RAD51 and DMC1, and therefore, being necessary to a timely proper homologous strand invasion.

Table 4.1. Recombination foci numbers presents in spermatocytes at different stages of prophase from the indicated genotypes. Data from RAD51, DMC1 and RPA staining analysis expressing the average and SEM of the number of foci present in spermatocytes at the indicated stages of prophase from the indicated genotypes.

		Early-leptonema	Late-leptonema	Early-zygonema	Late-zygonema	Pachynema	Diplonema
RAD51	$Atr^{+/+}$	187.6 ± 14.2, N=22	165.8 ± 14.0, N=12	162.0 ± 11.0, N=15	78.5 ± 5.3, N=38	21.0 ± 1.9, N=61	13.1 ± 3.0, N=15
	$Atr^{s/s}$	120.8 ± 17.9, N=12	151.4 ± 11.9, N=16	144.5 ± 5.4, N=53	82.8 ± 3.1, N=79	29.9 ± 1.6, N=104	11.9 ± 1.6, N=29
DMC1	$Atr^{+/+}$	180.0 ± 26.0, N=12	163.1 ± 13.4, N=9	118.5 ± 5.6, N=32	65.81 ± 3.0, N=58	19.3 ± 1.8, N=77	2.07 ± 0.5, N=28
	$Atr^{s/s}$	118.3 ± 8.2, N=22	95.2 ± 6.5, N=18	100.3 ± 6.5, N=27	57.73 ± 2.3, N=56	31.2 ± 1.9, N=80	3.2 ± 0.9, N=13
RPA	$Atr^{+/+}$	156.8 ± 11.7, N=15	152.5 ± 8.1, N=12	178.2 ± 6.7, N=18	121.4 ± 4.5, N=42	62.2 ± 4.8, N=58	4.9 ± 1.1, N=18
	$Atr^{s/s}$	193.0 ± 12.7, N=17	156.8 ± 5.3, N=19	132.9 ± 8.7, N=15	113.1 ± 2.4, N=41	56.8 ± 3.6, N=79	3.2 ± 0.6, N=24

4.1.6 The control of crossover formation

The generation of CO is critical to achieve proper reductional division at meiosis I. It is estimated that in mouse only approximately 10% of SPO11-generated DSBs are repaired as COs, reflecting the existence of robust mechanism controling CO formation (Martini et al. 2006; Jones & Franklin 2006; Cole et al. 2012). Thus, we asked whether recombination defects seen in Seckel spermatocytes could affect CO formation. To test this idea, we analyzed MLH1, which appears at destined CO sites at pachynema (Baker et al. 1996; Anderson et al. 1999). It is important to emphasize that the presence of physical linkages (chiasmata) between homologous chromosomes is crucial to accurately segregate homologous chromosomes at metaphase I, so that, at least one CO per bivalent is required to ensure a proper orientation of this bivalent on the first meiotic spindle (Marcon & Moens 2003; Moens et al. 2007). Given that MLH1 foci appear progressively from early-pachynema to mid/late pachynema when

MLH1 foci start to disappear (Anderson et al. 1999), to do this analysis only nuclei with bright MLH1 foci were analyzed. Considering this, immunofluorescence against MLH1 protein showed that the number of autosomal MLH1 foci present in Seckel mice spermatocytes was significantly lower than in control cells (22.6 ± 0.21 in $Atr^{+/+}$ (avg. ± SEM, N=90); 21.6 ± 0.24 in $Atr^{s/s}$ (N=101), p = 0.0049, Mann Whitney test, **Fig. 4.8a**). Interestingly, this reduction in MLH1 foci was correlated with a significant increase in the number of autosomal bivalents lacking one MLH1 foci at pachynema (1.4% of the bivalents in $Atr^{+/+}$ (N=1520); 3.2% of the bivalents in $Atr^{s/s}$ (N=1653), p=0.0009, Fisher's exact test, **Fig. 4.8b,c**).

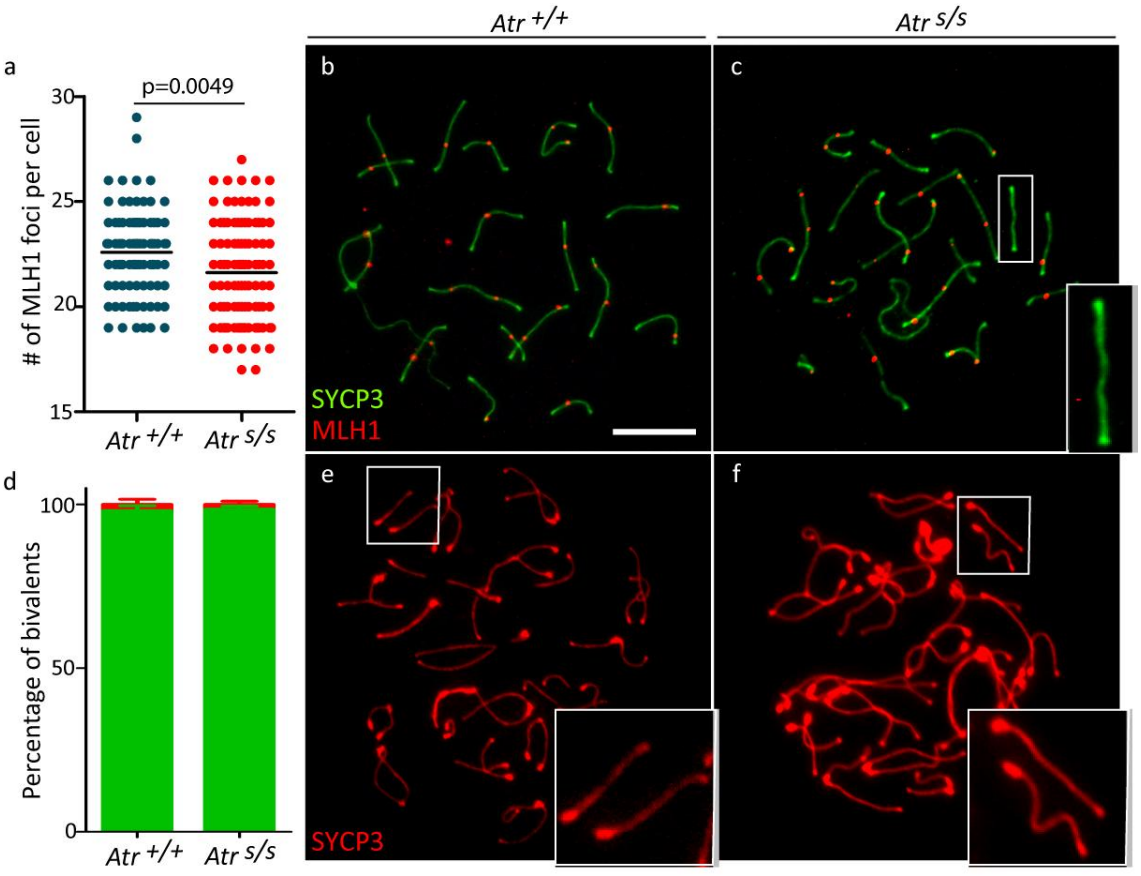

Figure 4.8. Autosomal MLH1 foci formation is delayed in Seckel mice spermatocytes. a) Quantification of autosomal MLH1 foci presents in $Atr^{+/+}$ and $Atr^{s/s}$ pachytene spermatocytes. Horizontal black lines denote the means. A significant reduction of MLH1 foci was observed in Seckel spermatocytes relative to control cells. **b-c)** Representative images of pachytene spermatocytes from the indicated genotypes immunostained against SYCP3 (green) and MLH1 (red). White box in $Atr^{s/s}$ spermatocytes (c) denotes the presence of a bivalent lacking an MLH1 focus, which is zoomed in the image inset. **d)** Percentage of chiasmate (green) and achiasmate bivalents present at diplonema (red) from the indicated genotypes. Columns and lines indicate the mean and standard error (SEM). **e-f)** Representative images of diplotene spermatocytes from the indicated genotypes immunostained against SYCP3 (red). White boxes denote the presence of achiasmate bivalents in both genotypes, which are zoomed in the image inset.

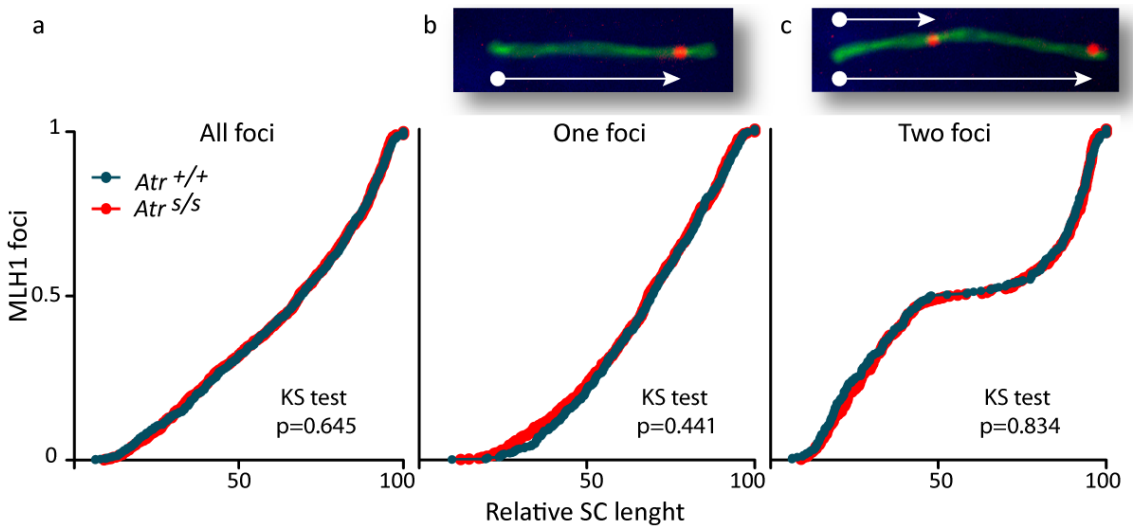

Figure 4.9. Study of MLH1 foci distribution along autosomal bivalents in control and Seckel mice spermatocytes. a) Cumulative frequency plot comparing MLH1 foci position along all autosomal bivalents from $Atr^{+/+}$ (N=924) and $Atr^{s/s}$ (N=932) pachytene spermatocytes. Note that both genotypes exhibit similar distribution of MLH1 foci. **b)** Cumulative frequency plot exhibiting similar MLH1 distribution in SC presenting one MLH1 focus from $Atr^{+/+}$ (N=581) and $Atr^{s/s}$ (N=601) pachytene spermatocytes. The image inset shows a representative pachytene autosomal bivalent immunostained against SYCP3 (green) and MLH1 (red). Arrow exemplifies how MLH1 focus distance from the centromere is measured. Foci tend to be located in the centromere-distal region of the SC. **c)** Cumulative frequency plot shows undistinguishable MLH1 distribution curves in pachytene bivalents presenting two MLH1 foci from $Atr^{+/+}$ (N=350) and $Atr^{s/s}$ (N=369) spermatocytes. The image inset shows a representative SC immunostained against SYCP3 (green) and MLH1 (red). Note that when bivalents present two foci, one tends to be located in the interstitial region of the SC, and the second one tends to appear in the centromere-distal telomeric region.

Since several studies have suggested a relationship between the total number of CO events present at pachynema and the SC length (Lynn et al. 2002; Kleckner et al. 2003), we evaluated whether lower MLH1 foci number found in $Atr^{s/s}$ pachytene spermatocytes was a result of a different SC length. The results obtained from the measure of total autosomal SC length for each control and mutant spermatocyte showed that on average total autosomal SC length was fundamentally similar between the two genotypes (159.3 ± 2.3 µm in $Atr^{+/+}$ (avg. ± SEM, N=39); 153.4 ± 3.0 µm in $Atr^{s/s}$ (N=40), p=0.1279, t test). This suggest that the reduction in MLH1 foci found in Seckel mice spermatocytes was not derived from the presence of shorter SCs. Therefore, at least two different scenarios might illustrate the reduction in MLH1 foci found in Seckel mice spermatocytes at pachynema. One would be that fewer DSBs were resolved as CO events. Alternatively, the other would be that in ATR mutants, CO formation was delayed. To discriminate between these two options, we analyzed the frequency of achiasmate autosomal chromosomes at diplonema. In control spermatocytes, only a minority of bivalents lack a chiasmata (1.5% of the bivalents (N=42), **Fig. 4.8d**). Achiasmate bivalents were observed as two separated univalents at diplonema (**Fig. 4.8e,f**). Mutant spermatocytes showed a normal number of achiasmate autosomal chromosomes (1.3% of the bivalents (N=48), p=0.8378, Fisher's exact test) indicating that most Seckel mouse spermatocytes

achieved at least one CO per autosomal bivalent at diplonema. Consistent with our previous results, these data suggest that CO formation is delayed in Seckel mice as a consequence of a delayed meiotic recombination.

It is widely accepted that CO control mechanisms regulate, not only the number of CO events, but also the location. This mechanism implies that the presence of one CO event is subjected to a positive interference leading to a non-random distribution of them (Jones & Franklin 2006; Baudat & de Massy 2007). In this way, we inquired how ATR reduction was affecting CO distribution along the autosomal SCs. To evaluate this, we measured the distance of each MLH1 focus to the centromeric end of the SC and we expressed these distances as a percentage of the length of the SC. The analysis of MLH1 foci position showed similar distribution of all MLH1 foci along the autosomal SCs in both genotypes (p=0.645, Kolmogorov-Smirnov tests, **Fig. 4.9a**). In those cases when only one MLH1 focus was formed in a bivalent, in both genotypes, this tended to be located near the centromere-distal telomeric region of the SC (p=0.441, Kolmogorov-Smirnov tests, **Fig. 4.9b**). Whereas, in the cases when two MLH1 foci were formed in a bivalent, the first foci tended to be located in the centromere-proximal half of the SC, and the second one, close to the centromere-distal telomeric region (p=0.834, Kolmogorov-Smirnov tests, **Fig 4.9c**).

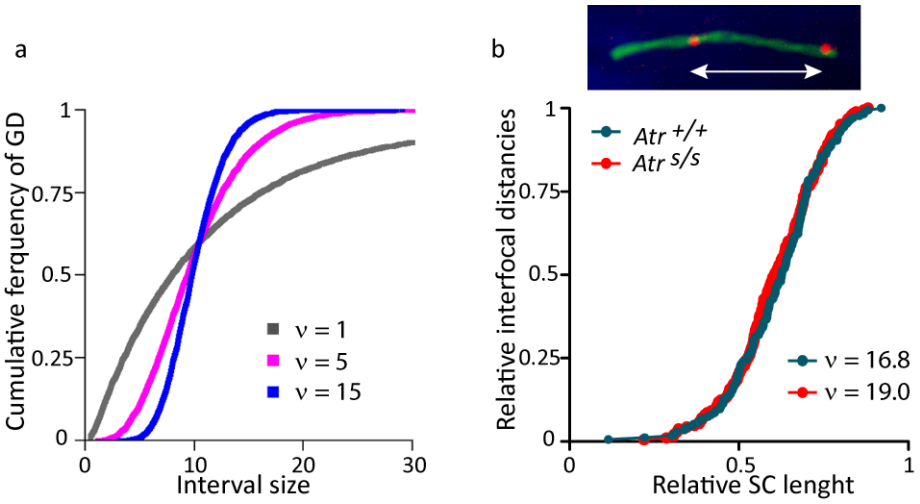

Figure 4.10. Cytological interference in autosomal chromosomes from control and Seckel mice. a) Example of cumulative plot of gamma distribution (GD). When interference between MLH1 foci in a bivalent is inexistent, an exponential frequency distribution is expected (gray curve) indicating that MLH1 foci are randomly distributed. The existence of interference modifies the distribution (blue and purple curves). Stronger interference between focus implies higher ν values. Image modified from (Barchi et al. 2008). **b)** MLH1 interfocal distances from $Atr^{+/+}$ and $Atr^{s/s}$ mice (blue and red curves, respectively) are undistinguishable showing normal patterns of MLH1 distribution along autosomal bivalents. The image inset shows a representative pachytene autosomal bivalent immunostained against SYCP3 (green) and MLH1 (red). Interfocal distances were measured in autosomal bivalents containing two MLH1 foci and are expressed as a percentage of total SC length.

Finally, we also measured the distance between two MLH1 foci as a cytological estimation of CO interference. Interference refers to the observation that the presence of one CO event in a chromosome region reduces the probability that another CO occurs in an adjacent chromosome region (Anderson et al. 1999; Jones & Franklin 2006; de Boer et al. 2006). As previously, interfocal distances were expressed as a percentage of total SC length (**Fig 4.9a**). The strength of cytological interference can be mathematically modeled using the gamma distribution (GD). The GD that best fits a particular set of interfocal distances is characterized by a shape parameter (ν) which is used as an indicator of the strength of the interference occurring in a particular sample. Thus, the higher ν value, the stronger the interference observed (**Fig. 4.10a**). Our analysis showed that Seckel mouse spermatocytes exhibited normal pattern of MLH1 foci interference analogous to the observed in control spermatocytes (ν=16.8 for inter-focus distances in $Atr^{+/+}$; ν=19.0 for inter-focus distances in $Atr^{s/s}$, GD tests, **Fig. 4.10b**). These results indicate that, although wild type levels of ATR are required for a timely correct number of CO events at pachynema, CO distribution is not affected in these conditions.

4.1.7 Recombination in sex chromosomes

Previous studies have demonstrated that sex chromosomes in males present high susceptibility to meiotic recombination failure (Mohandas et al. 1992; Shi et al. 2001; Hall et al. 2006). The X and Y chromosomes share only a small region of homology called the pseudoautosomal region (PAR) which estimated size is ~700kb (Perry et al, 2001). Given that X and Y chromosome homology search and pairing can only be mediated by DSBs occurring within the PAR, these chromosomes are naturally more susceptible to suffer synaptic alterations than the autosomes. Therefore, the X and Y pair is substantially more sensitive to suffer recombination defects causing sex chromosomes segregation to be particularly difficult in males (Page et al. 1987; Hunt & LeMaire 1992; Kauppi et al. 2012).

Recent studies found that PAR presents unusual characteristics during meiosis (Kauppi et al. 2011; Kauppi et al. 2013), including the formation of belated DSBs in this region, presumably as an inherent control mechanism in which unsynapsed chromosome axes are subjected to continued DSB formation. Consequently, recombination and pairing in male sex chromosomes are temporally delayed compared to autosomal chromosomes. As mentioned above, Seckel mouse spermatocytes showed an increased rate of unsynapsed X and Y chromosomes at late prophase stages. Then, we inquired whether DSB formation, repair and subsequent CO formation in the PAR might be inefficient in an ATR reduced scenario leading to the presence of unsynapsed sex chromosomes at pachytene and diplotene cells. Firstly, we indirectly analyzed DSB formation and processing in the PAR by scoring foci density of intermediate DSB markers on the X chromosome at early and late-zygotene stages. To assess this, we performed immunostaining against RAD51 or RPA, followed by FISH to identify X-PAR region detecting the PAR-proximal Scml2 gene in control and mutant spermatocytes.

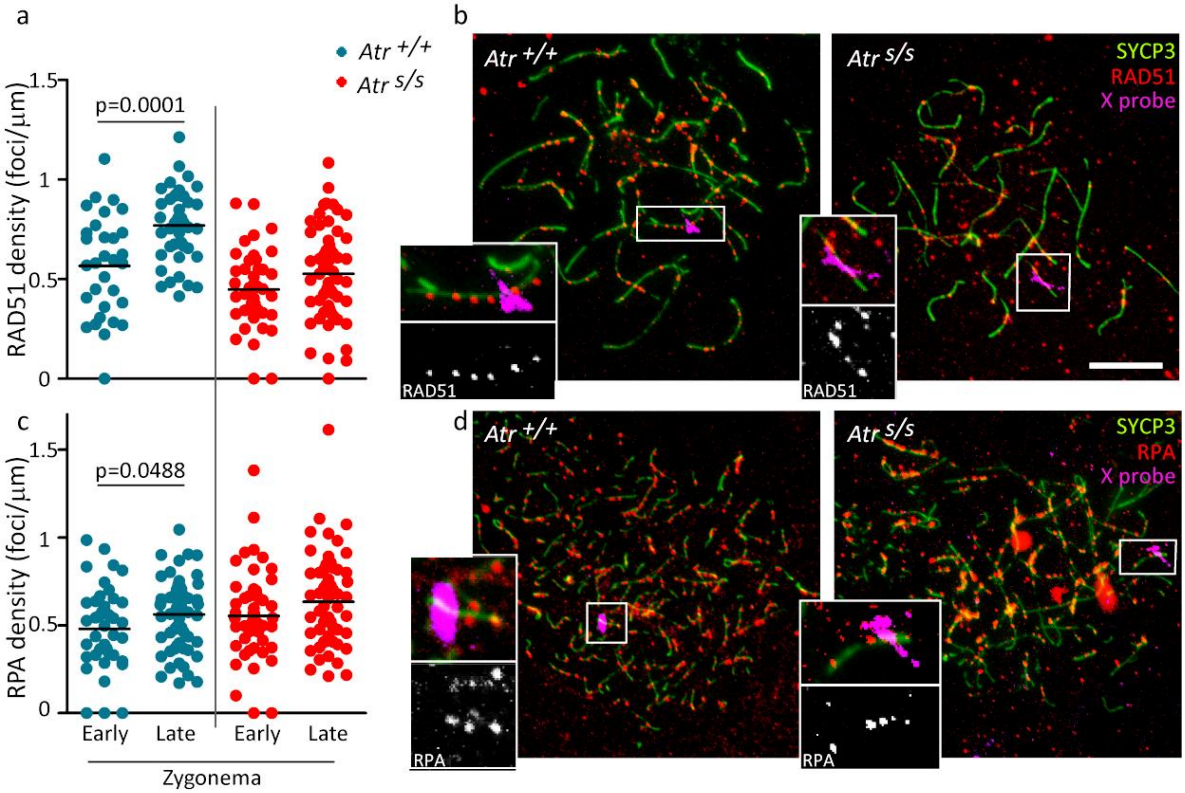

Figure 4.11. Seckel mice spermatocytes exhibit defects in meiotic DSB formation and repair in sex chromosomes. a) Quantification of RAD51 foci density along the entire measurable X chromosome axe for *Atr*$^{+/+}$ and *Atr*$^{s/s}$ spermatocytes at the indicated stages. Horizontal black lines denote the means. **b)** Representative images of late zygotene spermatocytes from the indicated genotypes. Images show overlays of immunoflourescence against SYCP3 (green) and RAD51 (red), and FISH for X-PAR region (purple). Bar in the image represent 10 µm. Inset images show RAD51 foci in the measurable X axis. **c)** RPA foci density present on the entire measurable X axes for *Atr*$^{+/+}$ and *Atr*$^{s/s}$ spermatocytes at the indicated stages. Horizontal black lines denote the means. **d)** Images of early zygotene spermatocytes from the indicated genotypes showing immunoflourescence against SYCP3 (green) and RPA (red), overlayed with FISH for X-PAR region (purple). Inset images show RPA foci counted in the measurable X axis.

Consistent with previous observations (Kauppi et al. 2013), in control spermatocytes the number of RAD51 foci counted on the entire measurable X axis, marked by SYCP3, revealed that at early-zygonema the X chromosome presented a limited number of RAD51 foci, which significantly increased at late-zygonema (0.57 ± 0.05 foci/µm at early-zygonema (avg. ± SEM, N=31); 0.77 ± 0.03 foci/µm at late-zygonema (N=43), p=0.0001, t test, **Fig 4.11a,b**). Nevertheless, although, mutant spermatocytes tended to accumulate more RAD51 foci throughout zygonema, this increase was not statistically significant (0.45 ± 0.03 foci/µm at early-zygonema (N=45); 0.53 ± 0.03 at late-zygonema (N=58), p=0.0698, t test). Moreover, mutant spermatocytes showed a significant reduction in the number of RAD51 foci at early-zygonema (p=0.0217, t test), as well as, at late-zygonema (p<0.0001, t test) compare to control cells. These findings suggest that even thought, in Seckel mouse spermatocytes DSB formation on X chromosome tend to rise through zygonema, at this stage they exhibit lower RAD51 foci on X chromosome compared to control cells, suggesting defects in sex chromosomes meiotic recombination.

At this point, we hypothesized that, similar to what we found in whole-nuclei recombination analysis, the reduction in RAD51 foci observed in the X chromosome from mutant spermatocytes might be originated by deficient loading of RAD51 into resected DSB sites. In order to determine this, we examined RPA staining on X chromosome at early and late-zygonema. The analyses revealed that, as we expected, in control spermatocytes the number of RPA foci tended to rise from early to late-zygonema (0.48 ± 0.03 foci/µm at early-zygonema (N=44); 0.56 ± 0.02 foci/µm at late-zygonema (N=63), p=0.0488, t test, **Fig 4.11c,d**). However, we did not found a significant increase in mutant spermatocytes (0.55 ± 0.03 foci/µm at early-zygonema (N=63); 0.63 ± 0.03 foci/µm at late-zygonema (N=62), p=0.0783, t test). In addition, we found that control and mutant spermatocytes exhibited similar RPA foci in the X chromosomes at early-zygonema, as well as, at late-zygonema (p=0.1427 and p=0.0783, respectively, t test). These data suggest that, whereas in control spermatocytes X chromosome tends to accumulate DSBs through zygonema, as demonstrated by the rise in RAD51 and RPA foci detected at these stages, Seckel mouse spermatocytes have a limited DSB formation on the X chromosome during zygonema. Our findings indicate that normal levels of ATR are necessary to achieve a timely proper DSB formation and repair on the sex chromosomes during zygonema, and consequently, X and Y synapsis.

To investigate more deeply meiotic sex chromosome recombination defects observed in Seckel mouse spermatocytes we analyzed whether X and Y chromosomes failed to form a CO. To do so, we examined MLH1 foci presence on PAR at pachynema, only in those cells that presented synapsed X and Y chromosomes. Consistent with the two fold increase of unsynapsed X and Y chromosomes in mutant spermatocytes at pachynema, MLH1 foci analyses showed that Seckel spermatocytes exhibited approximately two fold decrease in MLH1 foci present in the XY bivalent (56.3% of the XY bivalents analyzed in $Atr^{+/+}$ presented an MLH1 foci (N=87), while only 28.7% of the XY bivalents analyzed in $Atr^{s/s}$ had one (N=94), p=0.0198, Fisher's exact test, **Fig. 4.8b,c**). This data indicate that meiotic sex chromosome recombination is compromised in Seckel mice leading to defects in CO formation at pachytene stage. Accordingly to the normal levels of asynaptic sex chromosomes at diplonema, mentioned previously, these observations imply that reduction of ATR expression impairs meiotic sex chromosome recombination affecting the temporal regulation of DSB formation in PAR region during prophase, and subsequently, the presence of the obligate CO in the XY bivalent, at least, in a correctly time.

4.1.8 In vitro study of ATR functions during prophase

Recently, Sato and colleagues have developed a new organ culture system that allows the *in vitro* study of the first wave of spermatogenesis by using an agarose gel system at a gas-liquid interface (Sato et al. 2011). This new method could be useful to study the meiotic prophase *in vitro*. Thus, with the aim of verifying the meiotic recombination defects observed in Seckel mice, we used this new approach to analyze *in vitro* prophase progression targeting

ATR kinase with a recently discovered selective ATR inhibitor, AZ-20 (Foote et al. 2013). To do so, we cultivated testis tissue fragments from 5 dpp *Atr*$^{+/+}$ mice, which have not entered into meiosis, for 7 days. At 7 days of culture, in order to inhibit ATR, we added to the cultures different ATR inhibitor doses (ATRi) dissolved in DMSO (0.2 µM, 1 µM or 5 µM) and the corresponding volumes of the DMSO to control cultures (DMSO1, DMSO2 or DMSO3, respectively). Testis fragments where cultured for 7 more days when they were harvested.

In order to verify whether spermatogonia present in 5dpp testis fragments were able to initiate the first wave of spermatogenesis and maintain meiotic progression *in vitro*, we analyzed spermatocyte spreads from not-treated testis tissue fragments at 0, 7 and 14 days of culture (D0, D7 and D14, respectively). To follow initiation of meiosis and synapsis progression we used SYCP3 as a marker of meiosis entry (**Fig. 4.12a**). The analyses from D0 revealed that most of cells did not enter into meiosis at 5 dpp, as demonstrated by only ~1% of the cells presented SYCP3 staining (**Table 4.2**). Nonetheless, at D7 we found that ~13% of the cells presented SYCP3 staining. Accordingly, this value was maintained at D14, when ~16% of the cells were SYCP3-positive (p=0.4284, t test). This increase in SYCP3-positive cells indicates that spermatocytes are able to initiate the first wave of spermatogenesis under culture conditions. In addition, we analyzed prophase progression from cultured testis fragments (**Fig. 4.12b**). Our analyses showed that, whereas at D0, the minor SYCP3 positive cells found in spermatocyte spreads were at leptotene stage, as the culture continued spermatocytes progressed throughout the different prophase stages, and eventually reached pachytene stage at D14 (**Table 4.2**). These data confirm that cultivating neonatal testis tissue fragments we are able to obtain cells that initiate the first wave of spermatogenesis, and moreover, they progress until pachynema within 14 days of culture. Therefore, this method allows spermatocyte meiotic progression completing synapsis *in vitro*.

Next, in order to evaluate whether AZ-20 was down-regulating ATR function in testis cultures during meiotic prophase we analyzed meiosis progression at D14 in testis tissue fragments treated with different dosages of ATRi (**Fig. 4.12c**). Firstly, we analyzed the percentage of meiocytes presents at different ATRi dosages and the respectively DMSO controls. We found that spermatocyte spreads from testis tissue fragments treated with 0.2 µM AZ-20 and DMSO1 presented similar number of SYCP3 positive cells (p=0.8943, t test, **Table 4.2**). Nevertheless, we found statistically significant differences between 1 µM AZ-20 and DMSO2 treatments (p=0.0001, t test) and 5 µM AZ-20 and DMSO3 treatments (p<0.0001, t test), indicating that as ATRi dosage increased the number of spermatocytes found in culture decreased.

Secondly, we evaluated how prophase progression was accomplished at different ATRi dosages (**Fig. 4.12d**). To do so, we analyzed the percentage of spermatocytes present at different stages of prophase in each one of the treated samples. Testis tissue fragments treated with 0.2 µM AZ-20 and DMSO1 presented similar number of spermatocytes at

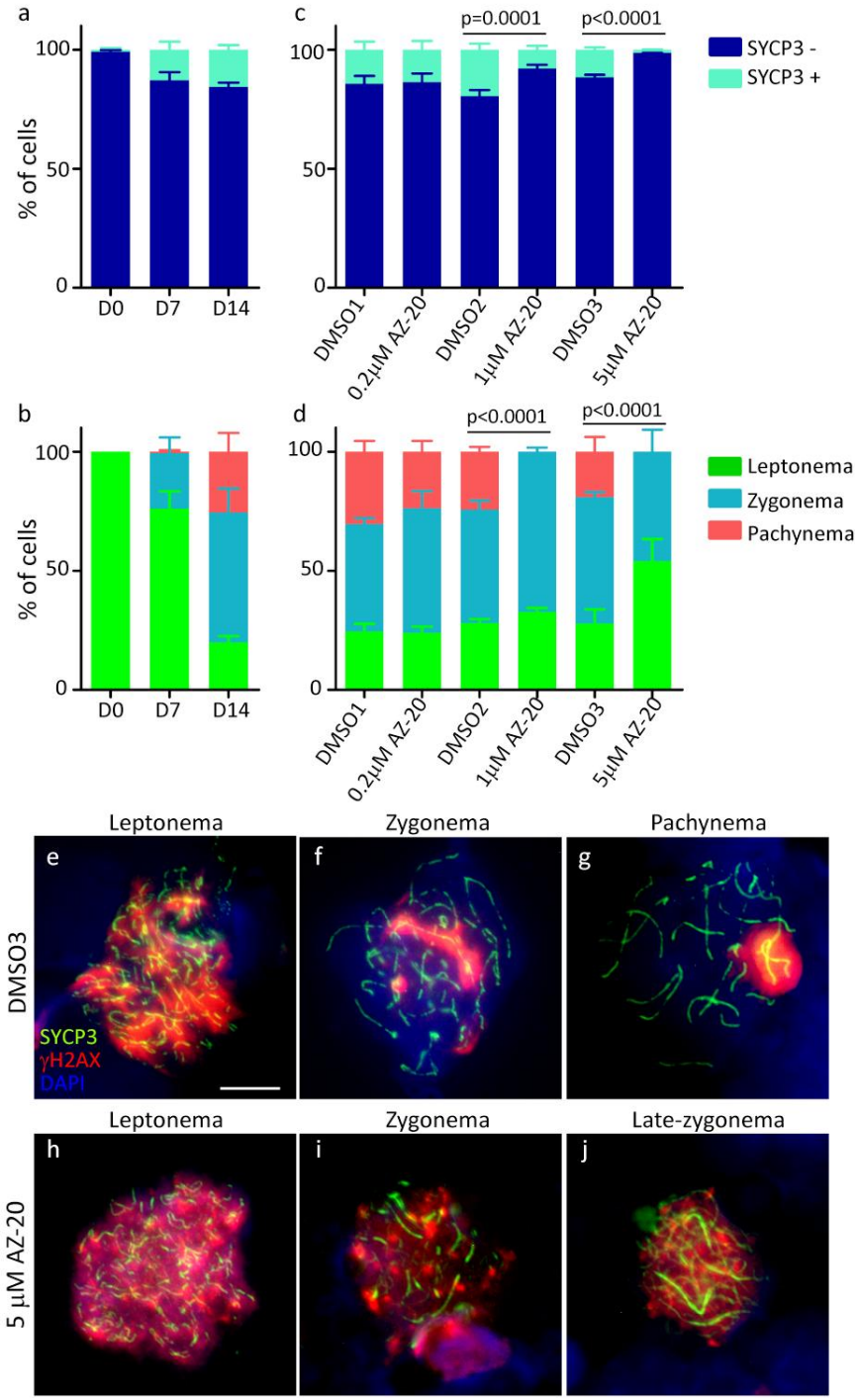

Figure 4.12. Evaluation of ATR involvement during *in vitro* meiotic progression. a) Percentage of SYCP3 positive cells present in not-treated testis tissue fragments at 0, 7 and 14 days of culture (D0, D7 and D14). Columns and lines indicate the mean and standard error (SEM) in all graphs. **b)** Percentage of spermatocytes present at the indicated stages of prophase in not-treated testis tissue fragments at the indicated day of culture. Note that ~25% of spermatocytes reach pachytene stage (red) at D14. **c)** Percentage of SYCP3 positive cells present at D14 in testis tissue fragments treated with the indicate dosages of ATRi (AZ-20) and their respective DMSO controls. Elevated doses of ATRi disturb meiosis entry. **d)** Proportion of spermatocytes present at different stages of meiotic prophase after D14 in the indicated treated samples. Samples treated with elevated doses of ATRi do not progress until pachytene stage. **e-j)** Representative images of spermatocytes from testis tissues treated with DMSO3 and 5µ ATRi showing progression of meiotic prophase followed immunofluorescence against SYCP3 (green), γH2AX (red) and DAPI (blue). Bar in the image represents 10 µm. Note the presence of SYCP3 patches in late-zygonema spermatocyte (j) exhibiting impaired synapsis progression.

different stages of prophase (p= 0.7148, G test, **Table 4.2**) indicating that synapsis progression was not affected at this ATRi dosage. In contrast, we detected statistically significant differences in the number of spermatocytes present at different stages of prophase between 1 µM AZ-20 and DMSO2 treatments (p<0.0001, G test) and 5 µM AZ-20 and DMSO3 treatments (p<0.0001, G test, **Fig. 4.12e-j**). In both cases, we did not find any spermatocytes at pachynema in testis cultured in the presence of AZ-20. Whereas, in testis tissue fragments treated with 1 µM AZ-20 ~68% of spermatocytes reached zygonema, in those treated with 5 µM AZ-20 less than 50% of spermatocytes reached this stage. These data suggest that as ATRi dosage is increased, synapsis progression is compromised. Moreover, comprehensive examination of meiocytes found in 5 µM AZ-20 samples revealed that zygotene spermatocytes exhibit defects in synapsis (**Fig. 4.12j**). Most spermatocytes present large unsynapsed axes with some patches of intense SYCP3 staining suggesting failure to complete synapsis. Together these results indicate that the ATRi treatment results in altered meiotic progression and synapsis defects.

Table 4.2. Frequency of spermatocytes from *in vitro* meiotic initiation and progression analysis. Data from culture testis tissue fragments. First column indicate the percentage of spermatocytes (avg. ± SEM) present at the indicated conditions of the culture. Succeeding columns show the proportion of spermatocytes at the indicated stages of prophase (avg. ± SEM) from the indicated conditions of the culture.

	SYCP3 +	Leptonema	Zygonema	Pachynema	N
D0	0.93 ± 0.7, N=525	100.0 ± 0.0	--	--	3
D7 – not-treated	12.8 ± 3.3, N=819	76.1 ± 7.3	23.3 ± 6.6	0.65 ± 0.65	324
D14 – not-treated	15.7 ± 1.9, N=983	20.0 ± 2.7	54.5 ± 10.0	25.6 ± 7.8	490
DMSO1	14.3 ± 3.3, N=825	24.6 ± 3.1	45.1 ± 2.4	30.3 ± 4.5	492
ATRi 0.2 µM	13.7 ± 3.7, N=860	23.9 ± 2.6	52.4 ± 7.2	23.7 ± 4.6	280
DMSO2	19.5 ± 2.5, N=829	28.0 ± 1.8	47.7 ± 3.8	24.3 ± 2.0	218
ATRi 1 µM	8.0 ± 1.6, N=829	32.7 ± 1.6	67.3 ± 1.7	--	486
DMSO3	11.5 ± 1.0, N=844	27.8 ± 5.9	53.1 ± 2.1	19.1 ± 6.2	400
ATRi 5 µM	1.4 ± 0.04, N=818	54.1 ± 9.3	45.9 ± 9.3	--	194

According to these findings, we decided to study meiotic recombination in cultured testis tissue fragments treated with the high concentration of ATRi in order to evaluate whether recombination defects observed in Seckel mice were recapitulated *in vitro*. We hypothesized that if ATR is implicated in the loading of RAD51 at resected DSB sites, as we observed in Seckel mouse spermatocytes, cultured testes treated with ATRi might present defects in RAD51 accumulation on chromosome axes. Therefore, we performed immunostaining against RAD51 protein on spermatocyte spreads from cultured testis treated with 5 µM AZ-20, DMSO3 and no treated samples cultured during 14 days (D14) as a control of the treatment. RAD51 foci counts in not-treated and DMSO3 samples showed that RAD51 dynamic in control samples was normal. In both controls, RAD51 foci accumulated at leptonema reaching a peak, although at early-leptonema we found a decrease in the number

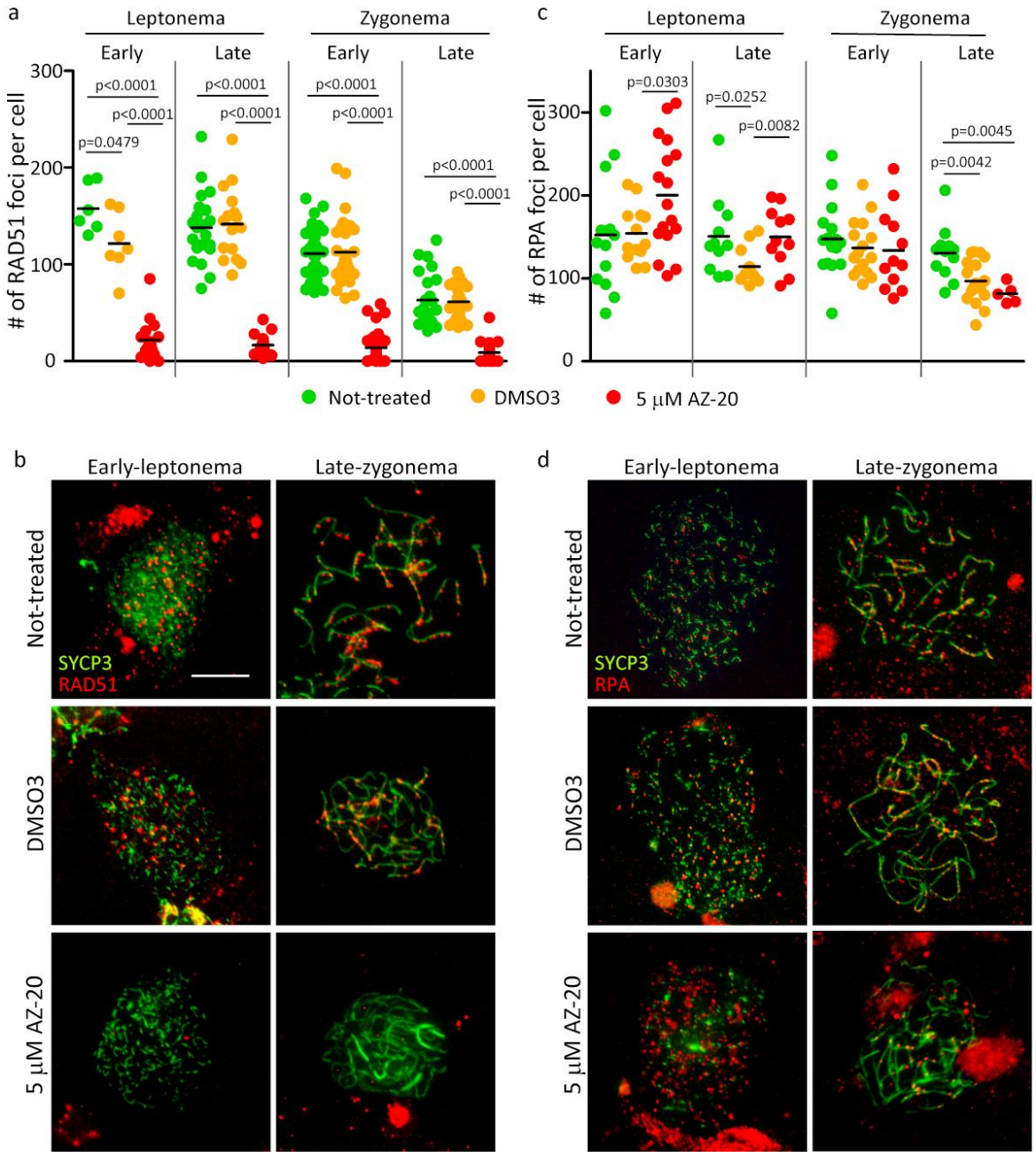

Figure 4.13. Evaluation of RAD51 and RPA foci from *in vitro* cultured spermatocytes. a) Quantification of total RAD51 foci per spermatocyte at the indicated stages in not-treated samples (green), samples treated with DMSO3 (orange) and 5μM ATRi (red). Horizontal lines denote the means in all graphs. **b)** Representative images of spermatocytes cultured with the indicated treatments immunostained against SYCP3 (green) and RAD51 (red). Severe reduction of RAD51 loading at DSB sites is showed in 5μM ATRi-treated spermatocytes in early-leptonema and late-zygonema. **c)** Quantification of total RPA foci per spermatocyte at the indicated stages in the indicated treatments. **d)** Representative spermatocytes cultured with the indicated treatments showing immunostaining against SYCP3 (green) and RPA (red). Note the reduced RPA foci numbers in 5μM ATRi-treated spermatocytes at late-zygonema.

of RAD51 present in DMSO3 compared to the not-treated sample (p=0.0479, t test, **Fig. 4.13a, Table 4.3**). In both not-treated and DMSO3 samples, as meiotic prophase progressed we observed a reduction in the number of RAD51 foci indicating DSBs were properly repaired. As we expected, the number of RAD51 foci found in 5 µM AZ-20 samples was significantly lower than the observed in control samples in all stages analyzed (p<0.0001, t test), indicating that inhibiting ATR function alters the correct loading of RAD51 on chromosome axes leading to recombination defects.

To further evaluate ATR implication in meiotic recombination, we analyzed RPA staining on *in vitro* cultured testis in 5 µM AZ-20, DMSO3 and not-treated (D14) samples. At this point, we reasoned that if down-regulation of ATR is affecting RAD51 loading, the reduction in the number of RAD51 foci observed in 5 µM AZ-20 might be accompanied by the persistence of RPA foci at DSB sites. Consistent with RAD51 data, RPA analysis revealed that at early-leptonema the number of foci counted in spermatocytes from 5 µM AZ-20 samples tended to be higher than in D14 (p=0.0693, t test, **Fig. 4.13b, Table 4.3**). Interestingly, RPA foci counts from 5 µM AZ-20 samples were identical to the observed in spermatocytes from D14 samples at late-leptotene and early-zygotene (p>0.05 in both cases, t test). However, at late-zygotene the number of RPA foci present in spermatocytes from 5 µM AZ-20 samples dropped in comparison to D14 spermatocytes (p=0.0045, t test). Thus, these progressive reduction in RPA counts, together with the lower RAD51 accumulation observed previously, suggest that DSBs might be repaired by an RAD51-independent pathway when ATR functions are inhibited. Nevertheless, we have to take into account that these results could be influenced by the vehicle in which the ATRi is dissolved, as noticeable by the reduction observed in RPA counts in late-leptonema and late-zygonema spermatocytes from DMSO3 compared to D14 samples (p=0.0252 and p=0.0042 respectively, t test).

Table 4.3 Recombination foci numbers counted at different stages of prophase from cultured testis tissue fragments. Data from RAD51 and RPA staining analysis expressing the average and SEM of foci present in spermatocytes at the indicated stages of prophase from the indicated culture treatments.

		Early-leptonema	Late-leptonema	Early-zygonema	Late-zygonema
RAD51	D14 – no treatment	157.7 ± 10.2, N=6	137.8 ± 7.9, N=21	111.2 ± 4.0, N=39	63.0 ± 5.5, N=24
	DMSO3	121.7 ± 12.1, N=7	141.6 ± 9.3, N=16	112.7 ± 6.6, N=27	61.5 ± 3.3, N=28
	ATRi 5 µM	21.8 ± 5.3, N=16	16.6 ± 3.1, N=14	13.9 ± 2.3, N=42	8.9 ± 2.4, N=21
RPA	D14 – no treatment	152.3 ± 19.8, N=13	150.6 ± 14.3, N=11	147.4 ± 10.9, N=16	130.5 ± 9.1, N=12
	DMSO3	154.0 ± 9.2, N=13	114.3 ± 6.2, N=12	136.6 ± 8.4, N=16	96.76 ± 6.4, N=17
	ATRi 5 µM	200.2 ± 16.2, N=17	149.9 ± 10.8, N=11	133.7 ± 14.1, N=12	81.4 ± 5.2, N=5

Remarkably, whereas in spermatocytes treated with 5 µM AZ-20 RPA counts diminished though prophase stages, RPA counts from not-treated samples spermatocytes do not change as meiotic prophase progresses. Considering that unsynapsed axes are subjected to continued DSB formation (Kauppi et al. 2013), one can imagine that during zygonema, ssDNA-bound RPA

levels are maintained by a balance between resected DSBs that are repaired and newly synthesized DSB formation occurring in unsynapsed chromosome axes. Thus in not-treated samples this balance leads to a non-significant reduction in approximately 10% of the number of RPA foci found in late zygonema compared to early zygonema ($p \geq 0.05$, t test). In contrast, RPA levels in 5 μM AZ-20 significantly decreased at late zygonema ($p = 0.0345$, t test), suggesting a limited DSB formation in chromosome axes during prophase, even thought, these spermatocytes exhibited long stretches of unsynapsed axes. These data are consistent with the previous results observed in Seckel mouse sex chromosomes in which the reduction in ATR levels results in a decrease in the number of RPA and RAD51 foci accumulated on X chromosome axis. Altogether, these findings indicate that down-regulation of ATR function alters meiotic recombination by at least two different mechanism, one by impeding the correct loading of RAD51 into DSB sites, and another one, by limiting accumulation of DSB throughout meiotic prophase.

4.2 Characterization of female Seckel mice phenotype during gametogenesis

Sexual dimorphism exhibit by mammalian germ cells during meiosis has revealed significant differences in the stringency of meiotic events in males and females. Although the main players involved in the DNA damage response machinery appear to be conserved in both sexes, male and female germ cells execute different checkpoint signaling machinery responses. For this reason, investigating ATR involvement during oogenesis is important to analyze these distinctions. In the present work, we study the complete process of gametogenesis in female Seckel mice in order to analyze regulation of meiotic prophase and the process of folliculogenesis to obtain a mature oocyte.

4.2.1 Analyzing the reduction of ATR levels in Seckel ovaries

Female Seckel mice have been reported to be sterile, in view of the fact that after hormone-induced superovulation of the mutant female, no viable oocytes were obtained (Murga et al. 2009). Consistent with these data, to evaluate fertility we decided to mate female Seckel mouse with demonstrated fertile males. After 3 months of breeding, whereas control females gave multiple births (3 births, 10.8 ± 1.5 litters/birth, N=2), no litters were obtained from Seckel female, supporting the previously reported infertility in mutated females.

In order to determine whether ATR expression was reduced in adult Seckel mouse ovaries, as we observed in Seckel mouse testis, we performed RT-PCR using total RNA from both ovaries from Seckel and control mice. Retrotranscription analyses showed that the levels of the ATR transcript were reduced in Seckel ovaries, indicating a substantial reduction of ATR expression levels in mutant ovaries (**Fig 4.14**).

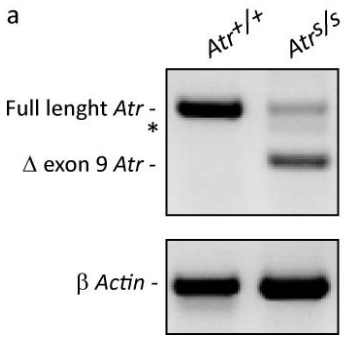

Figure 4.14. Ovaries from Seckel mouse present reduced expression of ATR. a) Products from RT-PCR of ATR using primers at exon 8 and exon 9 for the indicated genotips. Several reduction of RT-PCR product corresponding to full length Atr (477 bp) is showed in $Atr^{s/s}$ ovaries. RT-PCR product corresponding to Atr lacking exon 9 (284 bp) is present in $Atr^{s/s}$ ovaries. Asterisk denote unspecific RT-PCR product.

4.2.2 Assessing the involvement of ATR during female meiotic prophase

The successful execution of meiosis depends, in large part, on the precise coordination of meiotic prophase progression. As previously mentioned proper alignment and synapsis of homologous chromosomes, as well as, formation of meiotic cohesion are crucial events to

ensure a correct segregation of homologous chromosomes. DSB formation is essential to achieve a suitable synapsis in most organisms (Baudat et al. 2000; Romanienko & Camerini-Otero 2000; Baudat et al. 2013). The synaptonemal complex mediates homologous recombination resolution, and at the same time, ensures the correct establishment of synapsis and progression of meiotic prophase (Fraune et al. 2012). For this reason, in order to ascertain whether the infertility observed in female Seckel mice was attributable to the defective meiotic prophase, we analyzed synapsis and homologous recombination in fetal oocytes from control and mutant mice.

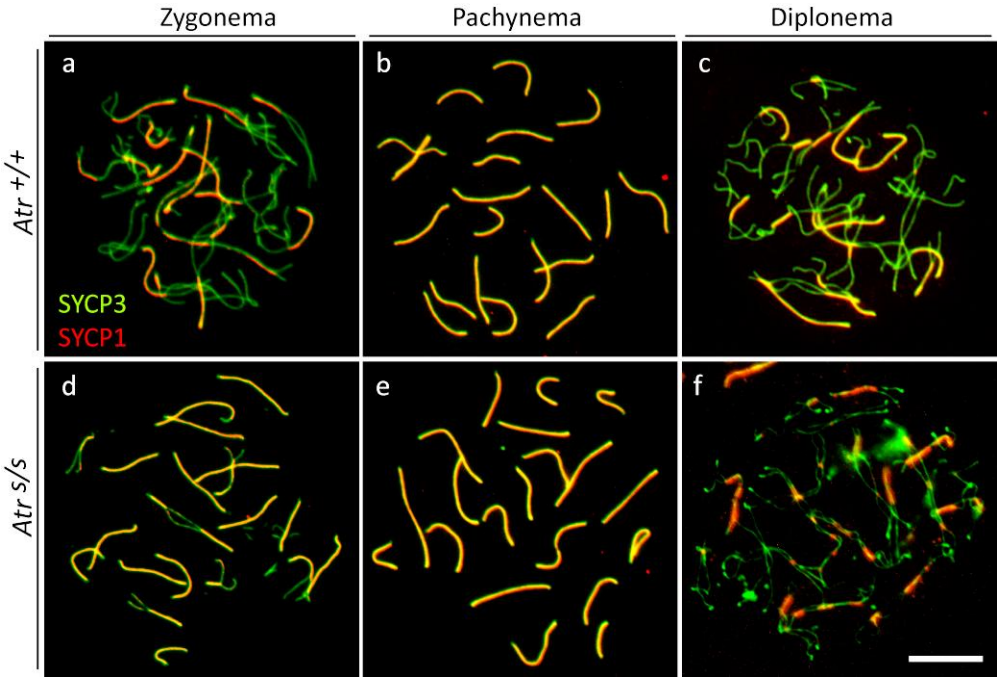

Figure 4.15. Synapsis and progression of meiotic prophase is not affected in Seckel mice oocytes. a-f) Representative images showing progression of meiotic prophase and SC formation followed by immunostaining of oocytes spreads from fetal ovaries against SYCP3 (green) and SYCP1 (red) from $Atr^{+/+}$ and $Atr^{s/s}$. Bar in the image represents 10μm. SC formation in Seckel mice oocytes (d-f) is properly completed leading to entire homologous chromosome synapsis.

Immunostaining against SYCP1 and SYCP3 proteins on oocyte surface spreads showed that in Seckel mice oocytes chromosome synapsis progressed properly through all prophase stages, indicating that SC formation between homologous chromosomes was comparable in control and mutant oocytes (**Fig 4.15a-f**). These findings suggested that wild type expression of ATR is not a requirement to achieve a complete homologous chromosome synapsis in the oocytes.

Furthermore, in order to examine how reduction of ATR levels might be affecting DSB repair progression in Seckel mice oocytes, we performed a global analysis of meiotic recombination by immunostaining γH2AX protein on oocyte nuclei spreads. As mentioned above, in mammals γH2AX signals SPO11-generated DSBs showing discrete staining patches along chromosomes axes, as well as, accumulates surrounding an entire chromosome, or a

part of it, in response to unsynapsis (Mahadevaiah et al. 2001; Turner et al. 2005; Burgoyne et al. 2009). The analyses revealed that in both genotypes, we observed similar γH2AX dynamic through the meiotic prophase. At the onset of prophase, γH2AX was present over all chromatin of leptotene oocytes (data not shown). During zygonema, γH2AX appeared forming patches at DSB sites, besides, forming large marks surrounding the unsynapsed regions of the genome (**Fig. 4.16a,b**). At pachynema, most oocytes displayed γH2AX patches along the SC marking unrepaired DSBs, although some oocytes still presented γH2AX involving large part of synapsed bivalents (**Fig. 4.16c,d**).

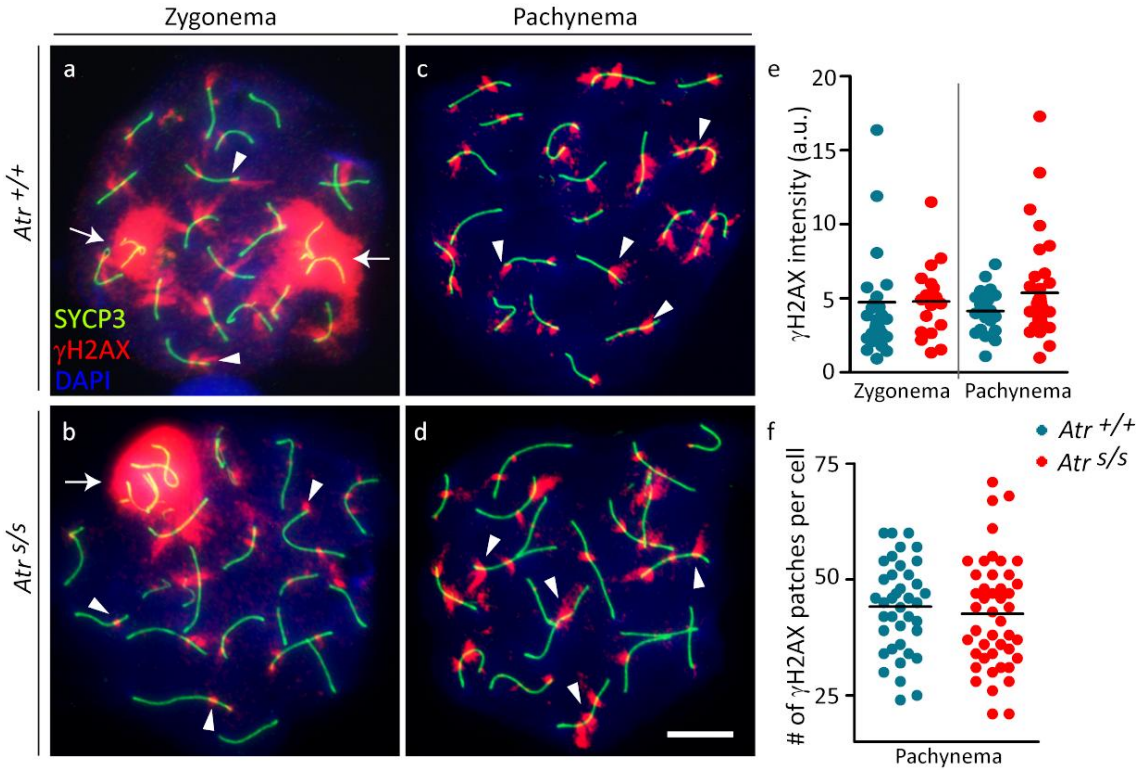

Figure 4.16. Seckel mice oocytes exhibit a proper phosphorilation of H2AX histone throughout meiotic prophase I. a-d) Immunostaining against SYCP3 (green), γH2AX (red) shows dynamic of γH2AX during zygonema (a,b) and pachynema (c,d) in *Atr*$^{+/+}$ and *Atr*$^{s/s}$ oocytes. DNA is stained with DAPI (blue). Bar in the image represents 10µm. Note the presence of large marks (arrows) and patches (arrowheads) of γH2AX staining in both genotypes. **e)** Quantification of total intensity of γH2AX staining at zygonema and pachynema in whole-nuclei at the indicated stages. Intensity of γH2AX is not statistically different between *Atr*$^{+/+}$ and *Atr*$^{s/s}$ oocytes in both indicated stages. Intensity is expressed in arbitrary units (a.u.) **f)** Quantification of total γH2AX foci present in each nucleus analyzed in *Atr*$^{+/+}$ and *Atr*$^{s/s}$ oocytes at pachynema. Seckel oocytes exhibit undistinguishable number of γH2AX patches compared to control cells. Horizontal back lines denote the means.

Taking this into account, in order to consider the total amount of γH2AX present in oocytes (discrete pacthes and large marks) we performed two different analyses to quantify γH2AX staining. Firstly, we analyzed the total intensity of γH2AX staining at zygonema and pachynema in whole-nuclei from control and Seckel mouse oocytes. Intensity of γH2AX staining was undistinguishable in control and mutant oocytes at zygonema (4.7 ± 0.8 in *Atr*$^{+/+}$

(avg. ± SEM, N=29); 4.8 ± 0.6 in *Atr*$^{s/s}$ (N=18), intensity is showed in arbitrary units, p=0.9659, t test, **Fig. 4.16e**), as at pachynema (4.1 ± 0.33 in *Atr*$^{+/+}$ (N=20); 5.4 ± 0.6 in *Atr*$^{s/s}$ (N=35), p=0.1282, t test). Secondly, we quantified the total number of γH2AX foci present in pachytene oocytes from control and Seckel mice. In those pachytene oocytes that exhibited large marks of γH2AX, these marks were counted as one patch for every bivalent that surrounded. Interestingly, in this case, we neither observed statistically significant differences in the number of γH2AX patches presented at pachynema between control and mutant oocytes (44.1 ± 1.6 in *Atr*$^{+/+}$ (N=39); 42.6 ± 1.8 in *Atr*$^{s/s}$ (N=45), p=0.5322, t test, **Figure 4.16f**). These results suggest that the dynamics of γH2AX staining appears grossly normal in mutant oocytes revealing that phosphorilation of histone H2AX is not majorly affected during female Seckel mouse meiotic prophase. Moreover, in contrast with what we observed in mutant males, in Seckel mouse oocytes, meiotic recombination progression is not mostly disturbed during meiotic prophase.

4.2.3 The control of crossover formation in female Seckel mice

Several works over the past years showed evidences of a striking sexual dimorphism in response to meiotic DSB repair (Roig et al. 2004; Tease & Hultén 2004; Morelli & Cohen 2005). It has been suggested that in mammalian females the progression of DSB repair, and consequently recombination, could be delayed compared to males. Moreover, the rate of CO counts in oocytes is always higher than in spermatocytes, despite the equivalent size of their genomes (Baudat & de Massy 2007). Nevertheless, homeostatic control of CO formation is strictly regulated in both males and females, since the number of SPO11-generated DSB is approximately 10 fold higher than the final number of COs (Cole et al. 2012).

Taking into account that COs are the final result from meiotic recombination, we decided to analyze whether CO formation regulation might be affected in female Seckel mice. To evaluate this, we performed immunostaining against MLH1, which marks strand exchanges at late stages of prophase (Baker et al. 1996), in control and mutant oocytes at pachynema (**Fig. 4.17a,b**). In this case, contrarily to the observed in Seckel males, the total number of MLH1 foci presented in pachytene oocytes was similar between control and mutant mice (26.5 ± 0.3 in *Atr*$^{+/+}$ (avg. ± SEM, N=107); 26.8 ± 0.4 in *Atr*$^{s/s}$ (N=95), p=0.4826, Mann Whitney test, **Fig. 4.17c**). Interestingly, Seckel mouse oocytes presented a significant increase in the number of bivalents without the obligate CO at pachynema (2.1% of the bivalents in *Atr*$^{+/+}$ (N=2140); 3.9% of the bivalents in *Atr*$^{s/s}$ (N=1900), p=0.0010, Fisher's exact test, **Fig. 4.17c inset**) as we observed in male Seckel mice. Hence, we hypothesize that the increase in the number of bivalents without MLH1 foci found in Seckel oocytes at pachynema correspond to an increase in the time to repair DSBs and consequently to form crossovers, consistent with the results obtained from the analyses of CO formation in Seckel mice spermatocytes. To test this hypothesis, and in light of MLH1 foci in females persist longer at COs sites (Baker et al. 1996), we analyzed the number of bivalents lacking MLH1 present at diplonema in control and

mutant oocytes. As we expected, there were not statistically significant differences between both genotypes at diplonema (1.5% of the bivalents in *Atr*$^{+/+}$ (N=260); 1.1% of the bivalents in *Atr*$^{s/s}$ (N=280), p=0.7164, Fisher's exact test) suggesting that the results observed at pachynema represent a delay in CO formation. Together, all these findings support the idea that ATR is required to achieve a proper timely meiotic homologous recombination, even though; meiotic prophase is not grossly altered in female Seckel mice.

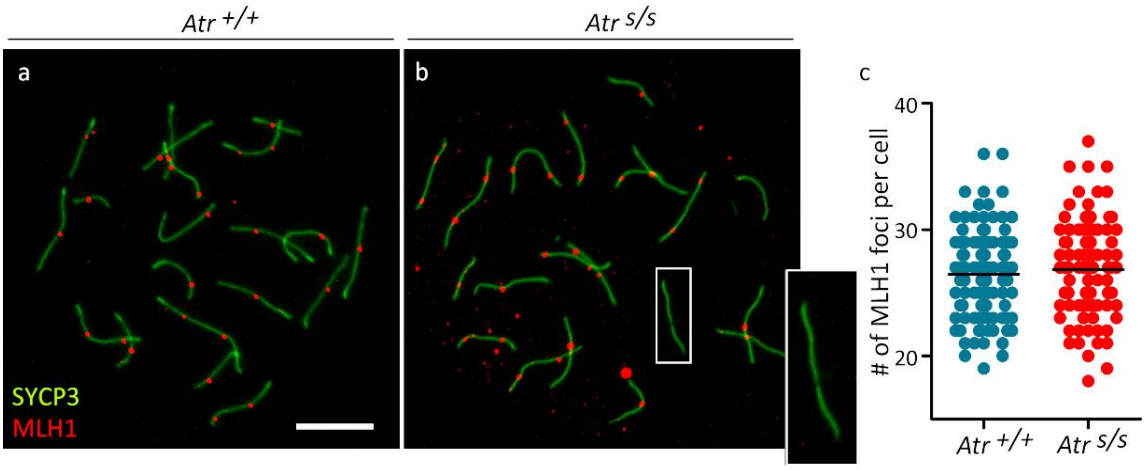

Figure 4.17. Total number of MLH1 foci is not altered in Seckel mouse oocytes. a-b) Representative images of pachytene oocytes from the indicated genotypes immunostained against SYCP3 (green) and MLH1 (red). Bar in the images represents 10 µm. White box denote the presence of a bivalent lacking MLH1 foci in *Atr*$^{s/s}$ oocytes (b), which is magnified in the image inset. **c)** Quantification of total MLH1 foci present in each pachytene oocyte analyzed in *Atr*$^{+/+}$ and *Atr*$^{s/s}$ samples. Horizontal black lines denote the means. Seckel mice do not exhibit statistically significant differences in total MLH1 foci number compared to control cells.

4.2.4 Folliculogenesis progression in an ATR reduced scenario

Female fertility in mammals depends upon the coordinated development between ovarian follicles and the oocytes contained within them (Gilchrist et al. 2004; Sánchez & Smitz 2012). In the fetal ovary, after germ cell colonization, there is a phase of mitotic proliferation followed by the entry of these cells into meiosis. After birth, oocytes arrested at diplonema initiate folliculogenesis to continue development. Follicle formation starts when oocytes become surrounded by a single layer of flattened somatic cells to form primordial follicles. Primordial follicles are stored within the ovary in a quiescent stage until they are recruited to initiate follicle growth, or folliculogenesis (De Felici et al. 2005; Jones 2008). Every step during follicle development is crucial, and errors during this process may result in infertility (Hu et al. 2012).

Given that, Seckel mouse oocytes did not exhibit substantial meiotic prophase I defects, we investigated the progression of folliculogenesis in control and mutant female mice. Folliculogenesis is characterized by an enormous increase in oocyte size. At the same time, somatic granulosa cells proliferate mitotically forming a multilayered follicle. Eventually, a

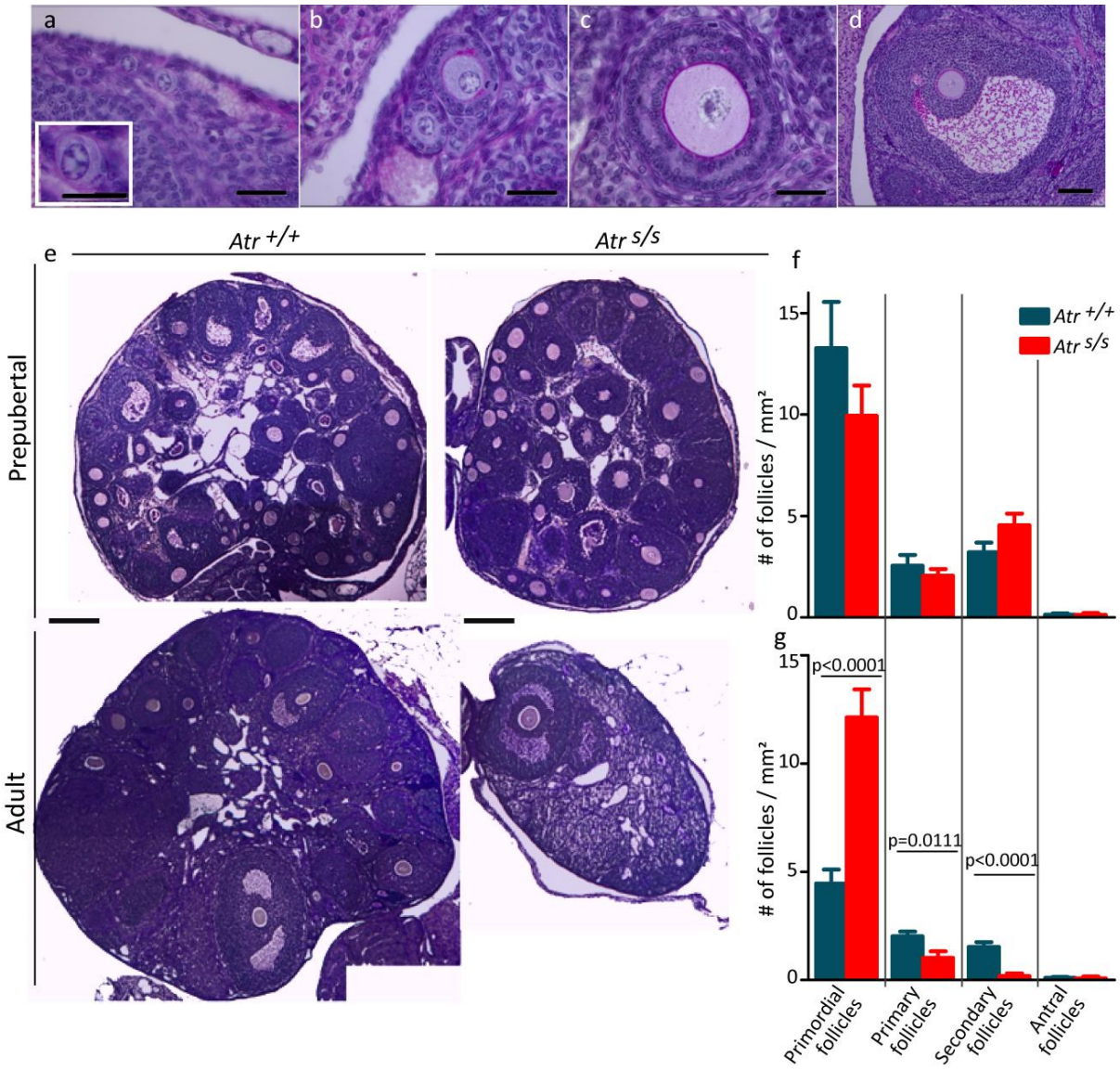

Figure 4.18. Folliculogenesis analysis of histological ovarian sections from prepubertal and adult mice. a-d) Representative images of folliculogenesis progression showing the four stages used to classify follicles: primordial (a), primary (b), secondary (c) and antral (d). Bars in the images represent 20 µm, except for the antral follicle that represents 50 µm. e) Histological ovarian sections stained with PAS-Hematoxylin from prepubertal (from 3-week old females) and adult mice (from 3-month old females) from $Atr^{+/+}$ and $Atr^{s/s}$ ovaries exhibiting all follicular stages. Bars in the images represent 200 µm. Note that Seckel adult mice ovarian section presents abundant stroma depleted of follicles. **f-g)** Quantification of the number of follicles present at different stages of eight alternate ovarian sections from two prepubertal (f) and two adult females (g) from the indicated genotypes. Values are expressed as the average of the number of follicle presents in each section relative to the entire measurable area of those sections. Columns and lines indicate the mean and standard error (SEM), respectively. Note that folliculogenesis progression is not altered in prepubertal Seckel females. Adult females present an increased number of primordial follicles, accompanied by a reduction of the more advanced follicles.

cavity appears among granulosa cells, forming the antrum when the follicle is completely developed (Sánchez & Smitz 2012; Li & Albertini 2013). Hence, we classified follicles into four different categories according to their morphology and organization (**Fig. 4.18a-d**). The pool of primordial follicles gives rise to primary follicles, which present a single layer of cuboidal granulosa cells. Primary follicles progress to secondary follicles, which present several layers of granulosa cells. Finally, we designate as antral follicles those that present a cavity (the antrum). Therefore, to study folliculogenesis progression we analyzed the number of follicles from these different categories in alternate histological sections from prepubertal and adult ovaries from control and mutant mice. As mentioned earlier, since Seckel mice exhibit several dwarfism (Murga et al. 2009), in order to account on the effect of a smaller ovary in this analysis, we measured the total area of each ovarian section. Then, we counted and classified the total number of follicles present in each of those sections and expressed these values as the number of follicles per measurable area of each ovarian section. Histological analysis revealed that both genotypes contained all follicular stages, in prepubertal as well as in adult ovaries (**Fig. 4.18e**), indicating that follicles in Seckel mice have the capacity to progress to pre-ovulatory stages. Nevertheless, although folliculogenesis progression was not affected in prepubertal Seckel ovaries (**Fig. 4.18f, Table 4.4**), we found that adult Seckel ovaries showed defects in follicular progression. Our analysis revealed approximately a three-fold increase in the number of primordial follicles compared to control ovaries ($p<0.0001$, t test, **Fig. 4.18g, Table 4.4**), accompanied by a significant reduction in primary ($p=0.0111$, t test) and secondary follicles ($p<0.0001$, t test). These data indicate that adult female Seckel mice present defects in primordial follicle recruitment to initiate follicle growth, as well as, in follicular development as suggested by the reduction of growing follicles.

Table 4.4. Number of follicles at different stages of folliculogenesis. Data from folliculogenesis analysis expressing the average and SEM number of follicles present in one histological ovarian section divided by the area of those sections (number of follicles/mm^2) at different follicular stages for the indicate genotypes and age. Asterisks denote statistically significant differences in the number of follicles at the stages indicated between *Atr*$^{+/+}$ and *Atr*$^{s/s}$ mice (*p<0.05, **p<0.001, t test). Corresponding p values are in the text.

		Primordial follicles/mm^2	Primary follicles/mm^2	Secondary follicles/mm^2	Antral follicles/mm^2	N
Prepubertal ovaries	*Atr*$^{+/+}$	13.3 ± 2.3	2.6 ± 0.53	3.2 ± 0.48	0.14 ± 0.07	16
	Atr$^{s/s}$	9.9 ± 1.5	2.1 ± 0.32	4.5 ± 0.57	0.13 ± 0.09	16
Adult ovaries	*Atr*$^{+/+}$	4.6 ± 0.64	2.0 ± 0.21	1.5 ± 0.22	0.09 ± 0.05	16
	Atr$^{s/s}$	12.1 ± 1.3**	1.0 ± 0.30*	0.18 ± 0.12**	0.08 ± 0.08	16

Adding onto that, a comprehensive examination of the ovarian sections showed that Seckel mouse ovaries showed an increased proportion of follicles containing large oocytes, which have increased in volume because they have initiated oocyte growth, although still enclosed by only one layer of flattened or cuboidal granulosa cells (0.83 ± 0.18 follicles/mm^2 in *Atr*$^{+/+}$ (avg. ± SEM, N=16); 2.1 ± 0.40 in *Atr*$^{s/s}$ (N=16), p=0.0082, **Fig. 4.19a,b**). These results together suggest that reduction of ATR expression in the ovary alters the correct development of follicles.

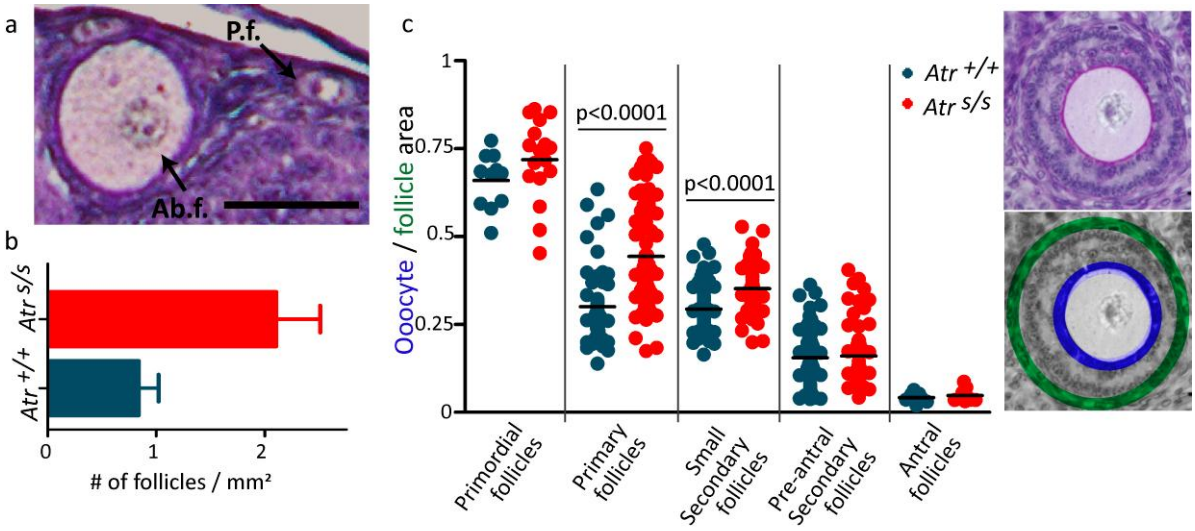

Figure 4.19. Seckel mouse oocytes occupy a larger area of the follicle. a) Representative image of an abnormal follicle (A.f) exhibiting a large oocyte surrounded by one flat layer of granulosa cells. Note the presence of a regular primordial follicle (P.f.) next to it. Bar represents 50 µm. **b)** Quantification of the number of abnormal follicles present in ovarian sections analyzed from the indicated genotypes. Columns and lines indicate the mean and standard error (SEM), respectively. *Atr*$^{s/s}$ ovaries show an increased presence of abnormal follicles. **c)** Indirect analysis of the number of follicular cells surrounding an oocyte. Each point represents the measure of the relative area occupied for an oocyte (blue circumference in the example image inset) in a particular follicle (green circumference) for the indicate genotypes at different stages of folliculogenesis. Horizontal black lines in the graph denote the means. Primary and small secondary follicles from Seckel ovaries present larger relative oocyte area than control follicles, suggesting a reduction in the number of granulosa cells surrounding those oocytes.

Correct proliferation of granulosa cells is necessary not only for follicular growth and development, but also for the creation of an appropriate environment for oocyte maturation (Albertini et al. 2003; Li & Albertini 2013). In order to study whether follicular growth was compromised in Seckel mouse ovaries, we indirectly evaluated follicular cell proliferation. To do so, on ovarian sections from control and Seckel mice, we measured the total area of a particular follicle and the area of the oocyte included into it. Then, we expressed this data as a relative area occupied by the oocyte in a particular follicle (**Fig. 4.19c**). In control mice, the relative area of an oocyte decreased throughout folliculogenesis progression, indicating an increase in the number of granulosa cells. Interestingly, although in Seckel mice the relative oocyte area also tended to decrease throughout folliculogenesis, we noticed that the area occupied by oocytes in growing follicles was larger than in control mice. Thus, while

examination of primordial follicles did not show statistically significant differences between control and mutant follicles (0.65 ± 0.02 in *Atr*$^{+/+}$ (avg. ± SEM, N=11); 0.72 ± 0.03 in *Atr*$^{s/s}$ (N=17), p = 0.1474, t test), Seckel ovaries presented larger oocytes enclosed in primary (0.3 ± 0.01 in *Atr*$^{+/+}$ (N=62); 0.44 ± 0.02 in *Atr*$^{s/s}$ (N=67), p<0.0001, t test), and small secondary follicles (with up to three layers of granulosa cells, 0.29 ± 0.01 in *Atr*$^{+/+}$ (N=81); 0.35± 0.01 in *Atr*$^{s/s}$ (N=45), p<0.0001, t test). Remarkably, we found undistinguishable relative area between control and Seckel pre-antral secondary follicles (with more than three layers of granulosa cells (0.16 ± 0.01 in *Atr*$^{+/+}$ (N=67); 0.16 ± 0.01 in *Atr*$^{s/s}$ (N=68), p=0.7360, t test) and, antral follicles (0.04 ± 0.01 in *Atr*$^{+/+}$ (N=7); 0.05 ± 0.01 in *Atr*$^{s/s}$ (N=8), p=0.4884, t test). Therefore, this approximation indicates that oocytes included in primary and small secondary follicles from mutant females occupied a larger area of the follicle compared to controls, suggesting that Seckel mouse follicles contain a reduced number of granulosa cells surrounding the oocyte than follicles from control mouse.

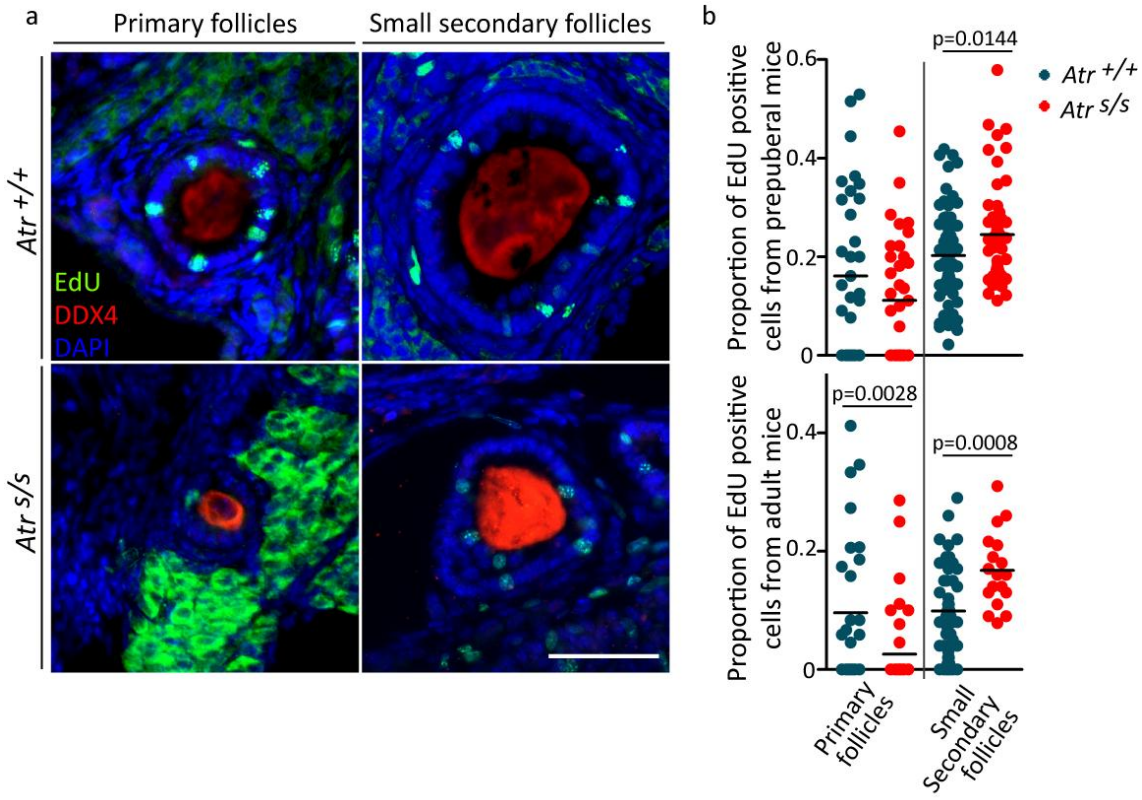

Figure 4.20. Follicular cell proliferation assay in ovarian cryosections from prepubertal and adult mice. a) Representative images of primary and secondary follicles for the indicated genotypes showing EdU positive cells (green), DDX4-oocyte marker (red) detected by immunofluorescence, and follicular cells detected by DAPI (blue). Bar represents 50 µm. **b)** Quantification of the number of EdU positive cells relative to the total number of granulosa cells present in each follicle analyzed for the indicate stages from prepubertal and adult cryosections from *Atr*$^{+/+}$ and *Atr*$^{s/s}$ ovaries. Horizontal black lines in the graph denote the means. Adult Seckel females exhibit significantly reduced proportion of EdU positive granulosa cells in primary follicles. Contrarily, small secondary follicles from adult and `prepubertal *Atr*$^{s/s}$ ovaries present increased proportion of EdU positive granulosa cells indicating elevated proliferative rate of those follicles.

Table 4.5 Data from follicular cell proliferation analysis from prepubertal and adult mice. Each chart shows the average and SEM proliferation rate, EdU positive cells, number of follicular cells found in each particular follicle and number of follicles studied (N) from the indicated genotype and age. Asterisks denote statistically significant differences between $Atr^{+/+}$ and $Atr^{s/s}$ mice (*p<0.05, **p<0.001, t test). Corresponding p values for proliferation rate are provided in the text.

			Proliferation rate	EdU positive cells	# of follicular cells	N
Prepubertal mice	Primary follicles	$Atr^{+/+}$	0.16 ± 0.03	3.0 ± 0.7	15.1 ± 1.2	34
		$Atr^{s/s}$	0.11 ± 0.02	1.7 ± 0.7	11.9 ± 1.0*	36
	Secondary follicles	$Atr^{+/+}$	0.20 ± 0.01	13.8 ± 1.0	70.0 ± 3.7	67
		$Atr^{s/s}$	0.24 ± 0.01*	13.8 ± 0.9	57.6 ± 2.9*	57
Adult mice	Primary follicles	$Atr^{+/+}$	0.10 ± 0.02	2.3 ± 0.6	18.1 ± 1.5	28
		$Atr^{s/s}$	0.03 ± 0.01**	0.35 ± 0.11**	10.5 ± 0.67**	43
	Secondary follicles	$Atr^{+/+}$	0.10 ± 0.01	5.7 ± 0.67	62.7 ± 3.6	56
		$Atr^{s/s}$	0.17 ± 0.01 **	7.2 ± 0.83	43.4 ± 3.7**	18

It is widely accepted that in multicellular organism, coordination of cell populations are strictly controlled by cell proliferation and cell loss, and these two functions are precisely balanced. In this way, successful follicle development depends in part on granulosa cells proliferation and prevention of apoptosis (Jiang et al. 2003; Liu 2007). Since regular follicular development is accompanied by high proliferation rate of granulosa cells we inquired whether the reduced ATR expression observed in the ovary might be altering cell proliferation and programmed cell death during folliculogenesis. Considering that we only recognized developmental problems in primary and small secondary follicles, we focused the following analyses on these two categories of follicles. Firstly, in order to evaluate granulosa cell proliferation, we used an EdU incorporation assay to detect follicular replicating cells on cryosections from prepubertal and adult ovaries from control and Seckel mice (**Fig. 4.20a**). To determine this, we analyzed the number of EdU positive cells relative to the total number of granulosa cells present in a particular follicle. Importantly, the number of granulosa cells counted in ATR mutant follicles tended to be lower than the observed in control follicles (**Table 4.5**), consistent with what we had indirectly determined before. EdU analyses revealed that follicular cell proliferation rate in Seckel mouse primary follicles tended to be inferior to the observed in control follicles. Nevertheless, whereas the reduction observed in prepubertal primary follicles were not statistically significant between control and Seckel mice (p=0.0791, t test, **Fig. 4.20b**, **Table 4.5**), primary follicles in adult Seckel ovaries exhibited a significant reduced proliferation rate of follicular cells compared to control follicles (p=0.0028, t test). We

found more than a three-fold reduction in the number of EdU positive cells counted in each follicle, and this reduction was accompanied with a two-fold reduction in the number of granulosa cells present in those follicles compared to control follicles. Interestingly, we observed that mutant small secondary follicles exhibited an increased granulosa cell proliferation rate than control small secondary follicles, in prepubertal (p=0.0144, t test) as in adult ovaries (p=0.0008, t test). In contrast to what we observed in Seckel primary follicles, the number of EdU positive cells counted in each small secondary follicle was similar between mutant and control follicles, even though, it presented a reduced number of granulosa cells compared to control follicles (**Table 4.5**). These findings indicate that Seckel follicles have a reduced granulosa cells proliferation rate, which intensifies as mice age, leading to problems on follicular development and folliculogenesis progression. Nevertheless, due to the increased proliferation rate detected in secondary follicles we suggest that those follicles that have the ability to progress throughout folliculogenesis present an increased granulosa cells proliferative capacity, which allow them a correct follicular development.

Table 4.6. Data from follicular cell apoptotic analysis from prepubertal and adult mice. Each chart shows the average and SEM from apoptotic cell rate, TUNEL positive cells, number of follicular cells and number of follicles studied (N) from the indicate mice, genotypes and age. Asterisks denote statistically significant differences in the number of TUNEL positive cells, and follicular cells at the indicated stages and ages between *Atr*$^{+/+}$ and *Atr*$^{s/s}$ mice (*p<0.05, **p<0.001, t test). Corresponding p values for apoptotic rate are provided in the text.

			Apoptotic cell rate	TUNEL positive cells	# of follicular cells	N
Prepubertal mice	Primary follicles	*Atr*$^{+/+}$	0.005 ± 0.004	0.06 ± 0.04	11.57 ± 0.89	35
		Atr$^{s/s}$	0.011 ± 0.007	0.15 ± 0.1	10.35 ± 1.14	20
	Secondary follicles	*Atr*$^{+/+}$	0.002 ± 0.001	0.18 ± 0.1	83.92 ± 3.67	96
		Atr$^{s/s}$	0.016 ± 0.003**	1.1 ± 0.16*	77.22 ± 3.06	55
Adult mice	Primary follicles	*Atr*$^{+/+}$	0.006 ± 0.004	0.06 ± 0.04	12.84 ± 0.85	32
		Atr$^{s/s}$	0.010 ± 0.004	0.11 ± 0.05	10.31 ± 0.70*	35
	Secondary follicles	*Atr*$^{+/+}$	0.001 ± 0.0005	0.06 ± 0.042	76.00 ± 4.38	53
		Atr$^{s/s}$	0.009 ± 0.005*	0.4 ± 0.24*	41.20 ± 4.81*	5

Next, in order to detect and quantify follicular cells death we performed TUNEL assays to evaluate apoptotic cells rate on histological sections from prepubertal and adult ovaries from control and Seckel mice. Similarly to proliferation analysis, we counted the number of TUNEL positive cells relative to the total number of granulosa cells present in a particular

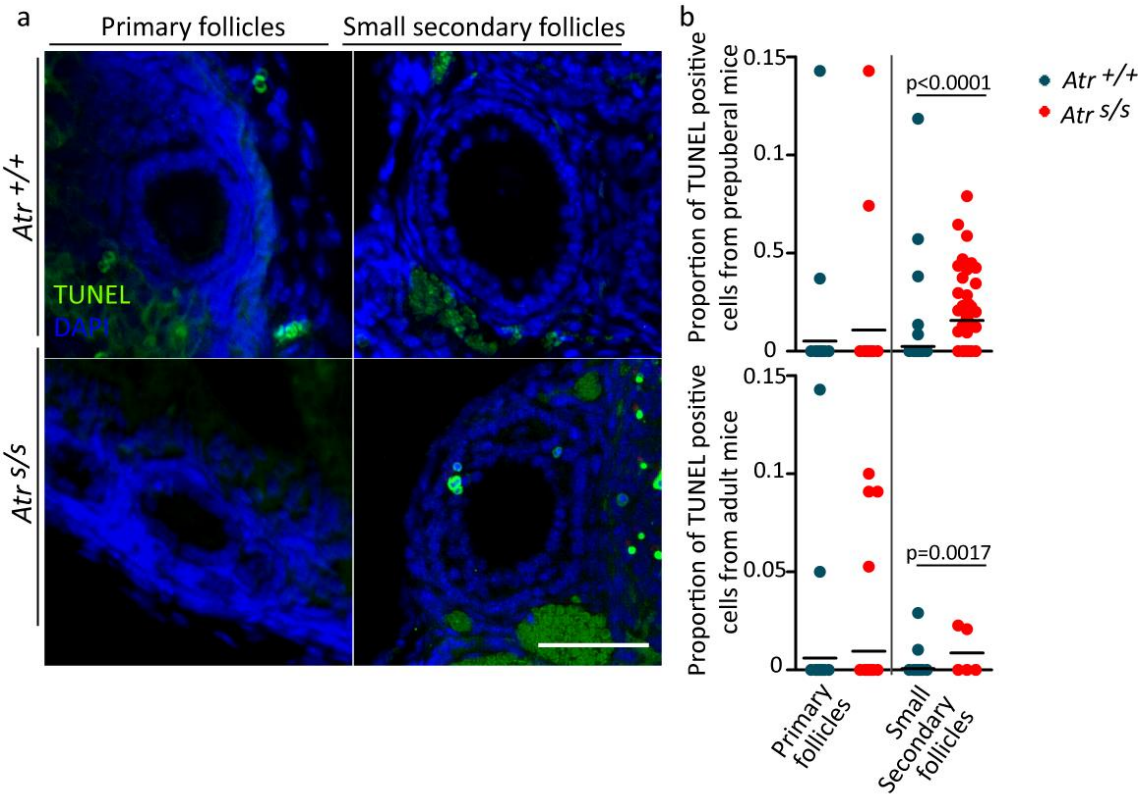

Figure 4.21. Follicular cells apoptotic assay in ovarian sections from prepubertal and adult mice. a) Representative images of primary and secondary follicles showing TUNEL positive cells (green), and follicular cells detected by DAPI (blue) from $Atr^{+/+}$ and $Atr^{s/s}$ ovaries. Bar represents 50 µm. **b)** Quantification of the number of TUNEL positive cells relative to the total number of granulosa cells present in each follicle analyzed from prepubertal and adult sections from $Atr^{+/+}$ and $Atr^{s/s}$ ovaries at the indicated stages. Horizontal black lines in the graph denote the means. Seckel females exhibit a significant increased proportion of TUNEL positive granulosa cells in secondary follicles indicating a rise in the follicular cells apoptotic rate.

follicle (**Fig. 4.21a**). The results obtained revealed that Seckel mouse follicles tended to present more apoptotic cells than control follicles in all follicular stages. Nevertheless, in this case, while in primary follicles apoptotic cells rate was not statistically different between control and mutant mouse follicles, neither in prepubertal (p=0.4849, t test, **Fig. 4.22b, Table 4.6**), not in adult mice (p=0.5967, t test), small secondary follicles presented a substantial increase of follicular cell apoptotic rate. We found five-fold increase in prepubertal (p<0.0001, t test) and around nine-fold increase in adult mice (p=0.0017). This increment in the apoptotic follicular cells rate present in Seckel ovaries supports the idea that reduction of ATR expression in the ovaries causes follicle development defects.

Hence, these data indicate that in Seckel mouse ovaries while follicles grow and the number of granulosa cells rise, the number of apoptotic granulosa cells increase, intensifying the developmental problems that experienced these follicles. Consistent with proliferation analysis, these results suggest that only those follicles that achieve a high proliferative capacity can overcome the increased apoptotic rate present in Seckel mouse follicles and thus progress

throughout folliculogenesis. Therefore, all these findings suggest that ATR is necessary to achieve a successful follicle development and consequently, a correct folliculogenesis progression. Deficient ATR levels in Seckel ovaries propitiate a reduction in the number of growing follicles.

DISCUSSION

Chapter 5

5.1 New strategies to investigate ATR roles in meiosis

The study of ATR role during mammalian meiosis has been a challenge for years. On the one hand, the essential requirement of ATR for embryo development has hampered for decades the generation of mammalian models for ATR deficiency that enable to investigate the function of this kinase during gametogenesis. On the other hand, the limitations to reproduce gametogenesis *in vitro* have impeded the use of culture methods to perform meiotic studies. In the present work we employed recently developed approaches in order to provide new advances in the study of ATR implications in meiosis and gametogenesis.

5.1.1 Seckel mouse constitutes a valid model to study the role of ATR during meiosis

In this study, we used a genetically engineered mouse model of ATR Seckel syndrome generated few years ago. This novel model was reported to be an ATR-knockdown mouse that causes loss of ATR-function in most organs (Murga et al. 2009). Here, we demonstrated that ATR levels were also affected in adult testis, as well as, in ovaries, as we observed by RT-PCR and western blot. According to these observations, we used the analysis of the known roles of ATR in MSCI in order to determine whether ATR function was also down-regulated during meiosis. In this way, we found evidences that ATR deficiency substantially reduced ATR function. Comparison of sex body formation between control and Seckel mice spermatocytes revealed that accumulation of ATR in unsynapsed sex chromosome axes was impaired. Most mutant spermatocytes accumulate ATR only in X and Y AE and, only few pachytene cells exhibited perceptible ATR translocation into the chromatin loops. Linked to these defects in the accumulation of ATR, we detected reduced levels of two epigenetic modifications, SUMO-1 and γH2AX protein on sex chromosome chromatin. These two measurements were consistent with the previously published roles of ATR in MSCI since ATR promotes accumulation of the SUMO-1 epigenetic modification into sex chromosomes, as well, phosphorylation of H2AX during zygotene and pachytene stages (Royo et al. 2013). Moreover, we observed increased MDC1 accumulation into the XY chromatin showing that reduced expression of ATR in spermatocytes is not affecting MDC1 location. Therefore, we demonstrated that the reduction of ATR observed in Seckel mouse testis is affecting the already known functions of ATR during meiosis in sex body formation. Furthermore, since correct MSCI is essential for male fertility and failure in sex body formation promotes a pachytene arrest when sex-linked genes are not transcriptionally silenced (Royo et al. 2010), we conclude that wild type levels of ATR are not essential to initiate and/or maintain sex chromosome meiotic silencing. Indeed, unpublished data from our group reveals that sex chromosome silencing is unaffected by ATR loss of function occurring in Seckel spermatocytes (M. Marcet-Ortega and I. Roig, unpublished data). We analyzed expression of X-linked gene *Zfx* in pachytene Seckel mouse spermatocytes in order to investigate MSCI efficiency. We observed proper meiotic silencing, as noticeable by

reduced levels of *Zfx* expression, in $Atr^{s/s}$ pachytene-stage cells compared to controls (p=1.0000, Fisher's exact test, **Fig. 5.1**).

On the basis of these findings, we propose that the Seckel mouse is a valid model to investigate the implications of ATR in mammalian meiotic recombination and during gametogenesis.

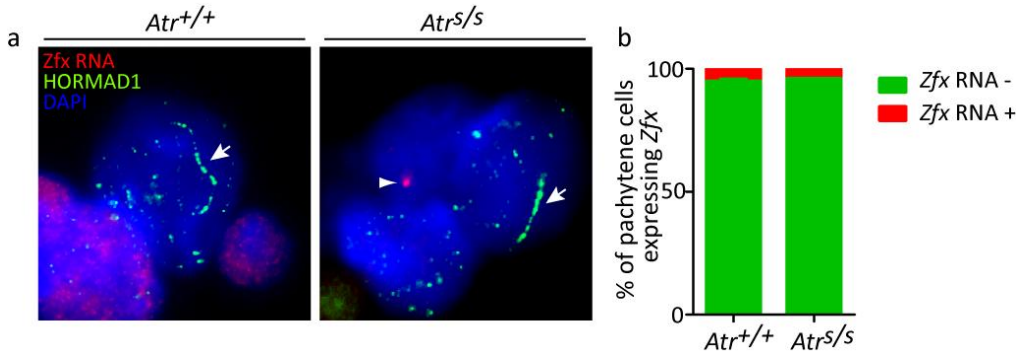

Figure 5.1. Seckel mouse spermatocytes exhibit proper meiotic sex chromosome meiotic inactivation. **a)** Representative images of early-pachytene spermatocytes from the indicated genotipes. Images show immunofluorescence against HORMAD1 proteins, which is mostly confined to sex chromosomes (arrows) at early-pachynema (green), overlayed with RNA FISH for X-linked gen (*Zfx*) (red), and DAPI (blue). Note that *Zfx* is not expressed in any cell evidencing proper sex chromosome meiotic silencing in both, $Atr^{+/+}$ and $Atr^{s/s}$ pachytene spermatocytes. One HORMAD1 negative cell is expressing the X-linked gen (arrowhead). **b)** Percentage of pachytene cells exhibiting *Zfx* RNA FISH signals (red) in $Atr^{+/+}$ (N=95) and $Atr^{s/s}$ (N=48). Columns and lines indicate the mean and standard error (SEM). Note that a similar proportion of pachytene cells are expressing X-linked genes in both genotypes.

5.1.2 Neonatal testis organ culture is a useful tool to study meiotic prophase in vitro

One of the technical challenges that have been holding up our understanding of spermatogenesis has been the absence of culture methods that reproduce spermatogenesis *in vitro.* Given the complexity of spermatogenesis and the fact that it occurs into the seminiferous tubules with the support of different somatic cell types, the complete process of spermatogenesis has been difficult to reproduce *in vitro* (Parks et al. 2003; Song & Wilkinson 2012). In the last years, Sato et al. reported the first strategy to recapitulate spermatogenesis from primitive spermatogonia using an organ culture method. In the present work, employing this new approach, we achieved spermatocyte meiotic progression *in vitro* from neonatal testis. We succeeded in promoting germ cells to progress into the first wave of spermatogenesis *in vitro*, and eventually reaching pachytene stage by 14 days of culture. Thus, for the first time we exploited the possibilities of the neonatal organ culture method to study the role of ATR during meiotic recombination using selective inhibitors to down-regulate ATR function.

Here we report new benefits for the use of *in vitro* spermatogenesis to the understanding of meiotic processes. Until now, to study the role of specific genes in

mammalian meiosis it has been necessary to produce genetically engineered animals, mostly mice, carrying targeted mutations in specific genes. Nonetheless, production of genetic modified mice is a complex process that requires enormous time and economical efforts. As we mentioned above, obtaining viable mutant models for ATR gene has been a challenge for years because of the intrinsic nature of this kinase. Notably, there are only two mouse models available to study ATR deficiency until date, one conditional ATR-knockdown system that down-regulates ATR expression in adult animals (Ruzankina et al. 2007), and the ATR-Seckel model, which has reduced ATR protein levels in all organs by introducing the mutation into the mouse germ line (Murga et al. 2009). Importantly, the Seckel model allows a certain level of *Atr* expression in testis (**Fig. 4.1**) that obscures the dramatic functions that ATR has in this process. We demonstrated here that administrating a selective ATR inhibitor in testis organ cultures we could target ATR kinase, and in this way, study the consequences of severe ATR down regulation during meiotic prophase.

Therefore, we propose that testis organ culture is a very useful tool that enables the manipulation meiotic events using drugs to target specific proteins during meiotic prophase. Consequently, this method could allow reduction of the number of experimental animals used in the experimental procedures being a complement of *in vivo* studies in mice.

5.2 ATR kinase is essential to complete meiotic recombination

Generation of haploid gametes during meiosis is a crucial step for sexually reproducing organisms. Critical events occur during prophase of the first meiotic division. Deliberated generation of DNA double strand breaks in the genome and their repair promote synapsis, recombination and CO formation between homologous chromosomes. All of these processes are essential to ensure homologous chromosomes accurately segregate originating haploid cells. Thence, meiocytes present highly regulated machinery that coordinates these processes to elicit the appropriate responses.

ATR is one of the players of the DNA damage response machinery. ATR is activated by RPA-coated ssDNA (Cimprich & Cortez 2008). In meiotic cells, RPA appears in response to SPO11-generated DSBs that are resected at the beginning of meiotic prophase. Later on at zygonema, ssDNA fragments appear during strand invasion of the homolog chromosome. RPA-ssDNA complex is a prerequisite for the association of RAD51 and DMC1 proteins in the DSB sites forming nucleoprotein filaments (Fanning et al. 2006; Bannister & Schimenti 2004b; Brown & Bishop 2014). RAD51 and DMC1 are both components of the recombination nodules and cooperate during meiotic recombination to mediate strand-exchange to establish proper interhomolog connections. Accordingly with the previously described presence of ATR in

recombination nodules (Keegan et al. 1996; Plug et al. 1998; Moens et al. 1999), we present here new evidences of ATR being directly involved in meiotic recombination.

5.2.1 Seckel mouse spermatocytes present a temporally delayed homologous recombination

Cytological studies have been commonly used to monitor the dynamic of recombination proteins accumulation on the genome during meiotic prophase. Different immunostaining studies have showed that RAD51 and DMC1 proteins are detected first at early-leptonema forming foci on chromosome axes. As synapsis proceeds, foci numbers decrease and eventually disappear at the mid/late-pachynema, when most RAD51/DMC1 foci are confined to the unsynapsed sex chromosome axes (Tarsounas et al. 1999; Moens et al. 2002). Therefore, based on the appearance of recombination protein foci during prophase meiotic recombination progression can be followed in spermatocytes.

Immunostaining analysis of the abovementioned recombination proteins showed that when ATR is down-regulated DSB repair progression is altered. In the first place, we noticed that deficiency of ATR produced changes in RAD51 and DMC1 accumulation during prophase. Reduced numbers of RAD51 and DMC1 foci were detected during leptonema in Seckel mouse spermatocytes indicating that correct temporary recruitment of these proteins on chromosome axis requires wild type levels of ATR. In addition, this decrease was accompanied by the presence of increased numbers of RPA foci at early-leptonema in these cells. In mouse, mutants with impaired loading of RAD51 have been reported to show high-abundance of RPA foci at early stages of meiotic prophase (Sharan et al. 2004; Yang et al. 2008b; Roig et al. 2010; Llano et al. 2012). Then, we suggest that in the absence of wild type levels of ATR, RAD51 and DMC1 cannot replace RPA at resected DSBs, at least in a normal timing, and subsequently RPA remains loaded longer in resected DSB sites.

Nevertheless, it could be possible that the increased abundance of RPA foci seen at leptonema may reflect an increased DSB levels inflicted by SPO11 at the onset of prophase. In order to discard this possibility, we collaborate with S. Keeney and J. Lange (MSKCC) to study the levels of meiotic DSB formation in adult Seckel mouse testis by analyzing SPO11-oligonucleotide complexes (Pan & Keeney 2009). The analysis showed that SPO11-oligonucleotide complexes signal in $Atr^{s/s}$ testes is reduced compared to control testes (26.5 ± 1.5 % of the $Atr^{+/+}$ signal) (**Fig. 5.2**). Nevertheless, considering that Seckel testes weight is ~25% of $Atr^{+/+}$ testes weight, we reason that the reduction observed in SPO11-oligonucleotide complexes is reflecting the reduction in testis size. Thus, according to this finding we discard the possibility that Seckel testes display increased SPO11-generated DSB levels.

Alternatively the increased number of RPA foci could also result from an accumulation of DNA damage produced during S-phase due to the reduction of ATR activity (Flynn & Zou 2011). One approximation to study this was to analyze RPA presence in leptonema from

Spo11$^{-/-}$ *Atr*$^{s/s}$ double mutant mice. Unfortunately, we did not obtain any double mutants from double heterozygous breedings (13 litters, 78 pups). Notably, while *Spo11*$^{-/-}$ *Atr*$^{+/s}$ mutants were obtained at expected ratios (11 pups obtained, p=0.8423, Chi Squared text), no *Spo11*$^{+/-}$ *Atr*$^{s/s}$ animals were obtained from these breedings (p=0.0185, Chi Squared text) suggesting that wild type levels of SPO11 could be necessary to permit embryo viability in an ATR reduced scenario. Therefore, although we cannot demonstrate that spermatocytes enter into meiosis without carrying DNA damage, we favor the conclusion that the pattern observed in Seckel mouse spermatocytes may reflect the persistence of RPA in DSB sites due to the impaired loading of RAD51/DMC1, since this is the best model to explain the observed RPA foci rise coupled to an RAD51/DMC1 foci reduction.

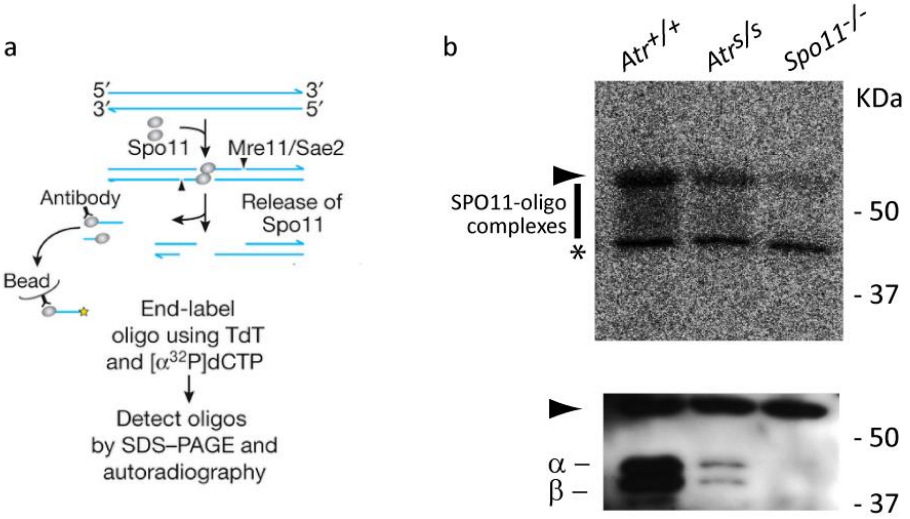

Figure 5.2. Levels of SPO11-oligonucleotide complexes are similar in Seckel and control testes. a) SPO11-oligonucleotide complexes were immunoprecipitated from testes extracts, labeled with terminal transferase and ^{32}P-nucleotide. Oligonucleotides were detected by SDS-PAGE and autoradiography. Image adapted from Thacker et al. 2014. **b)** Autoradiography (top image) shows the signal from SPO11-oligonucleotide complexes (vertical line) from the indicated genotypes. SPO11 western blot (bottom image) shows the two major SPO11 splicing isoforms, α and β. Asterisk indicates non-specific signal from the labeling reaction. Arrowheads denote the migration position of immunoglobulin heavy chain used to precipitate SPO11.

Accordingly to these data, we also found increased number of RAD51 and DMC1 foci at pachynema in Seckel mouse spermatocytes compared to control cells. These results along with the observation of persistent foci of the DSB signaling protein γH2AX at late stages of prophase suggest the presence of persistent DSBs in Seckel spermatocytes. Nevertheless, at diplonema the number of RAD51 and DMC1 foci was similar between *Atr*$^{s/s}$ and control cells indicating that Seckel mouse meiocytes can repair these DSBs, although they may require more time to accomplish meiotic recombination. The most straightforward explanation for these results is that ATR have a direct role in the loading of RAD51 or DMC1 proteins to the DSB site, and for this reason decreased levels of ATR protein lead to a delayed processing of DSBs.

Since X and Y chromosome homology is limited to the small PAR, sex chromosomes meiotic recombination is particularly susceptible to suffer small impairments (Mohandas et al. 1992; Hall et al. 2006). Hence, the XY pair should be more sensitive to the perturbations in DSB repair caused for ATR reduction. Indeed, Seckel mutant spermatocytes showed a two-fold increase of the XY synapsis failure found at pachynema, a fact that has been described to be related to deficient recombination events occurring at the PAR (Kauppi et al 2010). Interestingly, $Atr^{s/s}$ spermatocytes at diplonema exhibited normal levels of asynaptic sex chromosomes compare to $Atr^{+/+}$, reinforcing the idea that the defects observed in Seckel mouse spermatocytes are explainable by a delay in DSB repair.

Indeed, supporting this hypothesis, testis organ cultures treated with high doses of ATR inhibitor revealed that when ATR function was blocked, RAD51 presence on chromosome axes was dramatically reduced at all stages of prophase analyzed. In addition, in accordance to our previous observations in Seckel autosomal chromosomes, RPA foci were increased at early-leptonema, corroborating the deduction that ATR is necessary to incorporate RAD51 to resected DSB sites mediating RPA displacement from early-recombination nodules.

5.2.2 Down-regulation of ATR impaired synapsis due to failure to complete meiotic homologous recombination

It is widely accepted that defective HR results in a lack of coordination between DSB repair, synapsis and prophase progression (Bannister & Schimenti 2004b; MacQueen & Hochwagen 2011). Nonetheless, we only noticed a slight synapsis defect on the XY pair from *Atr*-mutant spermatocytes. Seckel mouse meiocytes display full autosomal synapsis and completed prophase I in a proper time as demonstrated by the presence of normal proportion of spermatocytes at different stages of prophase. In view of this, we propose that the reduction of ATR levels present in Seckel mice is not sufficient to impair homologous pairing and synapsis between autosomal chromosomes. We assume that the number of homologous recombination events is enough to complete homologous synapsis with this level of ATR reduction, although DSB repair appears slightly delayed. Interestingly, spermatocytes treated with ATRi exhibited defects in prophase progression, and these defects were more pronounced as the ATRi dosage increased. Analysis from spermatocytes treated with 5µM AZ-20 exhibited profound abnormalities in prophase progression. SYCP3 staining in these spermatocytes revealed patterns characteristics of leptotene and zygotene stages. Thus, these results indicated that ATR function is necessary to complete synapsis, probably due to failure to complete proper HR.

Our analysis of RPA in spermatocytes treated with 5 µM AZ-20 showed that the number of RPA foci decreased as meiotic prophase progressed indicating DSB repair events. Furthermore, the number of RPA foci found at late zygonema was significantly lower than the one found in not-treated samples. These findings probably suggest that in the absence of RAD51 assembly at recombination nodules, DSBs may be repaired by RAD51-independent

mechanisms. One RAD51-independent DSB repair pathway is non-homologous end joining (NHEJ), which is accomplished by the ligation of the DNA ends of both sides of DSB (Heyer et al. 2010). However, the protein KU70, which is essential to NHEJ, has been reported to be absent in the wild type spermatocyte nuclei until pachynema, when appears confined to the sex body presumably to allow DSB repair in sex chromosomes (Goedecke et al. 1999). Another well established RAD51-independent repair mechanism is the single strand annealing (SSA) mediated by RAD52. Studies in budding yeast demonstrated that RAD52 appears in response to SPO11-generated DSBs and co-localize with RPA (Gasior et al. 1998). SSA requires DSB resection to expose complementary sequences, and ssDNA-RPA coated to recruit RAD52 protein. Then, DNA repair involves reannealing of both ends of DSB. As DNA strand invasion is not involved in SSA, this repair mechanism is independent of RAD51 (Heyer et al. 2010; Krejci et al. 2012). Alternatively, a recent study carried out in human cells has demonstrated a mechanism, in which MUS81, a protein implicated in the formation of MLH1-independent COs during meiosis, interacts with RAD52 in an RAD51-independent manner during replication stress. Moreover, *in vitro* MUS81 acts in D-loops formed by RAD52, but not by RAD51 protein (Murfuni et al. 2013). However, whether RAD52 could catalyze strand invasion without RAD51 *in vivo* requires further investigation. Additional studies are still necessary to extend our understanding of how RAD51-independent DSB repair pathways may operate during meiosis.

Strikingly, RPA levels diminished faster in ATRi-treated than in not-treated spermatocytes as prophase progressed. As mentioned earlier, RPA foci found during meiosis are the result of at least two different events. Firstly, the resection of SPO11-generated DSBs. And secondly, the result of the strand invasion caused by RAD51/DMC1 activity that creates a fragment of ssDNA in the invaded chromosome. With this in mind, the fastest reduction of the RPA foci observed in ATRi-treated cells could be explained if DSB repair by RAD51-independent pathways did not involve D-loop formation, and thus RPA could not be incorporated after the strand invasion was performed. Nevertheless, considering that NHEJ pathways are inhibited until pachytene and SSA requires complementary DNA sequences to complete DSB re-annealing, the velocity by which RPA foci decreased is difficult to understand. An alternative explanation could be that ATRi-treated spermatocytes accumulate less DSBs in unsynapsed axes than not-treated spermatocytes. Considering that DSB formation in unsynapsed axes continues until synapsis is completed (Kauppi et al. 2013; Thacker et al. 2014), we propose that in ATR down-regulated spermatocytes the accumulation of DSBs in unsynapsed axes may be impaired (see a more detailed discussion below).

5.2.3 Model for ATR-dependent loading of RAD51 and DMC1 to DSB sites

Another intriguing question to consider from meiotic HR analysis is why DMC1 staining pattern is more affected than that of RAD51 in Seckel mouse spermatocytes. RAD51 foci can form in DMC1-deficient spermatocytes implying that functional DMC1 is not a requisite for RAD51 foci loading in chromosome axes (Yoshida et al. 1998; Pittman et al. 1998). Since

mutation in mouse *Rad51* results in early embryonic lethality (Lim & Hasty 1996; Tsuzuki et al. 1996), the role of RAD51 in DMC1 recruitment and the effects on homologous recombination in mammalian meiocytes has been inferred from studies in other organisms. In budding yeast, absence of RAD51 strongly impairs meiotic recombination and results in failure to repair DSBs and cell cycle arrest. In these mutants, DMC1 nucleofilament formation is considerably dimmer. Contrary, as occurs in mice, RAD51 formation appears normal in the absence of DMC1 (Bishop et al. 1992, 1994; Shinohara et al. 1992). Recent studies carried out on *S. cerevisiae* and *A. thaliana* have clarified the specific roles of these two proteins. These studies demonstrated that the strand-exchange activity of DMC1 by itself is sufficient to mediate meiotic interhomolog recombination, whereas RAD51 is essential for DMC1 foci formation, performing a crucial regulatory role by stimulating DMC1's D-loop formation activity, but not for its catalytic activity (Cloud et al. 2012; Da Ines et al. 2013). Different models have been proposed to explain the cytological localization of RAD51 and DMC1 proteins. It is widely accepted that RAD51 and DMC1 are usually confined to the same DSB site, although both foci do not precisely colocalize (Shinohara et al. 2000; Kurzbauer et al. 2012). This finding instigated a model where RAD51 forms a filament in one side of the resected DSB and DMC1 on the other (Shinohara et al. 2000; Hunter & Kleckner 2001). Nevertheless, this asymmetric model is not in accordance with the recent discoveries about RAD51 and DMC1 roles. Actually, Bishop and colleagues have proposed an attractive model in which loading of RAD51 occurs on both sides of the resected DSBs creating a homofilament in each end that serves as a mold to initiate DMC1 filament polymerization (Brown & Bishop 2014). On the basis of these observations, we propose that ATR directly promote the recruitment of RAD51, and possibly DMC1, to the resected DSB sties. Nevertherless, since RAD51 nucleofilament support DMC1 nucleofilament formation on DSB site, it is presumable that in a scenario where ATR kinase is a limiting factor, DMC1 loading to DSB sites is reduced and/or more delayed, because the available ATR is being used to mediate RAD51 assembly. In this way, it is plausible that ATR promotes HR phosphorylating RAD51, and possibly DMC1, to mediate recruitment to DSB sites. Indeed, there are several evidences that RAD51 could be activated in an ATR-dependent manner to promote HR repair. It has been demonstrated that RAD51 presents an S/T-Q cluster domain (SCD), which are potential phosphorylating sites for ATR and ATM (Cheung et al. 2012). Furthermore, a recent study in *S. cerevisiae* reports that Mec1-dependent RAD51 phosphorylation on S192 promotes HR in response to DNA damage (Flott et al. 2011). Likewise, given the structural and biochemical similarities between RAD51 and DMC1 (Masson & West 2001; Sheridan et al. 2008) and the fact that an SCD has also been detected in DMC1 (Cheung et al. 2012), ATR can also mediate DMC1 phosphorylation affecting its ability to form a nucleofilament with the ssDNA during meiosis.

So that, we propose a model in which RAD51 and DMC1 foci are recruited to SPO11-generated DSBs via phosphorylation mediated by ATR in order to promote HR repair. Thereby, if ATR is regulating RAD51 assembly, and possibly DMC1, it could be possible that in an ATR defective scenario, where RAD51 assembly is defective, RPA persist longer preventing also RAD51-independent DMC1 nucleofilament formation (**Fig 5.3**).

5.2.4 *Seckel mouse meiocytes showed a delay in CO formation*

Crossover formation is a tightly regulated process. The repair of some DSBs generate reciprocal exchanges (COs) that play an essential role in segregation during first meiotic division providing faithful connection between homologous chromosomes, which help to guide proper alignment on the meiotic spindle. During pachytene stage MLH1 staining appears in some recombination nodules marking most DSB sites resolved as COs (Baker et al. 1996; Edelmann et al. 1996). Here we reported that $Atr^{s/s}$ spermatocytes presented a decrease in the number of MLH1 foci numbers at pachynema. Consistent with the observation that wild type levels of ATR are essential to achieve a temporary normal meiotic recombination, we propose that Seckel meiocytes present a delay in CO formation.

Besides a decrease of total MLH1 foci numbers detected in Seckel mouse spermatocytes, both $Atr^{s/s}$ spermatocytes and oocytes showed an increased number of bivalents lacking an MLH1 focus at pachynema. Two different situations could explain this MLH1 foci reduction. Based on all the discussed above, the most straightforward interpretation is that $Atr^{s/s}$ meiocytes suffer a delay in CO formation. Alternatively, given that each DSB can either be repaired as a NCO or as a CO, a drop in MLH1 could reflect the involvement of ATR in the regulation of DSB repair pathway towards the CO pathways (Guillon et al. 2005). We favor the first interpretation in view of the number of bivalents lacking an MLH1 focus in oocytes is restored to control levels at diplonema. Moreover analysis of the number of achiasmate bivalents detected at late-diplonema in Seckel spermatocytes was undistinguishable between mutant and control cells. Even so, despite the wild type levels of achiasmate bivalents at diplonema, we cannot exclude the possibility that ATR promotes formation of MLH1-dependent COs, thus reduced levels of ATR could cause an increase in the number of MLH1-independent COs (Baker et al. 1996; Holloway et al. 2008). In mice, MUS81 has been reported to participate in CO formation in a MLH1-independent pathway (de los Santos et al. 2003; Holloway et al. 2008). Since MUS81-dependent COs are supposed to be non-interfering events, *Mus81-null* mice show reduced interference among MLH1 foci (Holloway et al. 2008). In base of this data, we predict that if more COs were resolved by MUS81-dependent pathway at the expense of that MLH1-dependent pathway in Seckel mouse spermatocytes interference would be increased due to the presence of more space between MLH1 foci. By contrast, Seckel mice spermatocytes showed undistinguishable interference compared to controls.

In addition, CO formation analysis on sex chromosomes showed that whereas Seckel mouse spermatocytes presented two-fold decrease in the number of XY pairs showing an MLH1 focus, the analysis of achiasmate XY pair at late-diplonema revealed a similar dynamic between mutant and control spermatocytes. Thus, these results reinforce the idea that Seckel mouse meiocytes exhibit a delayed meiotic recombination. Taken these observations together we propose that ATR is necessary to promote homologous recombination events, given that when ATR is reduced DSB repair, and consequently CO formation, are delayed.

During both mitosis and meiosis, the spindle assembly checkpoint blocks progression from metaphase to anaphase when spindle formation is defective or when chromosomes are misaligned in the spindle (Gorbsky 2014). Thus, reduction of chiasmata might originate premature separation of the bivalents, and subsequently the presence of univalents at MI. Univalents have been described to be not properly positioned on the meiotic spindle, thereby triggering a spindle assembly checkpoint that leads to cell death. Here we detected that seminiferous tubules from Seckel testes presented some apoptotic cells, presumably at MI stage. However, the few apoptotic cells found in Seckel testis do not seem to imply a biological impasse for fertility. Based on our detailed analysis, we think the minor arrest reported here could be reflecting subtle defects in CO formation. Although we have to consider the possibility that ATR is participating in the formation of the meiotic spindle (Cheung et al. 2012), we favor the interpretation that apoptotic cells observed in Seckel spermatocytes are associated with defects in CO formation in the sex chromosomes. It has been demonstrated than in spermatocytes, rather than in oocytes, the presence of a single unpaired bivalent, like the sex chromosomes, induces strong meiotic MI apoptosi (de Boer et al. 1991; LeMaire-Adkins et al. 1997; Kauppi et al. 2011). As we mentioned above, the XY pair are highly affected by recombination impairments because of the small PAR (Mohandas et al. 1992; Hall et al. 2006), even though sex chromosomes display special mechanisms to ensure synapsis and recombination (Kauppi et al. 2013). Taken together, we propose that sex chromosomes from *Atr*$^{s/s}$ spermatocytes presented defective CO formation due to the combined effect of the delayed recombination observed and the reduced DSB accumulation in sex chromosomes that could reduce the efficiency of DSB formation in PAR region (discussed below).

5.2.5 Seckel mice exhibited sexual dimorphism during meiotic prophase

The results reported here evidence that the phenotype associated to ATR reduction affects oocytes and spermatocytes in a different manner. Whereas spermatocytes showed a delay in the complete process of meiotic homologous recombination, oocytes showed meiotic prophase progression similar to controls, exhibiting only minor differences in the number of bivalents lacking MLH1 foci at pachynema, but not in global numbers. Thus, there is sexual dimorphism between meiocytes associated to the requisite of ATR kinase during meiotic prophase. Nevertheless, considering that we analyzed ATR expression by RT-PCR in mutant adult ovaries, even though meiosis in females starts in the fetal gonads, we contemplate the possibility that ATR levels during development in mutant fetal gonads are more elevated than in the adult organs. However, it could be also plausible that less ATR levels would be necessary to complete meiosis for an oocyte.

Sexually dimorphic phenotypes have been previously reported for many mutations that affect meiotic DSB repair pathways (Hunt & Hassold 2002; Morelli & Cohen 2005). Remarkably, in many of those mutations, males present a more severe phenotype with arrest at pachynema, while females progress through prophase I (Barlow et al. 1998; Libby et al. 2002;

Celeste et al. 2002; Sharan et al. 2004). The presence of unrepaired recombination intermediates cause early oocyte loss, whereas oocytes defective in homologous synapsis are eliminated late around two weeks after birth (Di Giacomo et al. 2005). This data indicate spermatocytes and oocytes show different behavior in meiotic prophase. So that, it could be reasonable to think that females take more time to repair DSB events during prophase. In this way, it could be possible that the delayed meiotic recombination observed in mutant spermatocytes was less dramatic in oocytes if DSB repair occurs in a prolonged time period. Nevertheless, further analyses are required to try to discriminate between these possibilities.

5.3 ATR is involved in the regulation of DSB accumulation in unsynapsed axes

DSB formation during meiosis is known to be a highly regulated process. DSB formation is proposed to be the result of a balancing act that maintains moderate DSB levels to allow proper meiotic progression. Preventing excessive DSBs to avoid recombination failure, but, ensuring adequate DSB formation to favor homologous synapsis (Keeney et al. 2014; Cooper et al. 2014). Several recent discoveries have pointed to ATR and ATM kinases as key regulators of the mechanisms that maintain DSB levels and control DSB formation (Lange et al. 2011; Gray et al. 2013; Carballo et al. 2013; Joshi et al. 2015). Indeed, different studies carried out in mouse, *D. melanogaster* and *S. cerevisiae* have implicated ATM signaling pathway in a negative feedback circuit that regulates DSB formation by inhibiting SPO11 activity (Lange et al. 2011; Joyce et al. 2011; Carballo et al. 2013; Pacheco et al. 2015).

Recent works have elucidated the presence of another feedback circuit associated to the successful engagement of homologous chromosomes that inhibit DSB formation (Kauppi et al. 2013; Gray et al. 2013; Thacker et al. 2014). Spermatocytes from a *Spo11*-null mouse carrying a transgenic construct expressing only a single copy of *Spo11β* splicing isoform (*Spo11*$^{-/-}$ *Tg(Spo11β)*$^{+/-}$), catalyze reduced levels of DSBs, accompanied by reduced ability to mediate homologous synapsis. Importantly, in these spermatocytes whereas the global DSB levels were diminished, continuous accumulation of RAD51 foci was detected in unsynapsed chromosome axes (Kauppi et al. 2013). Similarly, recent discoveries in yeast revealed that in *S. cerevisiae* strains exhibiting suboptimal DSB catalysis due to hypomorphic *Spo11* mutations, ssDNA products resulting from DSB resection activate Mec1 signaling pathway that, in turn, mediates a transient cell cycle arrest to allow further DSB formation until wild type levels are reached (Gray et al. 2013). In addition, an independent study showed that defective interactions between homologous chromosomes, caused by mutations in ZMM proteins needed for proper SC formation, also results in continuous DSB accumulation (Thacker et al. 2014). In mice, the naturally unsynapsed region of the X chromosome was reported to be subjected to a continuous RAD51 accumulation as meiotic prophase progresses (Kauppi et al. 2013). Accordingly, we showed that in control spermatocytes X chromosome axes accumulated

RAD51 foci, and RPA foci as well, from early to late-zygonema demonstrating accumulation of DSBs as prophase progressed. However, Seckel mouse spermatocytes did not showed significant increased numbers of RAD51 or RPA foci between early and late-zygotene. These findings lead us to propose that wild type levels of ATR are required to promote a local accumulation of DSBs in the unsynapsed X chromosome axis. Additionally, as we observed in autosomal chromosomes, Seckel mouse spermatocytes showed reduced number of RAD51 foci in X chromosome at early and late-zygonema compared to control cells, reflecting delayed RAD51 assembly. At this point, based in our previous findings we predicted that X chromosome in mutants may present increased numbers of RPA foci. By contrast, RPA foci counts in $Atr^{s/s}$ spermatocytes were undistinguishable from what we counted in $Atr^{+/+}$ spermatocytes in early, as well as, in late-zygonema. One model to explain this reduction in the number of RAD51 foci, not accompanied with an increased numbers of RPA foci, may be that Seckel spermatocytes form less DSBs in the X chromosome compared to control spermatocytes. Hence, decreased RAD51 foci in X chromosome may reflect delayed DSB repair combined with reduced DSB formation. These observations lead us to propose that ATR have a crucial role in promoting DSB formation on unsynapsed axes as meiotic prophase progresses. Furthermore, our results support previous findings suggesting the formation of late DSB during prophase progression is an indispensable requisite to promote XY recombination, to achieve proper synapsis within the PAR (Kauppi et al. 2011).

Interestingly, our results showed that spermatocytes from testis organ cultures treated with 5µM AZ-20 displayed defects in homologous chromosome synapsis, most likely due to impaired homologous recombination. In not-treated spermatocytes, we observed that when DSBs are repaired as prophase progresses -as noticeable by the pattern observed in RAD51 staining- the mean RPA foci number was maintained around the same levels from leptonema to late-zygonema. This data suggests that meanwhile some DSBs were repaired, which explains the dramatic reduction in RAD51/DMC1 foci (approximately 50%), new DSBs are created, likely on unsynapsed axes to promote completion of synapsis. At this point, accordingly with previously described data, we reasoned that if spermatocytes treated with 5 µM AZ-20 had impaired synapsis, these cells might accumulate highest levels of RPA foci. However, RPA foci numbers in ATRi-treated spermatocytes dropped as prophase progressed. This data has several implications: first, early-generated DSBs may be repaired via a RAD51-independent pathway which would explain why RPA numbers decreased as meiotic prophase progressed (as previously discussed). Secondly, the global reduction in the number of RPA foci may be indicative that chromosome axes that fail to synapse in ATRi-treated mouse spermatocytes may not be accumulating new DSBs as prophase progresses. On the basis of these observations we deduce that ATR is required to promote the accumulation of DSBs on unsynapsed chromosome axes as meiotic prophase progresses, separately of its role in promoting HR. Notably, consistent with this idea that ATR is involved in the regulation of DSB formation at late stages of prophase it has been proposed that in yeast whereas the control of early-DSB resection and interhomolog processing depends on ATM when DSB levels reach a

certain threshold, ATR is activated and DSB-resection and processing become dependent of both kinases (Joshi et al. 2015).

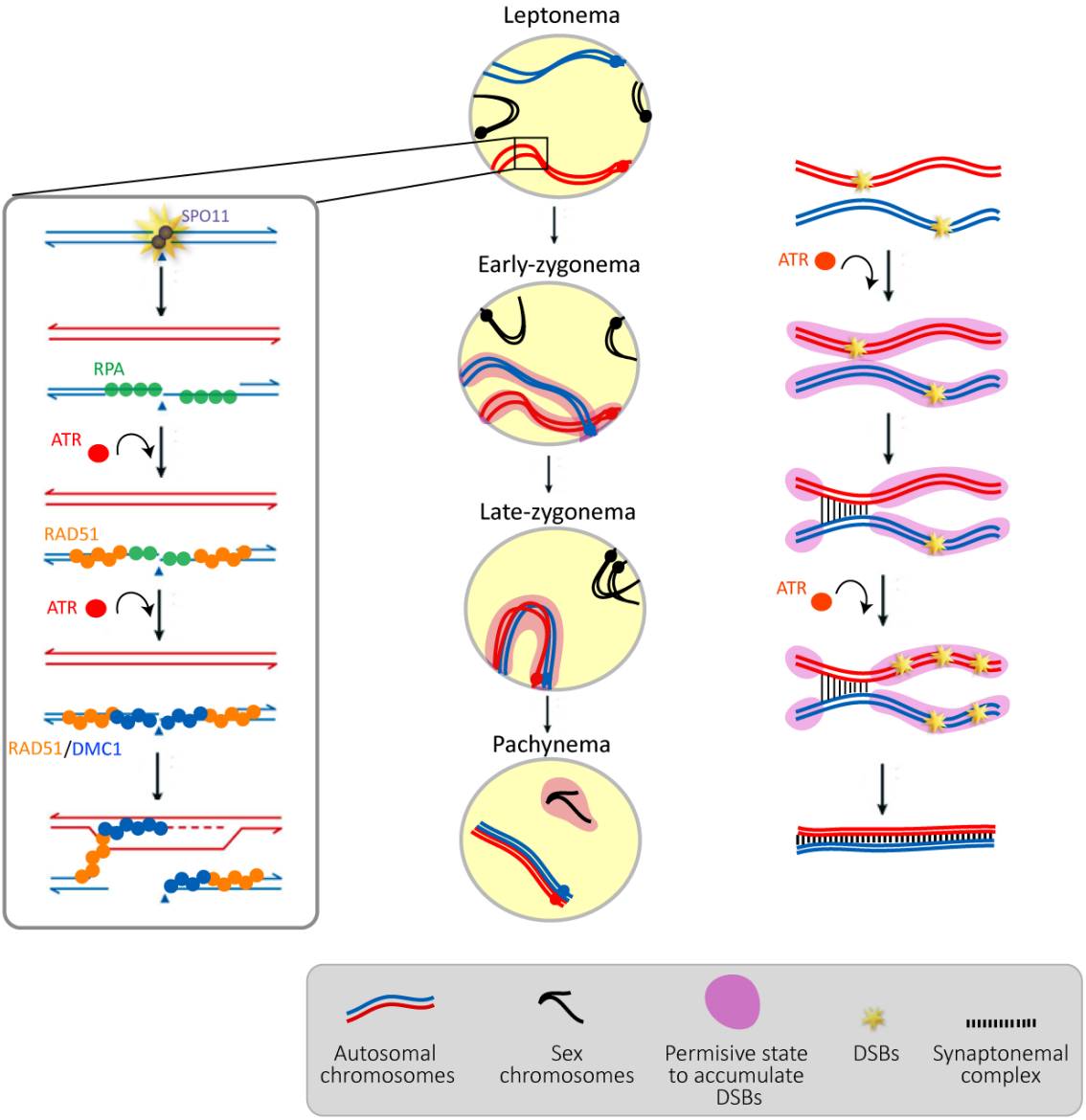

Figure 5.3. Working model for ATR role during meiotic prophase. ATR presents two independent functions during meiotic prophase. On the one hand, ATR plays a role in promoting HR (black box). Separately, ATR stimulate local DSB accumulation on unsynapsed axes. We propose that at leptonema, ATR phosphorylates HORMAD proteins mediating that chromosomes acquire a permissive state to generate DSBs (pink clouds). As synapsis occurs at sites of recombination, the permissive state of the chromosomes to receive DSBs is lost. Then, ATR is recruited at the axes that remain unsynapsed and promote continuous accumulation of DSBs to ensure correct synapsis. Completion of autosomal synapsis blocks further DSB accumulation, and ATR is restricted to the XY pair where maintain local permissive DSB accumulation and promote MSCI.

Hence, according to the understanding that in wild type spermatocytes DSB formation is suppressed when synapsis is accomplished, we propose that ATR kinase is regulating the local accumulation of DSBs in the axes that remain unsynapsed during meiotic prophase. A feasible model that accounts for ATR involvement in regulation of DSB levels is that unsynapsed regions could remain permissive to DSB formation until structural changes encompassing SC formation lock the "permissive state" of the chromosome to accumulate DSBs. In this way, HORMAD-domain proteins (HORMADs) localize to unsynapsed chromosome axes and, are displaced after SC formation (Wojtasz et al. 2009; Shin et al. 2010). It has been proposed that HORMADs displacement from synapsed chromosomes might suppress continuous DSB formation due to HORMADs are necessary to achieve normal DSB levels (Daniel et al. 2011). Furthermore, it is known that HORMADs proteins mediate ATR recruitment to unsynapsed axes (Daniel et al. 2011; Wojtasz et al. 2012), and HORMAD SCD motif are a phosphotarget of ATR (Carballo et al. 2008; Fukuda et al. 2012; Royo et al. 2013). Therefore, we propose a model in which in response to SPO11-generated DSBs, ATR phosphorylates HORMADs proteins that acts as a marker of unsynapsed axes, which in turn, mediates location of ATR at these unsynapsed regions. It might serve as a signal of asynapsis to ensure adequate levels of DSBs to favor homologous synapsis. Then, completion of synapsis leads to HORMADs displacement from autosomal chromosomes and suppress the "permissive state" to DSB formation. Once autosomal synapsis is accomplished, HORMADs proteins and ATR are restricted to the heterologous X and Y chromosomes where it promotes DSB accumulation to mediate correct XY synapsis and efficient sex body formation as well.

5.4 ATR is required to achieve proper follicular development

Seckel females have been reported to be infertile (Murga et al. 2009). Accordingly, our experimental findings showed that while meiotic prophase in oocytes appears to be fairly normal, histological analysis showed unusual disturbances in Seckel ovarian sections that were strengthen in adult ovaries. We observed severe reduction of growing follicles in adult ovaries, despite the presence of few antral follicles. In addition, adult sections presented abundant stroma devoid of follicles, which could be associated to the accelerated aging related to Seckel mutation (Murga et al. 2009; Fernandez-Capetillo 2010).

It is well known that coordinated regulation of oocyte and follicle growth and development is essential for fertility. Therefore, proficient communication between oocyte and their surrounding granulosa cells during folliculogenesis plays a crucial role to achieve a healthy oocyte ready for ovulation and fertilization (Sánchez & Smitz 2012; Li & Albertini 2013). Here we demonstrated that the reduction of ATR expression in Seckel ovaries originates follicular developmental defects that have critical consequences in fertility.

ATR controls and coordinates DNA replication origin firing, stabilizes replication forks, regulates cell cycle progression preventing premature mitotic entry and responds to DNA-

damage (Nam & Cortez 2011). Deficient ATR function could lead to errors produced during replication fork collapse, accumulating DNA damage and ultimately causing cell death (Cimprich & Cortez 2008). During follicular development, granulosa cells actively proliferate in order to generate multilayered antral follicles. Here we showed that granulosa cells from $Atr^{s/s}$ primary follicles display proliferation defects. We observed that in primary follicles the proliferation rate from $Atr^{s/s}$ granulosa cells was lower than the one found in $Atr^{+/+}$ cells. Remarkably, this defect was emphasized in adult ovaries. Strikingly, granulosa cells from mutant secondary follicles showed a greater proliferation rate than control cells, accompanied by an increase in the number of apoptotic cells. In view of these findings, we propose that when ATR levels are reduced, mitotic proliferation of granulosa cells is diminished and consequently, cells that accumulate excessive DNA damage due to replication stress activate programmed cell death. Thus, these follicles could not reach full size compromising folliculogenesis progression, as noticeable by the reduced number of granulosa cells found in these follicles. Nevertheless, a few follicles may be able to proliferate at highest rates and then overcome developmental problems. Therefore, only those follicles with the highest replicative capacity could proceed until antral stages and reach similar size than wild type follicles. Indeed, it was described that in Seckel mice particular tissues with high replicative indexes could suffer a positive selection for those cells in which the amount of productive (full length) ATR splicing was highest (Murga et al. 2009).

Importantly, in accordance with our findings, Seckel mice were reported to develop a progeroid phenotype (Murga et al. 2009). Despite Seckel mouse ovaries presented all stages of follicular development, from primordial to antral stages, histological analyses from prepubertal and adult mutant ovaries revealed that follicular development defects were stressed with age. Whereas prepubertal ovaries presented unaffected follicular progression, adult ovaries showed defects in the number of follicles present at different stages of folliculogenesis. Here we demonstrate that adult Seckel ovaries have an impaired activation of primordial follicles, given that the pool of dormant follicles observed was threefold higher than in control ovaries. Furthermore, this increase was accompanied by a reduction of primary and secondary follicles. In the mammalian ovary, the majority of oocytes remain dormant enclosed by flattened somatic cells forming the primordial follicles, which are selectively and continuously activated to progress throughout folliculogenesis. It has been demonstrated that somatic cell signaling factors are essential to initiate primordial follicle activation (Kerr et al. 2013; Zhang et al. 2014). Moreover, several studies have evidenced the role of granulosa cells to achieve proper oocyte-granulosa cells interactions in order to maintain correct follicle development (Dong et al. 1996; Carabatsos et al. 2000; Thomas & Vanderhyden 2006). Therefore, considering that Seckel granulosa cells suffer proliferation defects and elevated rates of apoptosis, it could be possible that somatic cell signaling factors -essential to activate primordial follicles and to maintain follicle growth- were deficient. Consequently, crosstalk between follicular cells and the oocytes might be impaired, compromising proper follicular growth.

Interestingly, even though the clear impact that the ATR reduction had on follicular cells development, the mean number of antral follicles reported in Seckel mouse ovaries was similar to that of control ovaries. Nevertheless, considering the severe reduction of ovarian size in Seckel females associated to dwarfism (Seckel ovary weight is ~33% of a wild type ovary, Murga et al. 2009), along with the large size characteristic of antral follicles, we reason that less antral follicles may fit in mutant ovaries in comparison to control. Bearing in mind the reduced area of Seckel ovarian sections (**Fig. 4.18**), we consider that the approximation obtained from the analysis of eight alternate sections from each ovary may not reflect the total number of antral follicles ready to ovulate present in the ovary at the same time. Even so, considering the possibility that global numbers of antral follicles was diminished in $Atr^{s/s}$, those that we analyzed appear to be morphologically normal.

At this point, in the light of the infertility associated to Seckel females, we contemplate different options to explain the origin of this sterility. Firstly, it is plausible that $Atr^{s/s}$ oocytes enclosed in antral follicles carry defects associated to errors occurring during meiotic progression at fetal stages, although our prophase analysis did not show major defects. Crossover defects may predispose meiocytes to errors during meiosis I division. As we mentioned above, decreased CO formation may originate the presence of univalents at MI and consequently defective chromosome attachment to the meiotic spindle (Woods et al. 1999; Gorbsky 2014). However, it is well known that the female spindle checkpoint at the first meiotic division is less stringent that in males (Hunt & Hassold 2002; Morelli & Cohen 2005). In this case, based on the fairly normal prophase progression described in Seckel oocytes we assume that most oocytes may be competent to progress through meiosis, to extrude the first polar body and become a fertilizable egg (Edelmann et al. 1996; Eaker et al. 2002).

Secondly, it is also possible that $Atr^{s/s}$ oocytes enclosed in antral follicles are not able to acquire the ability to resume meiosis and subsequently to ovulate. It have been demonstrated that nuclear maturation, cytoplasmatic maturation and subsequent developmental competency of the oocyte is orchestrated by communication between oocyte and cumulus cells by gap junctions (Li & Albertini 2013). Somatic cells play an important role in the control of oocyte development and allow metabolic transfer to regulate meiotic maturation (Simon et al. 1997; Albertini et al. 2003; Park et al. 2004). Therefore, considering the proliferation defects during follicular development reported here when ATR is deficient, communication defects between oocyte and granulosa cells could be explaining Seckel female infertility. However, since in Seckel mouse ovaries the follicles that achieve the antral stage may be those that have the highest proliferative capacity, we reason that they may be less likely to present communication problems.

Alternatively, we have to consider the possibility that Seckel mouse oocytes can be normally ovulated and be fertilized, but defects in fertility comes from embryo implantation. It is well established that implantation success requires a crosstalk between the embryo and the uterus that integrate many signaling processes. In response to the implanting embryo-derived

signals, the uterine stroma undergoes multiple transformations to prepare to embryo accommodation and implantation (Zhang et al. 2013). The reduced number of antral follicles present in Seckel mouse ovaries makes evident that few oocytes could be ovulated simultaneously to eventually be fertilized and become a zygote. Considering that, a plausible explanation of Seckel female infertility might be that the embryo-derived signaling molecules emitted by a much reduced number of embryos might not be able to regulate uterine preparation for implantation. Even though, further studies are necessary for understanding ATR deficiency defects associated to oogenesis, we favor this last interpretation. First, because Seckel mouse ovaries displayed all kinds of follicles including morphological normal corpus luteum, indicating that ovaries have the capacity to ovulate. And secondly, because those follicles that achieve ovulatory stage and overcome developmental problems in Seckel mouse ovaries appear to be morphologically undistinguishable than control antral follicles.

CONCLUSIONS

Chapter 6

1. Seckel mutant mouse model constitutes a valid model to investigate the functions of ATR during mammalian gametogenesis. Particularly, Seckel mouse model allows the analysis of ATR roles in meiotic prophase, including meiotic homologous recombination and meiotic silencing of unsynapsed chromosomes, and in folliculogenesis.

2. Testis organ culture is an advantageous method to study synapsis progression and meiotic recombination taking place during mammalian meiotic prophase. *In vitro* meiotic studies enable the manipulation of meiotic events using drugs to target specific proteins during meiotic prophase.

3. Mammalian meiocytes present sexual dimorphism associated to the requisite of ATR kinase during meiotic prophase. Reduction of ATR levels in spermatocytes results in a temporary delayed DSB repair progression impeding CO formation in a correct timing, whereas oocytes display normal meiotic prophase progression.

4. Reduced ATR levels in testis lead to an apparently normal progression of spermatogenesis although the presence of a minor arrest occurring at metaphase I stage, probably associated to CO formation defects in the XY pair.

5. ATR kinase plays an essential role during meiotic recombination mediating RAD51 protein assembly, and possibly DMC1, to DSB sites promoting strand invasion of the homolog chromosome and DSB repair.

6. *In vitro* down-regulation of ATR causes failure to complete homologous chromosome synapsis during meiotic prophase.

7. ATR kinase is required to promote local accumulation of DSB on unsynapsed axes to allow proper meiotic prophase progression, most likely independently of its role in promoting meiotic homologous recombination.

8. Wild type levels of ATR are required to reach proper DSB levels and accurate homologous recombination in the XY pair and to promote efficient synapsis within the pseudoautosomal region.

9. ATR is necessary to promote primordial follicle activation to initiate follicular growth and consequently, to allow appropriate follicular progression within the ovary.

10. Reduced ATR levels in ovaries cause impaired follicular development associated to defects in granulosa cells proliferation, which are strengthen with age. These defects result in a reduced number of ovulatory follicles leading to female infertility.

REFERENCES

Chapter 7

Adams, I. R., & McLaren, A. (2002). Sexually dimorphic development of mouse primordial germ cells: switching from oogenesis to spermatogenesis. Development (Cambridge, England), 129(5), 1155–64.

Albertini, D. F., Sanfins, A., & Combelles, C. M. H. (2003). Origins and manifestations of oocyte maturation competencies. Reproductive Biomedicine Online, 6(4), 410–5.

Alver, R. C., Chadha, G. S., & Blow, J. J. (2014). The contribution of dormant origins to genome stability: from cell biology to human genetics. DNA Repair, 19, 182–9.

Anderson, L. K., Reeves, A., Webb, L. M., & Ashley, T. (1999). Distribution of crossing over on mouse synaptonemal complexes using immunofluorescent localization of MLH1 protein. Genetics, 151(4), 1569–79.

Baarends, W. M., Hoogerbrugge, J. W., Roest, H. P., Ooms, M., Vreeburg, J., Hoeijmakers, J. H., & Grootegoed, J. A. (1999). Histone ubiquitination and chromatin remodeling in mouse spermatogenesis. Developmental Biology, 207(2), 322–33.

Baarends, W. M., Wassenaar, E., van der Laan, R., Hoogerbrugge, J., Sleddens-Linkels, E., Hoeijmakers, J. H. J., & Grootegoed, J. A. (2005). Silencing of unpaired chromatin and histone H2A ubiquitination in mammalian meiosis. Molecular and Cellular Biology, 25(3), 1041–53.

Baker, S. J., & Spears, N. (1999). The role of intra-ovarian interactions in the regulation of follicle dominance. Human Reproduction Update, 5(2), 153–65.

Baker, S. M., Plug, A. W., Prolla, T. A., Bronner, C. E., Harris, A. C., Yao, X., & Liskay, R. M. (1996). Involvement of mouse Mlh1 in DNA mismatch repair and meiotic crossing over. Nature Genetics, 13(3), 336–42.

Bannister, L. A., & Schimenti, J. C. (2004a). Homologous recombinational repair proteins in mouse meiosis. Cytogenetic and Genome Research, 107(3-4), 191–200.

Bannister, L. A., & Schimenti, J. C. (2004b). Homologous recombinational repair proteins in mouse meiosis. Cytogenetic and Genome Research, 107(3-4), 191–200.

Barchi, M., Mahadevaiah, S., Giacomo, M. Di, Rooij, D. G. De, Burgoyne, P. S., Jasin, M., & Keeney, S. (2005). Surveillance of Different Recombination Defects in Mouse Spermatocytes Yields Distinct Responses despite Elimination at an Identical Developmental Stage, 25(16), 7203–7215.

Barchi, M., Roig, I., Di Giacomo, M., de Rooij, D. G., Keeney, S., & Jasin, M. (2008). ATM promotes the obligate XY crossover and both

crossover control and chromosome axis integrity on autosomes. PLoS Genetics, 4(5), e1000076.

Barlow, C., Liyanage, M., Moens, P. B., Tarsounas, M., Nagashima, K., Brown, K., & Wynshaw-Boris, A. (1998). Atm deficiency results in severe meiotic disruption as early as leptonema of prophase I. Development (Cambridge, England), 125(20), 4007–17.

Barrionuevo, F., Bagheri-Fam, S., Klattig, J., Kist, R., Taketo, M. M., Englert, C., & Scherer, G. (2006). Homozygous inactivation of Sox9 causes complete XY sex reversal in mice. Biology of Reproduction, 74(1), 195–201.

Baudat, F., Buard, J., Grey, C., Fledel-Alon, A., Ober, C., Przeworski, M., & de Massy, B. (2010). PRDM9 is a major determinant of meiotic recombination hotspots in humans and mice. Science (New York, N.Y.), 327(5967), 836–40.

Baudat, F., & de Massy, B. (2007). Regulating double-stranded DNA break repair towards crossover or non-crossover during mammalian meiosis. Chromosome Research : An International Journal on the Molecular, Supramolecular and Evolutionary Aspects of Chromosome Biology, 15(5), 565–77.

Baudat, F., Imai, Y., & de Massy, B. (2013). Meiotic recombination in mammals: localization and regulation. Nature Reviews. Genetics, 14(11), 794–806.

Baudat, F., Manova, K., Yuen, J. P., Jasin, M., & Keeney, S. (2000). Chromosome synapsis defects and sexually dimorphic meiotic progression in mice lacking Spo11. Molecular Cell, 6(5), 989–98.

Bellani, M. A., Romanienko, P. J., Cairatti, D. A., & Camerini-Otero, R. D. (2005). SPO11 is required for sex-body formation, and Spo11 heterozygosity rescues the prophase arrest of Atm-/- spermatocytes. Journal of Cell Science, 118(Pt 15), 3233–45.

Berchowitz, L. E., & Copenhaver, G. P. (2010). Genetic interference: don't stand so close to me. Current Genomics, 11(2), 91–102.

Bishop, D. K. (1994). RecA homologs Dmc1 and Rad51 interact to form multiple nuclear complexes prior to meiotic chromosome synapsis. Cell, 79(6), 1081–92.

Bishop, D. K., Park, D., Xu, L., & Kleckner, N. (1992). DMC1: a meiosis-specific yeast homolog of E. coli recA required for recombination, synaptonemal complex formation, and cell cycle progression. Cell, 69(3), 439–56.

Blat, Y., Protacio, R. U., Hunter, N., & Kleckner, N. (2002). Physical and functional interactions among basic chromosome organizational features govern early steps of meiotic chiasma formation. Cell, 111(6), 791–802.

Bogdanov, Y. F., Grishaeva, T. M., & Dadashev, S. Y. (2007). Similarity of the domain structure of proteins as a basis for the conservation of meiosis. International Review of Cytology, 257, 83–142.

Borde, V., Robine, N., Lin, W., Bonfils, S., Géli, V., & Nicolas, A. (2009). Histone H3 lysine 4 trimethylation marks meiotic recombination initiation sites. The EMBO Journal, 28(2), 99–111.

Borum, K. (1961). Oogenesis in the mouse. A study of the origin of the mature ova. Experimental Cell Research, 45(1), 39–47.

Bowles, J., & Koopman, P. (2010). Sex determination in mammalian germ cells: extrinsic versus intrinsic factors. Reproduction (Cambridge, England), 139(6), 943–58.

Braun, R. E., Behringer, R. R., Peschon, J. J., Brinster, R. L., & Palmiter, R. D. (1989).

Genetically haploid spermatids are phenotypically diploid. Nature, 337(6205), 373–6.

Brick, K., Smagulova, F., Khil, P., Camerini-Otero, R. D., & Petukhova, G. V. (2012). Genetic recombination is directed away from functional genomic elements in mice. Nature, 485(7400), 642–5.

Brown, E. J., & Baltimore, D. (2000). ATR disruption leads to chromosomal fragmentation and early embryonic lethality. Genes & Development, 14(4), 397–402.

Brown, M. S., & Bishop, D. K. (2014). DNA Strand Exchange and RecA Homologs in Meiosis. Cold Spring Harbor Perspectives in Biology, 7(1).

Bullejos, M., & Koopman, P. (2004). Germ cells enter meiosis in a rostro-caudal wave during development of the mouse ovary. Molecular Reproduction and Development, 68(4), 422–8.

Burgoyne, P. S., Mahadevaiah, S. K., & Turner, J. M. a. (2009). The consequences of asynapsis for mammalian meiosis. Nature Reviews. Genetics, 10(3), 207–16.

Callender, T. L., & Hollingsworth, N. M. (2010). Mek1 suppression of meiotic double-strand break repair is specific to sister chromatids, chromosome autonomous and independent of Rec8 cohesin complexes. Genetics, 185(3), 771–82.

Carabatsos, M. J., Sellitto, C., Goodenough, D. A., & Albertini, D. F. (2000). Oocyte-granulosa cell heterologous gap junctions are required for the coordination of nuclear and cytoplasmic meiotic competence. Developmental Biology, 226(2), 167–79.

Carballo, J. a, Panizza, S., Serrentino, M. E., Johnson, A. L., Geymonat, M., Borde, V., & Cha, R. S. (2013). Budding yeast ATM/ATR control meiotic double-strand break (DSB) levels by down-regulating Rec114, an essential component of the DSB-machinery. PLoS Genetics, 9(6), e1003545.

Carballo, J. A., & Cha, R. S. (2007). Meiotic roles of Mec1, a budding yeast homolog of mammalian ATR/ATM. Chromosome Research : An International Journal on the Molecular, Supramolecular and Evolutionary Aspects of Chromosome Biology, 15(5), 539–50.

Carballo, J. A., Johnson, A. L., Sedgwick, S. G., & Cha, R. S. (2008). Phosphorylation of the axial element protein Hop1 by Mec1/Tel1 ensures meiotic interhomolog recombination. Cell, 132(5), 758–70.

Carpenter, A. T. (1979). Recombination nodules and synaptonemal complex in recombination-defective females of Drosophila melanogaster. Chromosoma, 75(3), 259–92.

Celeste, A., Petersen, S., Romanienko, P. J., Fernandez-Capetillo, O., Chen, H. T., Sedelnikova, O. A., Nussenzweig, A. (2002). Genomic instability in mice lacking histone H2AX. Science (New York, N.Y.), 296(5569), 922–7.

Chen, L., Russell, P. T., & Larsen, W. J. (1993). Functional significance of cumulus expansion in the mouse: roles for the preovulatory synthesis of hyaluronic acid within the cumulus mass. Molecular Reproduction and Development, 34(1), 87–93.

Chen, Y., & Poon, R. Y. C. (2008). The multiple checkpoint functions of CHK1 and CHK2 in maintenance of genome stability. Frontiers in Bioscience : A Journal and Virtual Library, 13, 5016–29.

Chesnel, F., & Eppig, J. J. (1995). Synthesis and accumulation of p34cdc2 and cyclin B in mouse oocytes during acquisition of competence to

resume meiosis. Molecular Reproduction and Development, 40(4), 503–8.

Cheung, H. C., San Lucas, F. A., Hicks, S., Chang, K., Bertuch, A. A., & Ribes-Zamora, A. (2012). An S/T-Q cluster domain census unveils new putative targets under Tel1/Mec1 control. BMC Genomics, 13(1), 664.

Chiquoine, A. D. (1954). The identification, origin, and migration of the primordial germ cells in the mouse embryo. The Anatomical Record, 118(2), 135–46.

Cimprich, K. a, & Cortez, D. (2008). ATR: an essential regulator of genome integrity. Nature Reviews. Molecular Cell Biology, 9(8), 616–27.

Clermont, Y., & Trott, M. (1969). Duration of the cycle of the seminiferous epithelium in the mouse and hamster determined by means of 3H-thymidine and radioautography. Fertility and Sterility, 20(5), 805–17.

Cloud, V., Chan, Y.L., Grubb, J., Budke, B., & Bishop, D. K. (2012). Rad51 is an accessory factor for Dmc1-mediated joint molecule formation during meiosis. Science (New York, N.Y.), 337(6099), 1222–5.

Cole, F., Baudat, F., Grey, C., Keeney, S., de Massy, B., & Jasin, M. (2014). Mouse tetrad analysis provides insights into recombination mechanisms and hotspot evolutionary dynamics. Nature Genetics, 46(10), 1072–80.

Cole, F., Kauppi, L., Lange, J., Roig, I., Wang, R., Keeney, S., & Jasin, M. (2012). Homeostatic control of recombination is implemented progressively in mouse meiosis. Nature Cell Biology, 14(4), 424–30.

Cooke, H.J., & Saunders,P.T. (2002). Mouse models of male infertility. Nature review genetics, 3(10):790-801.

Cooper, T. J., Wardell, K., Garcia, V., & Neale, M. J. (2014). Homeostatic regulation of meiotic DSB formation by ATM/ATR. Experimental Cell Research, 329(1), 124–31.

Cortez, D., Guntuku, S., Qin, J., & Elledge, S. J. (2001). ATR and ATRIP: partners in checkpoint signaling. Science (New York, N.Y.), 294(5547), 1713–6.

Cortvrindt, R., Smitz, J., & Van Steirteghem, A. C. (1997). Assessment of the need for follicle stimulating hormone in early preantral mouse follicle culture in vitro. Human Reproduction (Oxford, England), 12(4), 759–68.

Da Ines, O., Degroote, F., Goubely, C., Amiard, S., Gallego, M. E., & White, C. I. (2013). Meiotic Recombination in Arabidopsis Is Catalysed by DMC1, with RAD51 Playing a Supporting Role. PLoS Genetics, 9(9), e1003787.

Daniel, K., Lange, J., Hached, K., Fu, J., Anastassiadis, K., Roig, I., & Tóth, A. (2011). Meiotic homologue alignment and its quality surveillance are controlled by mouse HORMAD1. Nature Publishing Group, 13(5), 599–610.

de Boer, E., Stam, P., Dietrich, A. J. J., Pastink, A., & Heyting, C. (2006). Two levels of interference in mouse meiotic recombination. Proceedings of the National Academy of Sciences of the United States of America, 103(25), 9607–12.

de Boer, P., de Jong, J. H., & van der Hoeven, F. A. (1991). Meiosis in a sterile male mouse with an isoYq marker chromosome. Cytogenetics and Cell Genetics, 56(1), 36–9.

de Felici, M., Klinger, F. G., Farini, D., Scaldaferri, M. L., Iona, S., & Lobascio, M. (2005). Establishment of oocyte population in the fetal ovary: primordial germ cell proliferation and oocyte programmed cell death. Reproductive Biomedicine Online, 10(2), 182–91.

de Klein, A., Muijtjens, M., van Os, R., Verhoeven, Y., Smit, B., Carr, A. M., Hoeijmakers, J. H. (2000). Targeted disruption of the cell-cycle checkpoint gene ATR leads to early embryonic lethality in mice. Current Biology : CB, 10(8), 479–82.

de Kretser, D. M., Loveland, K. L., Meinhardt, A., Simorangkir, D., & Wreford, N. (1998). Spermatogenesis. Human Reproduction (Oxford, England), 13 Suppl 1, 1–8.

de los Santos, T., Hunter, N., Lee, C., Larkin, B., Loidl, J., & Hollingsworth, N. M. (2003). The Mus81/Mms4 endonuclease acts independently of double-Holliday junction resolution to promote a distinct subset of crossovers during meiosis in budding yeast. Genetics, 164(1), 81–94.

de Rooij, D. G. (1998). Stem cells in the testis. International Journal of Experimental Pathology, 79(2), 67–80. Retrieved from

de Rooij, D. G. (2001). Proliferation and differentiation of spermatogonial stem cells. Reproduction (Cambridge, England), 121(3), 347–54.

de Vries, F. A. T., de Boer, E., van den Bosch, M., Baarends, W. M., Ooms, M., Yuan, L., Pastink, A. (2005). Mouse Sycp1 functions in synaptonemal complex assembly, meiotic recombination, and XY body formation. Genes & Development, 19(11), 1376–89.

di Carlo, A. D., Travia, G., & De Felici, M. (2000). The meiotic specific synaptonemal complex protein SCP3 is expressed by female and male primordial germ cells of the mouse embryo. The International Journal of Developmental Biology, 44(2), 241–4.

di Giacomo, M., Barchi, M., Baudat, F., Edelmann, W., Keeney, S., & Jasin, M. (2005). Distinct DNA-damage-dependent and -independent responses drive the loss of oocytes in recombination-defective mouse mutants. Proceedings of the National Academy of Sciences of the United States of America, 102(3), 737–42.

Diaz, F. J., Wigglesworth, K., & Eppig, J. J. (2007). Oocytes are required for the preantral granulosa cell to cumulus cell transition in mice. Developmental Biology, 305(1), 300–11.

Don W. Fawcett, Susumu Ito, & D. S. (1959). The occurrence of intercellular bridges in groups of cells exhibiting synchronous differentiation. The Journal of Biophysical and Biochemical Cytology, 5(3), 453–60.

Dong, J., Albertini, D. F., Nishimori, K., Kumar, T. R., Lu, N., & Matzuk, M. M. (1996). Growth differentiation factor-9 is required during early ovarian folliculogenesis. Nature, 383(6600), 531–5.

Drabent, B., Bode, C., Bramlage, B., & Doenecke, D. (1996). Expression of the mouse testicular histone gene H1t during spermatogenesis. Histochemistry and Cell Biology, 106, 247–251.

Dragovic, R. A., Ritter, L. J., Schulz, S. J., Amato, F., Thompson, J. G., Armstrong, D. T., & Gilchrist, R. B. (2007). Oocyte-secreted factor activation of SMAD 2/3 signaling enables initiation of mouse cumulus cell expansion. Biology of Reproduction, 76(5), 848–57.

Drummond, A. E., & Findlay, J. K. (1999). The role of estrogen in folliculogenesis. Molecular and Cellular Endocrinology, 151(1-2), 57–64.

Durkin, S. G., & Glover, T. W. (2007). Chromosome fragile sites. Annual Review of Genetics, 41, 169–92.

Eaker, S., Cobb, J., Pyle, A., & Handel, M. A. (2002). Meiotic Prophase Abnormalities and Metaphase Cell Death in MLH1-Deficient Mouse

Spermatocytes: Insights into Regulation of Spermatogenic Progress. Developmental Biology, 249(1), 85–95.

Eddy, E. M. (2002). Male germ cell gene expression. Recent Progress in Hormone Research, 57, 103–28. Retrieved from

Edelmann, W., Cohen, P. E., Kane, M., Lau, K., Morrow, B., Bennett, S., & Kucherlapati, R. (1996). Meiotic pachytene arrest in MLH1-deficient mice. Cell, 85(7), 1125–34.

Eppig, J. J. (2001). Oocyte control of ovarian follicular development and function in mammals. Reproduction (Cambridge, England), 122(6), 829–38.

Ewen, K. A., & Koopman, P. (2010). Mouse germ cell development: from specification to sex determination. Molecular and Cellular Endocrinology, 323(1), 76–93.

Fanning, E., Klimovich, V., & Nager, A. R. (2006). A dynamic model for replication protein A (RPA) function in DNA processing pathways. Nucleic Acids Research, 34(15), 4126–37.

Feijoo, C., Hall-Jackson, C., Wu, R., Jenkins, D., Leitch, J., Gilbert, D. M., & Smythe, C. (2001). Activation of mammalian Chk1 during DNA replication arrest: a role for Chk1 in the intra-S phase checkpoint monitoring replication origin firing. The Journal of Cell Biology, 154(5), 913–23.

Feng, C.-W., Bowles, J., & Koopman, P. (2014). Control of mammalian germ cell entry into meiosis. Molecular and Cellular Endocrinology, 382(1), 488–97.

Fernandez-Capetillo, O. (2010). Intrauterine programming of ageing. EMBO Reports, 11(1), 32–6.

Fernandez-Capetillo, O., Mahadevaiah, S. K., Celeste, A., Romanienko, P. J., Camerini-Otero, R. D., Bonner, W. M., & Nussenzweig, A. (2003). H2AX is required for chromatin remodeling and inactivation of sex chromosomes in male mouse meiosis. Developmental Cell, 4(4), 497–508.

Flott, S., Kwon, Y., Pigli, Y. Z., Rice, P. A., Sung, P., & Jackson, S. P. (2011). Regulation of Rad51 function by phosphorylation. EMBO Reports, 12(8), 833–9.

Flynn, R. L., & Zou, L. (2011). ATR: a master conductor of cellular responses to DNA replication stress. Trends in Biochemical Sciences, 36(3), 133–40.

Foote, K. M., Blades, K., Cronin, A., Fillery, S., Guichard, S. S., Hassall, L., & Wood, C. (2013). Discovery of 4-{4-[(3R)-3-Methylmorpholin-4-yl]-6-[1-(methylsulfonyl)cyclopropyl]pyrimidin-2-y l}-1H-indole (AZ20): a potent and selective inhibitor of ATR protein kinase with monotherapy in vivo antitumor activity. Journal of Medicinal Chemistry, 56(5), 2125–2138.

Fraune, J., Schramm, S., Alsheimer, M., & Benavente, R. (2012). The mammalian synaptonemal complex: protein components, assembly and role in meiotic recombination. Experimental Cell Research, 318(12), 1340–6.

Fukuda, T., Pratto, F., Schimenti, J. C., Turner, J. M. a, Camerini-Otero, R. D., & Höög, C. (2012). Phosphorylation of chromosome core components may serve as axis marks for the status of chromosomal events during mammalian meiosis. PLoS Genetics, 8(2), e1002485.

Garcia-Cruz, R., Roig, I., Robles, P., Scherthan, H., & Garcia Caldés, M. (2009). ATR, BRCA1 and gammaH2AX localize to unsynapsed chromosomes at the pachytene stage in human oocytes. Reproductive Biomedicine Online, 18(1), 37–44.

Gasior, S. L., Wong, A. K., Kora, Y., Shinohara, A., & Bishop, D. K. (1998). Rad52 associates with RPA and functions with rad55 and rad57 to assemble meiotic recombination complexes. Genes & Development, 12(14), 2208–21.

Ge, X. Q., & Blow, J. J. (2010). Chk1 inhibits replication factory activation but allows dormant origin firing in existing factories. The Journal of Cell Biology, 191(7), 1285–97.

Ghabrial, A., & Schüpbach, T. (1999). Activation of a meiotic checkpoint regulates translation of Gurken during Drosophila oogenesis. Nature Cell Biology, 1(6), 354–7.

Gilchrist, R. B., Ritter, L. J., & Armstrong, D. T. (2004). Oocyte-somatic cell interactions during follicle development in mammals. Animal Reproduction Science, 82-83, 431–46.

Goedecke, W., Eijpe, M., Offenberg, H. H., van Aalderen, M., & Heyting, C. (1999). Mre11 and Ku70 interact in somatic cells, but are differentially expressed in early meiosis. Nature Genetics, 23(2), 194–8.

Gorbsky, G. J. (2014). The spindle checkpoint and chromosome segregation in meiosis. The FEBS Journal.

Gosden, R. G. (2002). Oogenesis as a foundation for embryogenesis. Molecular and Cellular Endocrinology, 186(2), 149–53.

Gray, S., Allison, R. M., Garcia, V., Goldman, A. S. H., & Neale, M. J. (2013). Positive regulation of meiotic DNA double-strand break formation by activation of the DNA damage checkpoint kinase Mec1(ATR). Open Biology, 3(7), 130019.

Greenbaum, M. P., Iwamori, T., Buchold, G. M., & Matzuk, M. M. (2011). Germ cell intercellular bridges. Cold Spring Harbor Perspectives in Biology, 3(8), a005850.

Griswold, M. D. (1998). The central role of Sertoli cells in spermatogenesis. Seminars in Cell & Developmental Biology, 9(4), 411–6.

Guillon, H., Baudat, F., Grey, C., Liskay, R. M., & de Massy, B. (2005). Crossover and noncrossover pathways in mouse meiosis. Molecular Cell, 20(4), 563–73.

Guillon, H., & de Massy, B. (2002). An initiation site for meiotic crossing-over and gene conversion in the mouse. Nature Genetics, 32(2), 296–9.

Hall, H., Hunt, P., & Hassold, T. (2006). Meiosis and sex chromosome aneuploidy: how meiotic errors cause aneuploidy; how aneuploidy causes meiotic errors. Current Opinion in Genetics & Development, 16(3), 323–9.

Handel, M. A., & Schimenti, J. C. (2010). Genetics of mammalian meiosis: regulation, dynamics and impact on fertility. Nature Reviews. Genetics, 11(2), 124–36.

Harper, J. W., & Elledge, S. J. (2007). The DNA damage response: ten years after. Molecular Cell, 28(5), 739–45.

Heyer, W.-D., Ehmsen, K. T., & Liu, J. (2010). Regulation of homologous recombination in eukaryotes. Annual Review of Genetics, 44, 113–39.

Hilscher, B., Hilscher, W., Bülthoff-Ohnolz, B., Krämer, U., Birke, A., Pelzer, H., & Gauss, G. (1974). Kinetics of gametogenesis. I. Comparative histological and autoradiographic studies of oocytes and transitional prospermatogonia during oogenesis and prespermatogenesis. Cell and Tissue Research, 154(4), 443–70.

Holloway, J. K., Booth, J., Edelmann, W., McGowan, C. H., & Cohen, P. E. (2008). MUS81 generates a subset of MLH1-MLH3-

independent crossovers in mammalian meiosis. PLoS Genetics, 4(9), e1000186.

Hu, M.-W., Wang, Z.B., Schatten, H., & Sun, Q.Y. (2012). New understandings on folliculogenesis/oogenesis regulation in mouse as revealed by conditional knockout. Journal of Genetics and Genomics = Yi Chuan Xue Bao, 39(2), 61–8.

Hu, Y.C., Wang, P.H., Yeh, S., Wang, R.S., Xie, C., Xu, Q., & Chang, C. (2004). Subfertility and defective folliculogenesis in female mice lacking androgen receptor. Proceedings of the National Academy of Sciences of the United States of America, 101(31), 11209–14.

Humphryes, N., & Hochwagen, A. (2014). A non-sister act: recombination template choice during meiosis. Experimental Cell Research, 329(1), 53–60.

Hunt, P. A., & Hassold, T. J. (2002). Sex matters in meiosis. Science (New York, N.Y.), 296(5576), 2181–3.

Hunt, P. A., & LeMaire, R. (1992). Sex-chromosome pairing: evidence that the behavior of the pseudoautosomal region differs during male and female meiosis. American Journal of Human Genetics, 50(6), 1162–70.

Hunter, N., & Kleckner, N. (2001). The single-end invasion: an asymmetric intermediate at the double-strand break to double-holliday junction transition of meiotic recombination. Cell, 106(1), 59–70.

Ichijima, Y., Ichijima, M., Lou, Z., Nussenzweig, A., Camerini-Otero, R. D., Chen, J., … Namekawa, S. H. (2011). MDC1 directs chromosome-wide silencing of the sex chromosomes in male germ cells. Genes & Development, 25(9), 959–71.

Inselman, A., Eaker, S., & Handel, M. A. (2003). Temporal expression of cell cycle-related proteins during spermatogenesis: establishing a timeline for onset of the meiotic divisions. Cytogenetic and Genome Research, 103(3-4), 277–84.

Jazayeri, A., Falck, J., Lukas, C., Bartek, J., Smith, G. C. M., Lukas, J., & Jackson, S. P. (2006). ATM- and cell cycle-dependent regulation of ATR in response to DNA double-strand breaks. Nature Cell Biology, 8(1), 37–45.

Jiang, J.Y., Cheung, C. K. M., Wang, Y., & Tsang, B. K. (2003). Regulation of cell death and cell survival gene expression during ovarian follicular development and atresia. Frontiers in Bioscience : A Journal and Virtual Library, 8, d222–37.

Jones, G. H., & Franklin, F. C. H. (2006). Meiotic crossing-over: obligation and interference. Cell, 126(2), 246–8.

Jones, K. T. (2008). Meiosis in oocytes: predisposition to aneuploidy and its increased incidence with age. Human Reproduction Update, 14(2), 143–58.

Joshi, N., Brown, M. S., Bishop, D. K., & Börner, G. V. (2015). Gradual Implementation of the Meiotic Recombination Program via Checkpoint Pathways Controlled by Global DSB Levels. Molecular Cell, 57(5), 797–811.

Joyce, E. F., Pedersen, M., Tiong, S., White-Brown, S. K., Paul, A., Campbell, S. D., & McKim, K. S. (2011). Drosophila ATM and ATR have distinct activities in the regulation of meiotic DNA damage and repair. The Journal of Cell Biology, 195(3), 359–67.

Kanai, Y., Hiramatsu, R., Matoba, S., & Kidokoro, T. (2005). From SRY to SOX9: mammalian testis differentiation. Journal of Biochemistry, 138(1), 13–9.

Kauppi, L., Barchi, M., Baudat, F., Romanienko, P. J., Keeney, S., & Jasin, M. (2011). Distinct

properties of the XY pseudoautosomal region crucial for male meiosis. Science (New York, N.Y.), 331(6019), 916–20.

Kauppi, L., Barchi, M., Lange, J., Baudat, F., Jasin, M., & Keeney, S. (2013). Numerical constraints and feedback control of double-strand breaks in mouse meiosis. Genes & Development, 27(8), 873–86.

Kauppi, L., Jasin, M., & Keeney, S. (2012). The tricky path to recombining X and Y chromosomes in meiosis. Annals of the New York Academy of Sciences, 1267, 18–23.

Keegan, K. S., Holtzman, D. a, Plug, a W., Christenson, E. R., Brainerd, E. E., Flaggs, G., & Hoekstra, M. F. (1996). The Atr and Atm protein kinases associate with different sites along meiotically pairing chromosomes. Genes & Development, 10(19), 2423–2437.

Keeney, S., Giroux, C. N., & Kleckner, N. (1997). Meiosis-specific DNA double-strand breaks are catalyzed by Spo11, a member of a widely conserved protein family. Cell, 88(3), 375–84.

Keeney, S., Lange, J., & Mohibullah, N. (2014). Self-organization of meiotic recombination initiation: general principles and molecular pathways. Annual Review of Genetics, 48, 187–214.

Kerr, J. B., Myers, M., & Anderson, R. A. (2013). The dynamics of the primordial follicle reserve. Reproduction (Cambridge, England), 146(6), R205–15.

Kleckner, N. (1996). Meiosis: how could it work? Proceedings of the National Academy of Sciences of the United States of America, 93(16), 8167–74.

Kleckner, N., Storlazzi, A., & Zickler, D. (2003). Coordinate variation in meiotic pachytene SC length and total crossover/chiasma frequency under conditions of constant DNA length. Trends in Genetics : TIG, 19(11), 623–8.

Kolas, N. K., Svetlanov, A., Lenzi, M. L., Macaluso, F. P., Lipkin, S. M., Liskay, R. M., & Cohen, P. E. (2005). Localization of MMR proteins on meiotic chromosomes in mice indicates distinct functions during prophase I. The Journal of Cell Biology, 171(3), 447–58.

Krawetz, S.A., De Rooij, D.G., & Hedger, M.P. (2009). Molecular aspects of male fertility. International Workshop on Molecular Andrology. EMBO Reproduction, 10(10):1087-92.

Krejci, L., Altmannova, V., Spirek, M., & Zhao, X. (2012). Homologous recombination and its regulation. Nucleic Acids Research, 40(13), 5795–818.

Kurzbauer, M.-T., Uanschou, C., Chen, D., & Schlögelhofer, P. (2012). The recombinases DMC1 and RAD51 are functionally and spatially separated during meiosis in Arabidopsis. The Plant Cell, 24(5), 2058–70.

Lange, J., Pan, J., Cole, F., Thelen, M. P., Jasin, M., & Keeney, S. (2011). ATM controls meiotic double-strand-break formation. Nature, 479(7372), 237–40.

Lam, I., Keeney, S., (2014). Mechanism and regulation of meiotic recombination initiation. Cold Spring Harbor Perspectives in Biology, 16;7(1):a016634.

Lawson, K. A., & Hage, W. J. (1994). Clonal analysis of the origin of primordial germ cells in the mouse. Ciba Foundation Symposium, 182, 68–84; discussion 84–91.

LeMaire-Adkins, R., Radke, K., & Hunt, P. A. (1997). Lack of checkpoint control at the metaphase/anaphase transition: a mechanism of meiotic nondisjunction in mammalian females. The Journal of Cell Biology, 139(7), 1611–9.

Li, R., & Albertini, D. F. (2013). The road to maturation: somatic cell interaction and self-organization of the mammalian oocyte. Nature Reviews. Molecular Cell Biology, 14(3), 141–52.

Li, X. C., Li, X., & Schimenti, J. C. (2007). Mouse pachytene checkpoint 2 (trip13) is required for completing meiotic recombination but not synapsis. PLoS Genetics, 3(8), e130.

Libby, B. J., De La Fuente, R., O'Brien, M. J., Wigglesworth, K., Cobb, J., Inselman, A., & Schimenti, J. C. (2002). The mouse meiotic mutation mei1 disrupts chromosome synapsis with sexually dimorphic consequences for meiotic progression. Developmental Biology, 242(2), 174–87.

Liebe, B., Alsheimer, M., Höög, C., Benavente, R., & Scherthan, H. (2004). Telomere attachment, meiotic chromosome condensation, pairing, and bouquet stage duration are modified in spermatocytes lacking axial elements. Molecular Biology of the Cell, 15(2), 827–37.

Lim, D. S., & Hasty, P. (1996). A mutation in mouse rad51 results in an early embryonic lethal that is suppressed by a mutation in p53. Molecular and Cellular Biology, 16(12), 7133–43.

Liu, K., Rajareddy, S., Liu, L., Jagarlamudi, K., Boman, K., Selstam, G., & Reddy, P. (2006). Control of mammalian oocyte growth and early follicular development by the oocyte PI3 kinase pathway: new roles for an old timer. Developmental Biology, 299(1), 1–11.

Liu, Y. X. (2007). Interaction and signal transduction between oocyte and somatic cells in the ovary. Frontiers in Bioscience : A Journal and Virtual Library, 12, 2782–96.

Llano, E., Herrán, Y., García-Tuñón, I., Gutiérrez-Caballero, C., de Álava, E., Barbero, J. L., & Pendás, A. M. (2012). Meiotic cohesin complexes are essential for the formation of the axial element in mice. The Journal of Cell Biology, 197(7), 877–85.

Lynn, A., Koehler, K. E., Judis, L., Chan, E. R., Cherry, J. P., Schwartz, S., & Hassold, T. J. (2002). Covariation of synaptonemal complex length and mammalian meiotic exchange rates. Science (New York, N.Y.), 296(5576), 2222–5.

MacQueen, A. J., & Hochwagen, A. (2011). Checkpoint mechanisms: the puppet masters of meiotic prophase. Trends in Cell Biology, 21(7), 393–400.

Mahadevaiah, S. K., Turner, J. M., Baudat, F., Rogakou, E. P., de Boer, P., Blanco-Rodríguez, J., Burgoyne, P. S. (2001). Recombinational DNA double-strand breaks in mice precede synapsis. Nature Genetics, 27(3), 271–6.

Marcon, E., & Moens, P. (2003). MLH1p and MLH3p localize to precociously induced chiasmata of okadaic-acid-treated mouse spermatocytes. Genetics, 165(4), 2283–7.

Maréchal, A., & Zou, L. (2013). DNA damage sensing by the ATM and ATR kinases. Cold Spring Harbor Perspectives in Biology, 5(9).

Martini, E., Diaz, R. L., Hunter, N., & Keeney, S. (2006). Crossover homeostasis in yeast meiosis. Cell, 126(2), 285–95.

Masson, J. Y., & West, S. C. (2001). The Rad51 and Dmc1 recombinases: a non-identical twin relationship. Trends in Biochemical Sciences, 26(2), 131–136.

McGee, E. A., & Hsueh, A. J. (2000). Initial and cyclic recruitment of ovarian follicles. Endocrine Reviews, 21(2), 200–14.

McKee, B. D., & Handel, M. A. (1993). Sex chromosomes, recombination, and chromatin conformation. Chromosoma, 102(2), 71–80.

McLaren, A. (1984). Meiosis and differentiation of mouse germ cells. Symposia of the Society for Experimental Biology, 38, 7–23.

McLean, D. J., Friel, P. J., Johnston, D. S., & Griswold, M. D. (2003). Characterization of spermatogonial stem cell maturation and differentiation in neonatal mice. Biology of Reproduction, 69(6), 2085–91.

Menke, D. B., Koubova, J., & Page, D. C. (2003). Sexual differentiation of germ cells in XX mouse gonads occurs in an anterior-to-posterior wave. Developmental Biology, 262(2), 303–12.

Moens, P. B., Kolas, N. K., Tarsounas, M., Marcon, E., Cohen, P. E., & Spyropoulos, B. (2002). The time course and chromosomal localization of recombination-related proteins at meiosis in the mouse are compatible with models that can resolve the early DNA-DNA interactions without reciprocal recombination. Journal of Cell Science, 115(Pt 8), 1611–22.

Moens, P. B., Marcon, E., Shore, J. S., Kochakpour, N., & Spyropoulos, B. (2007). Initiation and resolution of interhomolog connections: crossover and non-crossover sites along mouse synaptonemal complexes. Journal of Cell Science, 120(Pt 6), 1017–27.

Moens, P. B., Tarsounas, M., Morita, T., Habu, T., Rottinghaus, S. T., Freire, R., & Wynshaw-Boris, A. (1999). The association of ATR protein with mouse meiotic chromosome cores. Chromosoma, 108(2), 95–102.

Mohandas, T. K., Speed, R. M., Passage, M. B., Yen, P. H., Chandley, A. C., & Shapiro, L. J. (1992). Role of the pseudoautosomal region in sex-chromosome pairing during male meiosis: meiotic studies in a man with a deletion of distal Xp. American Journal of Human Genetics, 51(3), 526–33.

Molyneaux, K. A., Stallock, J., Schaible, K., & Wylie, C. (2001). Time-lapse analysis of living mouse germ cell migration. Developmental Biology, 240(2), 488–98.

Morelli, M. A., & Cohen, P. E. (2005). Not all germ cells are created equal: aspects of sexual dimorphism in mammalian meiosis. Reproduction (Cambridge, England), 130(6), 761–81.

Murfuni, I., Basile, G., Subramanyam, S., Malacaria, E., Bignami, M., Spies, M., & Pichierri, P. (2013). Survival of the replication checkpoint deficient cells requires MUS81-RAD52 function. PLoS Genetics, 9(10), e1003910.

Murga, M., Bunting, S., Montaña, M. F., Soria, R., Mulero, F., Cañamero, M., & Fernandez-Capetillo, O. (2009). A mouse model of ATR-Seckel shows embryonic replicative stress and accelerated aging. Nature Genetics, 41(8), 891–8.

Nakatsuji, N., & Chuma, S. (2001). Differentiation of mouse primordial germ cells into female or male germ cells. The International Journal of Developmental Biology, 45(3), 541–8.

Nam, E. A., & Cortez, D. (2011). ATR signalling: more than meeting at the fork. The Biochemical Journal, 436(3), 527–36.

O'Driscoll, M. (2009). Mouse models for ATR deficiency. DNA Repair, 8(11), 1333–7.

O'Driscoll, M., Ruiz-Perez, V. L., Woods, C. G., Jeggo, P. A., & Goodship, J. A. (2003). A splicing mutation affecting expression of ataxia-telangiectasia and Rad3-related protein (ATR) results in Seckel syndrome. Nature Genetics, 33(4), 497–501.

Oakberg, E. F. (1956). Duration of spermatogenesis in the mouse and timing of stages of the cycle of the seminiferous

epithelium. The American Journal of Anatomy, 99(3), 507–16.

Ohinata, Y., Payer, B., O'Carroll, D., Ancelin, K., Ono, Y., Sano, M., Surani, M. A. (2005). Blimp1 is a critical determinant of the germ cell lineage in mice. Nature, 436(7048), 207–13.

Pacheco, S., Marcet-Ortega, M., Lange, J., Jasin, M., Keeney, S., & Roig, I. (2015). The ATM Signaling Cascade Promotes Recombination-Dependent Pachytene Arrest in Mouse Spermatocytes. PLOS Genetics, 11(3), e1005017.

Page, D. C., Bieker, K., Brown, L. G., Hinton, S., Leppert, M., Lalouel, J. M., & White, R. (1987). Linkage, physical mapping, and DNA sequence analysis of pseudoautosomal loci on the human X and Y chromosomes. Genomics, 1(3), 243–56.

Page, S. L., & Hawley, R. S. (2003). Chromosome choreography: the meiotic ballet. Science (New York, N.Y.), 301(5634), 785–9.

Page, S. L., & Hawley, R. S. (2004). The genetics and molecular biology of the synaptonemal complex. Annual Review of Cell and Developmental Biology, 20, 525–58.

Palmer, S. J., & Burgoyne, P. S. (1991). In situ analysis of fetal, prepuberal and adult XX----XY chimaeric mouse testes: Sertoli cells are predominantly, but not exclusively, XY. Development (Cambridge, England), 112(1), 265–8.

Pan, J., & Keeney, S. (2009). Detection of SPO11-oligonucleotide complexes from mouse testes. Methods in Molecular Biology (Clifton, N.J.), 557, 197–207.

Pangas, S. A. (2012). Regulation of the ovarian reserve by members of the transforming growth factor beta family. Molecular Reproduction and Development, 79(10), 666–79.

Park, J.Y., Su, Y.Q., Ariga, M., Law, E., Jin, S.-L. C., & Conti, M. (2004). EGF-like growth factors as mediators of LH action in the ovulatory follicle. Science (New York, N.Y.), 303(5658), 682–4.

Parks, J., Lee, D., Huang, S., & Kaproth, M.. (2003). Prospects for spermatogenesis in vitro. Theriogenology, 59(1), 73–86.

Pelttari, J., Hoja, M. R., Yuan, L., Liu, J. G., Brundell, E., Moens, P., & Höög, C. (2001). A meiotic chromosomal core consisting of cohesin complex proteins recruits DNA recombination proteins and promotes synapsis in the absence of an axial element in mammalian meiotic cells. Molecular and Cellular Biology, 21(16), 5667–77.

Pepling, M. E. (2006). From primordial germ cell to primordial follicle: mammalian female germ cell development. Genesis (New York, N.Y. : 2000), 44(12), 622–32.

Pepling, M. E., & Spradling, A. C. (2001). Mouse ovarian germ cell cysts undergo programmed breakdown to form primordial follicles. Developmental Biology, 234(2), 339–51.

Peschon, J. J., Behringer, R. R., Brinster, R. L., & Palmiter, R. D. (1987). Spermatid-specific expression of protamine 1 in transgenic mice. Proceedings of the National Academy of Sciences of the United States of America, 84(15), 5316–9.

Peters, A. H., Plug, A. W., van Vugt, M. J., & de Boer, P. (1997). A drying-down technique for the spreading of mammalian meiocytes from the male and female germline. Chromosome Research : An International Journal on the Molecular, Supramolecular and Evolutionary Aspects of Chromosome Biology, 5(1), 66–8.

Picton, H., Briggs, D., & Gosden, R. (1998). The molecular basis of oocyte growth and

development. Molecular and Cellular Endocrinology, 145(1-2), 27–37.

Pittman, D. L., Cobb, J., Schimenti, K. J., Wilson, L. A., Cooper, D. M., Brignull, E., & Schimenti, J. C. (1998). Meiotic prophase arrest with failure of chromosome synapsis in mice deficient for Dmc1, a germline-specific RecA homolog. Molecular Cell, 1(5), 697–705.

Plug, A. W., Peters, A. H., Keegan, K. S., Hoekstra, M. F., de Boer, P., & Ashley, T. (1998). Changes in protein composition of meiotic nodules during mammalian meiosis. Journal of Cell Science, 111 (Pt 4, 413–23.

Print, C. G., & Loveland, K. L. (2000). Germ cell suicide: new insights into apoptosis during spermatogenesis. BioEssays : News and Reviews in Molecular, Cellular and Developmental Biology, 22(5), 423–30.

Raudsepp, T., Das, P. J., Avila, F., & Chowdhary, B. P. (2012). The pseudoautosomal region and sex chromosome aneuploidies in domestic species. Sexual Development : Genetics, Molecular Biology, Evolution, Endocrinology, Embryology, and Pathology of Sex Determination and Differentiation, 6(1-3), 72–83.

Robles, R., Morita, Y., Mann, K. K., Perez, G. I., Yang, S., Matikainen, T., Tilly, J. L. (2000). The aryl hydrocarbon receptor, a basic helix-loop-helix transcription factor of the PAS gene family, is required for normal ovarian germ cell dynamics in the mouse. Endocrinology, 141(1), 450–3.

Rodriguez, I., Ody, C., Araki, K., Garcia, I., & Vassalli, P. (1997). An early and massive wave of germinal cell apoptosis is required for the development of functional spermatogenesis. The EMBO Journal, 16(9), 2262–70.

Roig, I. (2005). Aparellament i sinapsis en oòcits humans. Doctoral Thesis. ISBN: 846900459X. B-40245-2006.

Roig, I., Dowdle, J. A., Toth, A., de Rooij, D. G., Jasin, M., & Keeney, S. (2010). Mouse TRIP13/PCH2 is required for recombination and normal higher-order chromosome structure during meiosis. PLoS Genetics, 6(8).

Roig, I., Liebe, B., Egozcue, J., Cabero, L., Garcia, M., & Scherthan, H. (2004). Female-specific features of recombinational double-stranded DNA repair in relation to synapsis and telomere dynamics in human oocytes. Chromosoma, 113(1), 22–33.

Romanienko, P. J., & Camerini-Otero, R. D. (2000). The mouse Spo11 gene is required for meiotic chromosome synapsis. Molecular Cell, 6(5), 975–987.

Rouyer, F., Simmler, M. C., Johnsson, C., Vergnaud, G., Cooke, H. J., & Weissenbach, J. (1986). A gradient of sex linkage in the pseudoautosomal region of the human sex chromosomes. Nature, 319(6051), 291–5.

Royo, H., Polikiewicz, G., Mahadevaiah, S. K., Prosser, H., Mitchell, M., Bradley, A., & Turner, J. M. A. (2010). Evidence that meiotic sex chromosome inactivation is essential for male fertility. Current Biology : CB, 20(23), 2117–23.

Royo, H., Prosser, H., Ruzankina, Y., Mahadevaiah, S. K., Cloutier, J. M., Baumann, & M., Turner, J. M.. (2013). ATR acts stage specifically to regulate multiple aspects of mammalian meiotic silencing. Genes and Development, 27(13), 1484–1494.

Russell, D. L., & Robker, R. L. (2007). Molecular mechanisms of ovulation: co-ordination through the cumulus complex. Human Reproduction Update, 13(3), 289–312.

Russell, L. D., Ettlin, R. A., Hikim, A. P. S., & Clegg, E. D. (1993). Histological and Histopathological Evaluation of the Testis. International Journal of Andrology, 16(1), 83–83.

Ruzankina, Y., Pinzon-Guzman, C., Asare, A., Ong, T., Pontano, L., Cotsarelis, G., & Brown, E. J. (2007). Deletion of the developmentally essential gene ATR in adult mice leads to age-related phenotypes and stem cell loss. Cell Stem Cell, 1(1), 113–26.

Sakai, Y., & Yamashina, S. (1989). Mechanism for the removal of residual cytoplasm from spermatids during mouse spermiogenesis. The Anatomical Record, 223(1), 43–8.

Saitou, M., & Yamaji, M., (2012). Primordial germ cells in mice. Spring Harbor Perspectives in Biology, 1;4(11).

Sánchez, F., & Smitz, J. (2012). Molecular control of oogenesis. Biochimica et Biophysica Acta, 1822(12), 1896–912.

Sato, T., Katagiri, K., Gohbara, A., Inoue, K., Ogonuki, N., Ogura, A., & Ogawa, T. (2011). In vitro production of functional sperm in cultured neonatal mouse testes. Nature, 471(7339), 504–7.

Seki, Y., Yamaji, M., Yabuta, Y., Sano, M., Shigeta, M., Matsui, Y., & Saitou, M. (2007). Cellular dynamics associated with the genome-wide epigenetic reprogramming in migrating primordial germ cells in mice. Development (Cambridge, England), 134(14), 2627–38.

Sekido, R., Bar, I., Narváez, V., Penny, G., & Lovell-Badge, R. (2004). SOX9 is up-regulated by the transient expression of SRY specifically in Sertoli cell precursors. Developmental Biology, 274(2), 271–9.

Shanske, A., Caride, D. G., Menasse-Palmer, L., Bogdanow, A., & Marion, R. W. (1997). Central nervous system anomalies in Seckel syndrome: report of a new family and review of the literature. American Journal of Medical Genetics, 70(2), 155–8.

Sharan, S. K., Pyle, A., Coppola, V., Babus, J., Swaminathan, S., Benedict, J., & Handel, M. A. (2004). BRCA2 deficiency in mice leads to meiotic impairment and infertility. Development (Cambridge, England), 131(1), 131–42.

Sheridan, S. D., Yu, X., Roth, R., Heuser, J. E., Sehorn, M. G., Sung, P., & Bishop, D. K. (2008). A comparative analysis of Dmc1 and Rad51 nucleoprotein filaments. Nucleic Acids Research, 36(12), 4057–66.

Shi, Q., Spriggs, E., Field, L. L., Ko, E., Barclay, L., & Martin, R. H. (2001). Single sperm typing demonstrates that reduced recombination is associated with the production of aneuploid 24,XY human sperm. American Journal of Medical Genetics, 99(1), 34–8.

Shin, Y.-H., Choi, Y., Erdin, S. U., Yatsenko, S. A., Kloc, M., Yang, F., & Rajkovic, A. (2010). Hormad1 mutation disrupts synaptonemal complex formation, recombination, and chromosome segregation in mammalian meiosis. PLoS Genetics, 6(11), e1001190.

Shinohara, A., Ogawa, H., & Ogawa, T. (1992). Rad51 protein involved in repair and recombination in S. cerevisiae is a RecA-like protein. Cell, 69(3), 457–70.

Shinohara, M., Gasior, S. L., Bishop, D. K., & Shinohara, A. (2000). Tid1/Rdh54 promotes colocalization of rad51 and dmc1 during meiotic recombination. Proceedings of the National Academy of Sciences of the United States of America, 97(20), 10814–9.

Simon, A. M., Goodenough, D. A., Li, E., & Paul, D. L. (1997). Female infertility in mice lacking connexin 37. Nature, 385(6616), 525–9.

Song, H.-W., & Wilkinson, M. F. (2012). In vitro spermatogenesis: A long journey to get tails. Spermatogenesis, 2(4), 238–244.

Sørensen, C. S., Hansen, L. T., Dziegielewski, J., Syljuåsen, R. G., Lundin, C., Bartek, J., & Helleday, T. (2005). The cell-cycle checkpoint kinase Chk1 is required for mammalian homologous recombination repair. Nature Cell Biology, 7(2), 195–201.

Soriano, P., Keitges, E. A., Schorderet, D. F., Harbers, K., Gartler, S. M., & Jaenisch, R. (1987). High rate of recombination and double crossovers in the mouse pseudoautosomal region during male meiosis. Proceedings of the National Academy of Sciences of the United States of America, 84(20), 7218–20.

Stocco, C., Telleria, C., & Gibori, G. (2007). The molecular control of corpus luteum formation, function, and regression. Endocrine Reviews, 28(1), 117–49.

Stracker, T. H., Usui, T., & Petrini, J. H. J. (2009). Taking the time to make important decisions: the checkpoint effector kinases Chk1 and Chk2 and the DNA damage response. DNA Repair, 8(9), 1047–54.

Su, Y.-Q., Sugiura, K., & Eppig, J. J. (2009). Mouse oocyte control of granulosa cell development and function: paracrine regulation of cumulus cell metabolism. Seminars in Reproductive Medicine, 27(1), 32–42. d

Subramanian, V. V, & Hochwagen, A. (2014). The Meiotic Checkpoint Network: Step-by-Step through Meiotic Prophase. Cold Spring Harbor Perspectives in Biology, 6(10).

Sun, S.C., & Kim, N.H. (2012). Spindle assembly checkpoint and its regulators in meiosis. Human Reproduction Update, 18(1), 60–72.

Surani, M. A. (2001). Reprogramming of genome function through epigenetic inheritance. Nature, 414(6859), 122–8.

Svingen, T., & Koopman, P. (2013). Building the mammalian testis: origins, differentiation, and assembly of the component cell populations. Genes & Development, 27(22), 2409–26.

Syrjänen, J. L., Pellegrini, L., & Davies, O. R. (2014). A molecular model for the role of SYCP3 in meiotic chromosome organisation. eLife, 3, e02963.

Szybek, K. (1972). In-vitro maturation of oocytes from sexually immature mice. The Journal of Endocrinology, 54(3), 527–8.

Tajima, K., Orisaka, M., Mori, T., & Kotsuji, F. (2007). Ovarian theca cells in follicular function. Reproductive Biomedicine Online, 15(5), 591–609.

Tam, P. P., & Snow, M. H. (1981). Proliferation and migration of primordial germ cells during compensatory growth in mouse embryos. Journal of Embryology and Experimental Morphology, 64, 133–47.

Tarsounas, M., Morita, T., Pearlman, R. E., & Moens, P. B. (1999). RAD51 and DMC1 form mixed complexes associated with mouse meiotic chromosome cores and synaptonemal complexes. The Journal of Cell Biology, 147(2), 207–20.

Tease, C., & Hultén, M. A. (2004). Inter-sex variation in synaptonemal complex lengths largely determine the different recombination rates in male and female germ cells. Cytogenetic and Genome Research, 107(3-4), 208–15.

Thacker, D., Mohibullah, N., Zhu, X., & Keeney, S. (2014). Homologue engagement controls meiotic DNA break number and distribution. Nature, 510(7504), 241–6.

Thomas, F. H., & Vanderhyden, B. C. (2006). Oocyte-granulosa cell interactions during mouse follicular development: regulation of kit ligand expression and its role in oocyte growth. Reproductive Biology and Endocrinology : RB&E, 4, 19.

Thomson, A. M., Gillespie, P. J., & Blow, J. J. (2010). Replication factory activation can be decoupled from the replication timing program by modulating Cdk levels. The Journal of Cell Biology, 188(2), 209–21.

Tingen, C., Kim, A., & Woodruff, T. K. (2009). The primordial pool of follicles and nest breakdown in mammalian ovaries. Molecular Human Reproduction, 15(12), 795–803.

Tsuzuki, T., Fujii, Y., Sakumi, K., Tominaga, Y., Nakao, K., Sekiguchi, M., & Yoshimura, Y. (1996). Targeted disruption of the Rad51 gene leads to lethality in embryonic mice. Proceedings of the National Academy of Sciences, 93(13), 6236–6240.

Turner, J. M. a. (2007). Meiotic sex chromosome inactivation. Development (Cambridge, England), 134(10), 1823–31.

Turner, J. M. a, Mahadevaiah, S. K., Fernandez-Capetillo, O., Nussenzweig, A., Xu, X., Deng, C.-X., & Burgoyne, P. S. (2005). Silencing of unsynapsed meiotic chromosomes in the mouse. Nature Genetics, 37(1), 41–7.

Turner, J. M. A., Aprelikova, O., Xu, X., Wang, R., Kim, S., Chandramouli, G. V. R., Deng, C. X. (2004). BRCA1, histone H2AX phosphorylation, and male meiotic sex chromosome inactivation. Current Biology, 14(23), 2135–2142.

Van den Hurk, R., & Zhao, J. (2005). Formation of mammalian oocytes and their growth, differentiation and maturation within ovarian follicles. Theriogenology, 63(6), 1717–51.

Vigodner, M. (2009). Sumoylation precedes accumulation of phosphorylated H2AX on sex chromosomes during their meiotic inactivation. Chromosome Research : An International Journal on the Molecular, Supramolecular and Evolutionary Aspects of Chromosome Biology, 17(1), 37–45.

Wagner, T., Wirth, J., Meyer, J., Zabel, B., Held, M., Zimmer, J., & Scherer, G. (1994). Autosomal sex reversal and campomelic dysplasia are caused by mutations in and around the SRY-related gene SOX9. Cell, 79(6), 1111–20.

Wang, X., Zou, L., Lu, T., Bao, S., Hurov, K. E., Hittelman, W. N., & Li, L. (2006). Rad17 phosphorylation is required for claspin recruitment and Chk1 activation in response to replication stress. Molecular Cell, 23(3), 331–41.

Wickramasinghe, D., Ebert, K. M., & Albertini, D. F. (1991). Meiotic competence acquisition is associated with the appearance of M-phase characteristics in growing mouse oocytes. Developmental Biology, 143(1), 162–72.

Wojtasz, L., Cloutier, J. M., Baumann, M., Daniel, K., Varga, J., Fu, J., & Tóth, A. (2012). Meiotic DNA double-strand breaks and chromosome asynapsis in mice are monitored by distinct HORMAD2-independent and -dependent mechanisms. Genes & Development, 26(9), 958–73.

Wojtasz, L., Daniel, K., Roig, I., Bolcun-Filas, E., Xu, H., Boonsanay, V., & Toth, A. (2009). Mouse HORMAD1 and HORMAD2, two conserved meiotic chromosomal proteins, are depleted from synapsed chromosome axes with the help

of TRIP13 AAA-ATPase. PLoS Genetics, 5(10), e1000702.

Woods, L. M., Hodges, C. A., Baart, E., Baker, S. M., Liskay, M., & Hunt, P. A. (1999). Chromosomal influence on meiotic spindle assembly: abnormal meiosis I in female Mlh1 mutant mice. The Journal of Cell Biology, 145(7), 1395–406.

Wu, H., Mathioudakis, N., Diagouraga, B., Dong, A., Dombrovski, L., Baudat, F., Kadlec, J. (2013). Molecular basis for the regulation of the H3K4 methyltransferase activity of PRDM9. Cell Reports, 5(1), 13–20.

Wu, H.Y., Ho, H. C., & Burgess, S. M. (2010). Mek1 kinase governs outcomes of meiotic recombination and the checkpoint response. Current Biology : CB, 20(19), 1707–16.

Yan, S., & Michael, W. M. (2009). TopBP1 and DNA polymerase alpha-mediated recruitment of the 9-1-1 complex to stalled replication forks: implications for a replication restart-based mechanism for ATR checkpoint activation. Cell Cycle (Georgetown, Tex.), 8(18), 2877–84.

Yang, F., De La Fuente, R., Leu, N. A., Baumann, C., McLaughlin, K. J., & Wang, P. J. (2006). Mouse SYCP2 is required for synaptonemal complex assembly and chromosomal synapsis during male meiosis. The Journal of Cell Biology, 173(4), 497–507.

Yang, F., Eckardt, S., Leu, N. A., McLaughlin, K. J., & Wang, P. J. (2008a). Mouse TEX15 is essential for DNA double-strand break repair and chromosomal synapsis during male meiosis. The Journal of Cell Biology, 180(4), 673–9.

Yang, F., Eckardt, S., Leu, N. A., McLaughlin, K. J., & Wang, P. J. (2008b). Mouse TEX15 is essential for DNA double-strand break repair and chromosomal synapsis during male meiosis. The Journal of Cell Biology, 180(4), 673–9.

Yang, F., & Wang, P. J. (2009). The Mammalian synaptonemal complex: a scaffold and beyond. Genome Dynamics, 5, 69–80.

Yoshida, K., Kondoh, G., Matsuda, Y., Habu, T., Nishimune, Y., & Morita, T. (1998). The Mouse RecA-like Gene Dmc1 Is Required for Homologous Chromosome Synapsis during Meiosis. Molecular Cell, 1(5), 707–718.

Youds, J. L., & Boulton, S. J. (2011). The choice in meiosis - defining the factors that influence crossover or non-crossover formation. Journal of Cell Science, 124(Pt 4), 501–13.

Yuan, L., Liu, J. G., Zhao, J., Brundell, E., Daneholt, B., & Höög, C. (2000). The murine SCP3 gene is required for synaptonemal complex assembly, chromosome synapsis, and male fertility. Molecular Cell, 5(1), 73–83.

Zeman, M. K., & Cimprich, K. A. (2014). Causes and consequences of replication stress. Nature Cell Biology, 16(1), 2–9.

Zhang, H., Risal, S., Gorre, N., Busayavalasa, K., Li, X., Shen, Y., & Liu, K. (2014). Somatic cells initiate primordial follicle activation and govern the development of dormant oocytes in mice. Current Biology : CB, 24(21), 2501–8.

Zhang, L., Kim, K. P., Kleckner, N. E., & Storlazzi, A. (2011). Meiotic double-strand breaks occur once per pair of (sister) chromatids and, via Mec1/ATR and Tel1/ATM, once per quartet of chromatids. Proceedings of the National Academy of Sciences of the United States of America, 108(50), 20036–41.

Zhang, S., Lin, H., Kong, S., Wang, S., Wang, H., Wang, H., & Armant, D. R. (2013). Physiological and molecular determinants of embryo implantation. Molecular Aspects of Medicine, 34(5), 939–80.

AGRAÏMENTS

Aquesta tesi és fruit de l'esforç de moltes persones que directa o indirectament han col·laborat per tirar endavant aquest treball.

En primer lloc, he d'agrair al meu director de tesi, l'Ignasi, per acollir-me al seu grup i permetrem formar part d'aquest projecte. T'he d'agrair moltes coses. La teva dedicació a la ciència, a la gent que formem part del teu grup i tot el temps que ens has destinat sempre que hem tingut un problema. Gracies per la teva manera de veure les coses i aquesta capacitat de fer que tot sigui fàcil per complicat que sembli. Durant aquests anys m'has ensenyat molt en professionalment, a desenvolupar-me en l'àmbit científic, però també a créixer com a persona.

Durant aquesta etapa he treballat amb molta gent, que han estat companys, però alhora amics. Vull agrair especialment a la Marina, per estar sempre al meu costat i recolzar-me. Per oferir-te a ajudar-me cada cop que ha sorgit alguna dificultat, tant del laboratori com personal, i per la teva infinita paciència amb els Westerns. Els dies al laboratori no haguessin estat el mateix sense els cafès de les tardes i els teus consells. A la Laia, per fer que el dia a dia del laboratori sigui una mica més fàcil i més alegre, i a la Rita, pel seu optimisme i sempre tenir un somriure per dedicar-te. També a la gent que ha arribat més tard al laboratori. A la Rosa Ana, la teva experiència m'ha ajudat a enfrontar-me al problemes d'aquest món científic, a l'Ana, a l'Elena, i particularment a la Cris, per tot els temps que has dedicat als cultius i tots els diumenges que hem hagut de passar al laboratori per fer que funcionin.

També he d'agrair a total la gent de la Unitat de Citologia i Histologia, que des dels inicis m'han ajudat a integrar-me al laboratori, i molt especialment al Josep, per dedicar tantes hores a ensenyar-me les tècniques d'histologia i acompanyar-me durant les hores al micròtom entretenint-me amb històries. A la Mar, del Institut de Neurociències per estar sempre disponible per ajudar-me amb el criòtom, i també a l'Almudena i la Francesca de l'IBB, per encarregar-se de que tot estigui sempre a punt i facilitar-nos la feina.

Vull donar també les gracies als que han col·laborat amb aquest projecte. A l'Oscar Fernandez-Capetillo del CNIO, per proporcionar-nos els ratolins Seckel; i a l'Scott Keeney i al Julian Lange per accedir a fer els anàlisis dels complexes d'oligonucleotids d'SPO11.

Sens dubte, he d'agrair a tota la gent que sense haver-hi participat directament, m'han ajudat a tirar endavant aquest projecte, i molts cops sense adonar-vos-en, simplement perquè formeu part de la meva vida. En primer lloc, a la meua família; als meus pares perquè sempre han fet tan per mi, i sé que seguiran esforçant-se per fer-ho, i a Iris, perquè no imagine com es pot ser millor germana i persona a la vegada. El vostre amor i suport incondicional us l'agrairé sempre. També a Marco, per haver aguantat les dificultats d'aquest últims mesos, haver-me recolzat en tot moment i especialment per intentar aprendre`t amb tanta il·lusió que es la meiosi i que hi fa ATR per allà al mig. Finalment, a tots els que heu estat al meu costat durant aquest temps, els que seguiu prop i als que els vostres camins us han portat lluny. Cadascun

dels consells que heu sabut donar-me, en el bons moments, però sobretot en els difícils, m'han conduit fins on em trobe ara. Veure que crèieu amb mi m'ha fet ser capaç de fer-ho, així que tots vosaltres us mereixeu un trosset d'aquest treball. Gracies per estar al meu costat i ser gent tan bonica.